# Algorithm Theoretical Basis Document for ASTER Level-1 Data Processing (Ver. 3.0)

Level-1 Data Working Group
ASTER Science Team, Japan

November 1, 1996

**ERSDAC**

Earth Remote Sensing
Data Analysis Center

Approval:

_____

Hiroji Tsu
ASTER Science Team Leader

## Level-1 Data Working Group Members

| | | |
|---|---|---|
| Chairman | Hiroyuki Fujisada | Electrotechnical Laboratory |
| Member | Kohei Arai | University of Saga |
| Member | Kiyonari Fukue | Tokai University |
| Member | Akira Iwasaki | Electrotechnical Laboratory |
| Member | Manabu Kaku | Bishimetal Exploration Co. |
| Member | Fumihiro Sakuma | National Research Laboratory of Metrology |
| Member | Isao Sato | Geological Survey of Japan |
| Member | Minoru Urai | Geological Survey of Japan |
| Observer | Hiroshi Watanabe | ERSDAC |
| Manager | Masatane Kato | ERSDAC |

# REVISION  RECORD

|        |              |      |
|--------|--------------|------|
| Ver.1.0 | March 24,    | 1994 |
| Ver.1.1 | November 1,  | 1994 |
| Ver.1.2 | April 28,    | 1995 |
| Ver.2.0 | October 24,  | 1995 |
| Ver.2.1 | December 26, | 1995 |
| Ver.3.0 | November 1,  | 1996 |

## Major  Changes  from  Ver.2.0  to  Ver.2.1

1. The pointing stability data of the ASTER instrument was added.

     Table 2-23 in page 13

2. Temperature coefficients were given for each detector instead of each band.

     Figure 2-4 in page 19

3. Non-linear temperature coefficients were added to the correction of offset for SWIR.

     Figure 2-4 in page 19

4. Some VNIR supplement data were deleted.

     Table 2-24, No.35 & 36 in page 20

5. Coordinate transformation module for map projection was moved to the Level-1B processing from the Level-1A processing.

     Figures 3-1, 3-16, 3-17, 3-18 and 3-21 in pages 25, 49, 50, 51 and 55, respectively

6. Flexibility for the map projection and the resampling methods was added in the Level-1B processing.

     Figures 3-21 and 3-22 in pages 55 and 56, respectively

7. The psudo-affin coefficients were removed from the Level-1A data product.

     Figure 3-19 in page 52

8. The size of the scene for band 3B was increased from 63 km to 69 km in the along-track direction to compensate the terrain error contribution.

     Section 3.8 in page 48
     Figures 3-19 and 3-23 in pages 52 and 57, respectively

9. The pixel size of the Level-1A scene for band 3B was increased from 4100 to 5000 in the cross-track direction.

     Figure 3-19 in page 52

10. Description on "Theoretical Basis of Radiometric Correction" was largely revised.

     Section 8.3 in pages from 100 to 105

## Major Changes from Previous Version (Ver.2.1)

1. The spacecraft position knowledge and pointing knowledge are updated.

    Table 2-2 in page 2 and Table 2-4 in page 3

**2.** The geolocation knowledge of the spacecraft is updated.

    Table 2-5 in page 4

3. The spectral and the radiometric performances are updated using the measured results.

    Table 2-9 in page 7 and Table 2-11 in page 8

3. The instrument pointing performances are updated using the results of PFT.

    Tables 2-19 to 2-23 in pages 12 and 13

4. The Pixel geolocation knowledge table is added.

    Table 2-24 in page 14

5. The sensor radiometric model and the data base are slightly modified.

    Section 2.2.6 in pages 18 to 19

6. The radiometric coefficients generation method is slightly modified.

    Section 3.4 in pages 36 to 40

7. The DC clamp correction is slightly modified.

    Section 3.5 in page 41

8. The inter-telescope geometric correction algorithm is slightly modified.

    Section 3.7 in pages 44 to 48

9. The contents of the Level-1A products are slightly modified.

    Figure 3-19 in page 52

10. The Level-1B processing method is slightly modified.

    Section 3.12 in pages 56 and 57

11. GCP Preparation Plan is added

    Section 4.4 in page 63

12. The description of the granularization is simplified.

    Chapter 6 in page 81

13. One test data is added.

    Figure 7-5 in page 89

14. The algorithm evaluation results of the SWIR parallax correction are updated.

    Section 7.3. in pages 90 to 92

15. The algorithm evaluation results of the inter-telescope registration correction are updated.

    Section 7.4 in pages 93 to 97

16. The theoretical basis of the geometric system correction is largely updated.

    Section 8.2 in pages 103 to 108

17. The theoretical basis of the radiometric correction is largely updated.

    Section 8.3 in pages 108 to 113

# Response to Review Panel Recommendation

1. Band-to-Band Registration:

<u>Recommendation</u>
The Review Panel showed some concern about band-to-band registration by image matching and recommended to investigate the possibility of employing both optical alignment methods and alternative spectral acquisition timing.

<u>Response</u>
We understand that automated image matching is indispensable for ASTER Level-1 processing, although it is very challenging techniques.

We can not accept Panel recommendation, because of a big impact to instrument design. Instrument design was finalized at CDRs in last November.

The evaluation results for the automated image matching are included in this version of ATBD.

2. Signal-to-Noise:

<u>Recommendation</u>
The Review Panel showed some concern about low signal-to-noise characteristics and recommended changing gains.

<u>Response</u>
Each ASTER spectral band has a independent variable gain function, although it would not have a significant effect on the signal-to-noise ratios. The signal-to-noise could not be significantly improved without sacrificing either spectral and spatial resolutions.

The measured values of the signal-to-noise characteristics for PFM are included in this version of ATBD as the back ground information of the instrument.

3. Calibration:

<u>Recommendation</u>
 The Review Panel noted that the Level-1 ATBD did not describe much detail on calibration procedure and recommended to dedicate considerable attention to the instrument calibration problem.

<u>Response</u>
We understand that we need more work to establish the calibration procedure.

An our idea on update methodology for radiometric and geometric coefficients is described in this version of ATBD.

# TABLE OF CONTENTS

# 1. INTRODUCTION

ASTER is an advanced multispectral imager which is selected by NASA to fly on EOS-AM1 polar orbiting spacecraft with other 4 sensors in June 1998, and covers a wide spectral region from visible to thermal infrared by 14 spectral bands with high spatial and spectral and radiometric resolutions. ASTER stands for the Advanced Spaceborne Thermal Emission and Reflection radiometer. The EOS-AM1 spacecraft will operate in a circular, near polar orbit at 705 km altitude. The orbit is sun-synchronous with a local time of 10:30 a.m. The recurrent cycle is 16 days.

The basic concept of ASTER is to acquire quantitative spectral data of reflected and emitted radiation from the earth's surface in the 0.5-2.5 and 8-12 μm atmospheric windows at spatial and spectral resolutions appropriate for various science objectives. The general purpose of the science investigation by ASTER is to study the interaction among the geosphere, hydrosphere cryosphere, and atmosphere of the earth from geophysical point of view. Special features to be stressed for ASTER compared to other optical imagers are; (1) spectral data acquisition with a high spatial resolution of 15 m in visible and near infrared regions, (2) stereoscopic capability in the along track direction, (3) high spectral resolution in short wave infrared region, and (4) high spectral and spatial resolutions in thermal infrared region.

More specific areas of the science investigation can be listed as; (a) geology and soil - the detailed compositional and geomorphologic mapping of surface soil and bedrocks to study the land surface processes and the Earth's history, (b) volcano monitoring - monitoring of eruptions and precursive events such as emission of volcanic gases to atmosphere, eruption plumes, development of lava lakes and fumerolic activity, eruptive history and eruptive potential, (c) carbon cycling and marine ecosystem - the atmospheric carbon dioxide being fixed into coral reefs by measuring the accumulation rate of coral reefs, (d) aerosol and cloud - observation of atmospheric aerosol characteristics and various cloud types, which are useful for the atmospheric correction of the surface retrieval, (e) evapotranspiration - the knowledge of the difference between air temperature measured in situ and canopy temperature derived from ASTER radiance measurements, (f) hydrology - understanding of global energy and hydrologic processes and their relationship to global changes, (g) vegetation and ecosystem dynamics - investigation of vegetation and soil distribution and their changes to estimate biological productivity to understand land-atmosphere interaction and to detect ecosystem changes, and (h) land surface climatology - investigation of land surface parameters, surface temperature etc., to understand land-atmosphere interaction the energy and moisture fluxes.

To meet a wide spectral coverage, optical signal sensing units of ASTER are separated into three subsystems, that is, visible and near infrared radiometer(VNIR) subsystem, short wave infrared radiometer(SWIR) subsystem and thermal infrared radiometer(TIR) subsystem, depending on spectral regions from technological point of view. Both VNIR and SWIR images are obtained by the pushbroom scanning employing linear array detectors of Si-CCD and PtSi-CCD, respectively. The Si-CCD for the VNIR includes 5000 detectors for each spectral bands. Only 4100 detectors among 5000 are enough for nadir looking images with a swath of 60 km, including a redundancy. For backward stereo images, extra detectors are necessary to compensate the earth rotation to cover 60 km swath. Therefore, full 5000 detectors are used for the stereo data acquisition. The PtSi-CCD for the SWIR subsystem consists of 2048 detectors for each spectral band. While TIR images are obtained by mechanical scanning with 10 HgCdTe PC type detectors for each spectral band, that is, 50 detectors in total.

The ASTER instrument configuration mentioned above gives rise to necessity of the ground processing on the generation of Level-1 data products which are radiometrically calibrated and geometrically registered. This document describes the concept of Level-1 processing algorithm on the ASTER Ground Data System, including the theoretical basis of the algorithm.

# 2. BACKGROUND INFORMATION

## 2.1. Spacecraft Orbit and Pointing Information

### 2.1.1. Orbit Parameters

Geometric parameters depend on the orbit parameters. For example pixel and scene sizes depend on the altitude of the spacecraft. Therefore, orbit parameters and their accuracies must be considered for the Level-1 algorithm development. The instrument design on the geometric parameters is based on a nominal spacecraft altitude of 705 km at the equator. The orbit parameters listed in Table 2-1 will be considered to develop the algorithm.

Table 2-1 Orbit Parameters

| Orbit | Sun synchronous Descending |
|---|---|
| Semi-major axis (Mean) | 7078 km |
| Eccentricity | 0.0012 |
| Time of day | 10:30 ± 15 min. am |
| Altitude range | 700 - 737 km (705 km at equator) |
| Inclination | 98.2° ± 0.15° |
| Repeat cycle | 16 days (233 revolutions/16 days) |
| Distance between adjacent orbits | 172 km |
| Orbit period | 98.9 min |
| Orbit position knowledge | ±150 m/3 axes, 3σ |
| Repetition accuracy | ±20 km, 3σ |

The design values of the position knowledge is much better than the specified ones. Table 2-2 shows these values presented at the spacecraft CDR.

Table 2-2 Prediction of Position Knowledge

| Direction | Specification (3σ) | Prediction (3σ) |
|---|---|---|
| Radial Position (m) | ±150 | 3.6 |
| Along-track (m) | ±150 | 11.1 |
| Cross-track (m) | ±150 | 5.4 |

Notes
Three non-optimal 9 minute TDRS contacts per orbit, GJM2 Geopotential (30 x 30), solar flux of 175, 5 % Cd error, TDRS ephemeris error of 75 meters.

## 2.1.2. Pointing Performance

The pointing performance of the instrument and the spacecraft is vital for band-to-band registration of ASTER, since ASTER optics consists of three telescopes. Boresights of each telescope must be stable enough to satisfy the required registration accuracies which are ±0.2 pixels for intra-telescopes and ±0.3 pixels for inter-telescopes. The pointing stability consists of the instrument allocation (instrument boresight-to-mounting interface) and the spacecraft allocation (mounting interface-to-Earth frame of reference). These allocations are described in ASTER UIID so as to meet the required band-to-band registration. The pointing performance at CDR stage is shown in Table 2-3 and compared with the allocated requirements for the Spacecraft. Total requirements for the jitter and stability of boresight are described in Section 2.2.4.

Table 2-3 Pointing Stability Performance of Spacecraft

(Unit; arcsec-3σ, Peak-to-Peak)

| Time Scale | Requirements | | | Design Values | | | Note |
|---|---|---|---|---|---|---|---|
| | Roll | Pitch | Yaw | Roll | Pitch | Yaw | |
| 1.0 s at SWIR & TIR | 3 | 3 | 4 | - | - | - | ITR |
| 1.8 s at SWIR | 2.7 | 2.7 | 4 | 2.0 | 0.8 | 2.0 | BBR |
| 9 s at VNIR | 10 | 10 | 10 | 3.2 | 1.9 | 8.3 | DEM |
| 420 s at MISR | 14 | 14 | 14 | 10.4 | 7.9 | 15.6 | |
| 480 s at VNIR | 17 | 16 | 16 | - | - | - | Geolocation |

Note    BBR; Band-to-Band Registration
        ITR; Inter-Telescope Registration     DEM; Digital Elevation Model
  TIR pointing mirror disturbance is not included in the design values. Therefore, the
  final design values including the TIR disturbance might be slightly increased.

Table 2-4 shows the pointing knowledge and accuracy of the spacecraft. Design values are those expressed at the spacecraft CDR.

Table 2-4 Pointing Knowledge and Accuracy of Spacecraft

| | Specification (Each Axis) | Design Values | | | | | |
|---|---|---|---|---|---|---|---|
| | | Dynamic Error | | | Static Error | | |
| | | Roll | Pitch | Yaw | Roll | Pitch | Yaw |
| Pointing knowledge (arcsec, 3σ) | ±90 | ±10.6 | ±13.1 | ±9.3 | ±43.2 | ±32.6 | ±50.4 |
| Pointing accuracy (arcsec, 3σ) | ±150 | ±11.7 | ±14.2 | ±12.8 | ±53.3 | ±45.1 | ±83.0 |

Table 2-5 shows the pixel geolocation performance of the spacecraft which is calculated with RSS of the pointing knowledge and the position knowledge shown in Tables 2-2 and 2-4, respectively, for the nadir direction. The along-track and the cross-track values are calculated by the pitch and the roll errors, respectively. The yaw axis pointing errors and the radial axis position errors do not have significant meaning. The errors for the nadir direction may be considered as common values with a good accuracy for all detectors even for a maximum pointing angle of 8.55 degree for the normal operation.

Table 2-5  Preciction of Pixel Geolocation Knowledge of Spacecraft

| Direction | Specification (3σ) | Predicted Values (3σ) | |
| --- | --- | --- | --- |
| | | Dynamic | Static |
| Along-track(m) | ±342 | ±28 | ±111 |
| Cross-track (m) | ±342 | ±25 | ±148 |

. Notes
Three non-optimal 9 minute TDRS contacts per orbit, GJM2 Geopotential (30 x 30),
solar flux of 175, 5 % Cd error, TDRS ephemeris error of 75 meters.

## 2.1.3.  Ancillary   Information

The Level-1 processing needs the spacecraft orbit and pointing informations for system correction.  These informations are provided from the spacecraft to the instrument as the ancillary data listed in Table 2-6.  The ASTER instrument multiplexes the ancillary data with the science data and send them to the spacecraft as the ASTER instrument source data, which is almost identical to Level-0 data.  Therefore, the ASTER Level-0 data include the spacecraft ancillary data to make it possible to carry out the Level-1 processing without telemetry data separately transmitted from the spacecraft to the ground station.

The performance information (TONS position and pointing knowledge) shown in Tables 2-2 and 2-4 represent near real-time calculations on-board the spacecraft and are provided in the ancillary data sent to ASTER over the C&T bus every 1.024 seconds.  These attitude and position data is refreshed every 1.024 seconds which is same as a communication frequency between the spacecraft and the ASTER instrument.

The attitude and position data is sent to ASTER at minor cycle (8 ms) number 77.  This results in a time lag of 616 milliseconds between the time stamp in the ancillary data and the clock time at the communication between the spacecraft and the instrument.  The sampling time of the ancillary data relative to the epoch of the time stamp is zero milliseconds for the TONS-derived spacecraft position and velocity data (real-time calculation using the rate data).

## Table 2-6 Spacecraft Ancillary Data Message Contents (GIIS)

| Description | Notes | Resolution* | Range* | Sampling time** |
|---|---|---|---|---|
| PacketHeader | CCSDS packet header for downlink, used for ground routing and processing. May be ignored by instruments | N/A | N/A | N/A |
| Secondary Header ID Flag | Flag indicating "Non-CCSDS-Defined Secondary Header" Always a data zero. This field is part of the secondary header of the packet for downlink. | N/A | N/A | N/A |
| Time Stamp | Epock of the data in the ancillary data message. Spacecraft clock time in CCSDS Day-Segmented Format. The "P-field" is implied, and equals "01000001" binary. The code epoch is 1958 January 1. This field is part of the secondary header of the packet for downlink. | 1 μsec | 1958-2047 | N/A |
| Flag Byte | Flags for ground data processing control. First (most significant) bit is the "quick look" bit which, when set to a data one, indicates that quick-look processing should be performed. Other bits are reserved and will contain data zeros. This field is part of the secondary header of the packet for downlink. | N/A | N/A | N/A |
| Time Conversion | Estimated difference between UTC and the Spacecraft Clock. This may be added to the Spacecraft Clock time to derive UTC time. | 1 μsec | $\pm 8.3 \times 10^6$ μsec | 0 |
| Spacecraft Position (X,Y,Z) | Estimated position of the spacecraft, expressed in the Earth Center Inertial frame (mean Equator and Equinox of J2000) | 0.125 m | $\pm 268 \times 10^6$ m | 0 |
| Spacecraft Velocity (X,Y,Z) | Estimated velocity of the spacecraft, expressed in the Earth Center Inertial frame (mean Equator and Equinox of J2000) | $244 \times 10^{-6}$ m/s | $\pm 524 \times 10^3$ m/s | 0 |
| Attitude Angle (Roll,Pitch,Yaw) | The estimated attitude of the spacecraft, expressed in the Orbital Reference frame. | 1.0 arcsec | $\pm 2048$ arcsec | See Note 1 |
| Attitude Rate (Roll,Pitch,Yaw) | The estimated attitude rates of the spacecraft, expressed in the Orbital Reference frame. | 0.5 arcsec/s | $\pm 1024$ arcsec/s | See Note 1 |
| Magnetic Coil Current (X,Y,Z) | Currents flowing in each of the magnetic torquer coils used for Spacecraft momentum unloading. | $15.6 \times 10^{-3}$ A | $\pm 2.0$ A | See Note 2 |
| Solar Array Current | Current flowing from the Spacecraft solar array. | 1.0 A | 0 - 256 A | See Note 2 |
| Solar Position (X,Y,Z) | Components of a unit vector, expressed in the Spacecraft Reference frame, pointing in the direction of the Sun. | $7.8 \times 10^{-3}$ | 1 | 0 |
| Moon Position (X,Y,Z) | Components of a unit vector, expressed in the Spacecraft Reference frame, pointing in the direction of the Moon. | $7.8 \times 10^{-3}$ | 1 | 0 |
| Reserved | Denotes fields within message which are reserved for future application. These fields must not be interpreted by instrument. | N/A | N/A | N/A |

Spacecraft issues an ancillary data message to each instrument once per major cycle(1.024 seconds).

(*); Resolutions and Ranges are approximate. Exact values are defined by format.

(**); Sampling time of data relative to epoch of Time Stamp, in milliseconds.

1. Telemetry sampled once per 1.024 seconds.

2. Telemetry sampled once per 8.192 seconds

## 2.2. Instrument Characteristics

### 2.2.1. Instrument Performance Overview

Table 2-7 shows the baseline performance requested in accordance with the science mission. Table 2-8 shows more detail spectral passbands. Optical signal sensing units of ASTER are separated into three subsystems, that is, visible and near infrared radiometer(VNIR) subsystem, short wave infrared radiometer(SWIR) subsystem and thermal infrared radiometer(TIR) subsystem, depending on spectral regions from technological point of view. ASTER has 3 spectral bands in VNIR region with a spatial resolution of 15 m, 6 spectral bands in SWIR region with a spatial resolution of 30 m and 5 spectral bands in TIR region with a spatial resolution of 90 m. In addition, ASTER has a stereoscopic capability with a base-to-height ratio of 0.6 by using near infrared band 3 in the along-track direction. Both VNIR and SWIR images will be obtained by the pushbroom scanning with linear array detectors. The TIR images will be obtained by mechanical scanning with 10 detectors for each band to decrease NE$\Delta$T.

Table 2-7  Base Line Performance Requirements

| | |
|---|---|
| Spectral coverage | 0.52 - 11.65 $\mu$m |
| Spatial resolution | 15 m (Bands 1 - 3)<br>30 m (Bands 4 - 9)<br>90 m (Bands 10 - 14) |
| Radiometric resolution | $\leq$ 0.5% NE$\Delta\rho$ (Bands 1 - 3)<br>$\leq$ 0.5 - 1.3% NE$\Delta\rho$ (Bands 4 - 9)<br>$\leq$ 0.3K NE$\Delta$T(Bands 10 - 14) |
| Absolute radiometric accuracy | $\leq \pm$ 4% |
| Absolute temperature accuracy | $\leq$ 3 K (200 - 240 K)<br>$\leq$ 2 K (240 - 270 K)<br>$\leq$ 1 K (270 - 340 K)<br>$\leq$ 2 K (340 - 370 K) |
| Signal quantization levels | 8 bits (Bands 1 - 9)<br>12 bits (Bands 10 - 14) |
| Base-to-height ratio of stereo capability | 0.6 (along-track) |
| Swath width | 60 km |
| Total coverage in cross-track direction by pointing function | 232 km |
| Mission life | 5 years |
| MTF at Nyquist frequency | 0.25 (cross-track)<br>0.20 (along-track) |
| Peak data rate | 89.2 Mbps |
| Mass | 406 kg |
| Peak power | 726 W |

Table 2-8  Spectral Passbands

| Subsystem | Band No. | Spectral range (µm) | Radiometric resolution | Spatial resolution (m) |
|---|---|---|---|---|
| VNIR | 1 | 0.52 - 0.60 | ≤ 0.5% | 15 |
| | 2 | 0.63 - 0.69 | | |
| | 3 | 0.76 - 0.86 | | |
| SWIR | 4 | 1.600 - 1.700 | ≤ 0.5% | 30 |
| | 5 | 2.145 - 2.185 | ≤ 1.3% | |
| | 6 | 2.185 - 2.225 | ≤ 1.3% | |
| | 7 | 2.235 - 2.285 | ≤ 1.3% | |
| | 8 | 2.295 - 2.365 | ≤ 1.0% | |
| | 9 | 2.360 - 2.430 | ≤ 1.3% | |
| TIR | 10 | 8.125 -8.475 | ≤ 0.3K | 90 |
| | 11 | 8.475 - 8.825 | | |
| | 12 | 8.925 - 9.275 | | |
| | 13 | 10.25 -10.95 | | |
| | 14 | 10.95 - 11.65 | | |

## 2.2.2.  Spectral   Performance

The ASTER spectral bands are shown in Table 2-8.  The VNIR bands will be used for topographic interpretation because of its high spatial resolution, and will be also useful to assess vegetation and iron oxide minerals.  The SWIR bands are selected mainly for the purpose of surface mineralogical mapping. The ASTER SWIR will permit more detailed surface lithologic mapping than Landsat TM and JERS-1 OPS. Discrimination of clouds from snow will also be possible using the SWIR bands.  The TIR bands will be used to separate temperature and emissivity of surface targets.  Emissivity patterns derived from the five TIR bands will be a powerful tool to estimate silica contents, which is important to characterize silicate rocks that are the most abundant rock type on the earth surface.  Table 2-9 shows the spectral performance of PFM at PQR.
.

Table 2-9  Accuracy of Spectral Bands

| Bands | Central wavelength (µm) | | Mometum Center (µm) | Band width (µm) | |
|---|---|---|---|---|---|
| | Specified Value | Measured Value | Measured Value | Specified Value | Measured Value |
| 1 | 0.56 ± 0.01 | 0.556 | 0.556 | 0.08 ± 0.02 | 0.09 |
| 2 | 0.66 ± 0.01 | 0.659 | 0.661 | 0.06 ± 0.02 | 0.06 |
| 3N | 0.81 ± 0.01 | 0.807 | 0.807 | 0.10 ± 0.02 | 0.10 |
| 3B | 0.81 ± 0.01 | 0.804 | 0.804 | 0.10 ± 0.02 | 0.11 |
| 4 | 1.650 ± 0.010 | 1.657 | 1.656 | 0.10 ± 0.020 | 0.092 |
| 5 | 2.165 ± 0.007 | 2.169 | 2.167 | 0.04 ± 0.010 | 0.035 |
| 6 | 2.205 ± 0.007 | 2.209 | 2.209 | 0.04 ± 0.010 | 0.040 |
| 7 | 2.260 ± 0.007 | 2.263 | 2.262 | 0.05 ± 0.010 | 0.047 |
| 8 | 2.330 ± 0.010 | 2.334 | 2.336 | 0.07 ± 0.015 | 0.070 |
| 9 | 2.395 ± 0.010 | 2.400 | 2.400 | 0.07 ± 0.015 | 0.068 |
| 10 | 8.30 ± 0.08 | 8.274 | 8.291 | 0.35 ± 0.08 | 0.344 |
| 11 | 8.65 ± 0.08 | 8.626 | 8.634 | 0.35 ± 0.08 | 0.347 |
| 12 | 9.10 ± 0.08 | 9.072 | 9.075 | 0.35 ± 0.08 | 0.361 |
| 13 | 10.60 ± 0.10 | 10.654 | 10.657 | 0.70 ± 0.12 | 0.667 |
| 14 | 11.30 ± 0.10 | 11.303 | 11.318 | 0.70 ± 0.12 | 0.593 |

## 2.2.3. Radiometric Performance

The input energy is defined by the target radiance in front of each radiometer and called input radiance. The maximum, the high level and the low level radiances are specified as shown in Table 2-10. The specification on radiometric accuracy is applied to the high level radiance, unless otherwise specified.

Table 2-10  Input Radiance (W/m$^2$/sr/μm)

| Band No. | Maximum Input Radiance | High Level Input Radiance | Low Level Input Radinace |
|---|---|---|---|
| 1 | 427 | 356 | 71.2 |
| 2 | 358 | 298 | 59.6 |
| 3 | 218 | 182 | 36.4 |
| 4 | 55.0 | 45.8 | 9.16 |
| 5 | 17.6 | 14.7 | 2.94 |
| 6 | 15.8 | 13.2 | 2.64 |
| 7 | 15.1 | 12.6 | 2.52 |
| 8 | 10.55 | 8.79 | 1.76 |
| 9 | 8.04 | 6.70 | 1.34 |
| 10-14 | Radiance of 370 K Blackbody | Radiance of 300 K Blackbody | Radiance of 200 K Blackbody |

The radiometric resolution is defined by signal to noise ratio (S/N) for VNIR and SWIR bands and noise equivalent temperature difference (NEΔT) for TIR bands. The radiometric resolution of PFM at PQR stage is shown in Table 2-11 for the high and low level input radiances.

The instrument parameter for the radiometric resolution is signal-to-noise ratio (S/N) rather than NEΔρ required by the science mission team. Therefore, NEΔρ is translated into S/N by using the relation, S/N = (target reflectance)/NEΔρ. User's requirement is applied to the high level input radiance. Therefore, 70 % target reflectance which is employed to estimate the high level input radiance is used for the conversion between NEΔρ and S/N. For TIR bands, the radiometric resolution is specified directly by user required parameter NEΔT which is convenient for instrument performance test.

Table 2-11  S/N or NEΔT

| Band | For High Level Input Radiance | | For Low Leve Input Radiance | |
|---|---|---|---|---|
| | Specification | Measured Value (Max - Min) | Specification | Measured Value (Max - Min) |
| 1 | ≥ 140 | 370 - 278 | ≥ 40 | 170 - 78 |
| 2 | ≥ 140 | 306 - 256 | ≥ 40 | 122 - 74 |
| 3N | ≥ 140 | 202 - 173 | ≥ 40 | 70 - 58 |
| 3B | ≥ 140 | 183 - 150 | ≥ 40 | 72 - 56 |
| 4 | ≥ 140 | 466 - 292 | ≥ 35 | 368 - 63 |
| 5 | ≥ 54 | 254 - 163 | ≥ 13.5 | 77 - 45 |
| 6 | ≥ 54 | 229 - 150 | ≥ 13.5 | 73 - 36 |
| 7 | ≥ 54 | 234 - 151 | ≥ 13.5 | 72 - 35 |
| 8 | ≥ 70 | 258 - 165 | ≥ 17.5 | 81 - 34 |
| 9 | ≥ 54 | 231 - 156 | ≥ 13.5 | 73 - 44 |
| 10 | ≤ 0.3 K | 0.17 - 0.07 K | ≤ 2.5 K | 1.34 - 0.68 K |
| 11 | ≤ 0.3 K | 0.14 - 0.09 K | ≤ 2.5 K | 1.27 - 0.63 K |
| 12 | ≤ 0.3 K | 0.13 - 0.07 K | ≤ 2.5 K | 1.05 - 0.42 K |
| 13 | ≤ 0.3 K | 0.09 - 0.05 K | ≤ 1.5 K | 0.49 - 0.26 K |
| 14 | ≤ 0.3 K | 0.13 - 0.09 K | ≤ 1.5 K | 0.65 - 0.33 K |

The VNIR and SWIR bands have 3 and 4 gains, respecively, as shown in Table 2-12.  The gain setting for each band can be selected independently.

Table 2-12  Gain Switching Function

| Band No. | High Gain | Normal Gain | Low Gain - 1 | Low Gain - 2 |
|----------|-----------|-------------|--------------|--------------|
| 1 | 2.5 | 1.0 | 0.75 | N/A |
| 2 | 2.0 | 1.0 | 0.75 | N/A |
| 3 | 2.0 | 1.0 | 0.75 | N/A |
| 4 | 2.0 | 1.0 | 0.75 | 0.75(TBR) |
| 5 | 2.0 | 1.0 | 0.75 | 0.17(TBR) |
| 6 | 2.0 | 1.0 | 0.75 | 0.16(TBR) |
| 7 | 2.0 | 1.0 | 0.75 | 0.18(TBR) |
| 8 | 2.0 | 1.0 | 0.75 | 0.17(TBR) |
| 9 | 2.0 | 1.0 | 0.75 | 0.12(TBR) |
| 10 - 14 | N/A | N/A | N/A | N/A |

## 2.2.4.   Geometric   Performance

The instrument parameter on the spatial resolution in the cross-track direction is the instantaneous field of view described with angle (IFOV angle).  Therefore, the spatial resolution on the ground depends on the platform altitude.  Table 2-13 shows the IFOV angle which is specified so as to meet the spatial resolution described in Table 2-7 for the nadir direction from a spacecraft altitude of 705 km.  The instantaneous field of view in the cross-track direction is defined by pixel-to-pixel distance of linear array detector for VNIR and SWIR bands and data sampling distance for TIR bands.

Table 2-13  IFOV

| | |
|---|---|
| VNIR nadir bands (1 - 3) | 21.3 ± 0.6 μrad |
| VNIR stereo band (3B) | 18.6 ± 0.5 μrad |
| SWIR band (4 - 9) | 42.6 ± 1.2 μrad |
| TIR bands (10 - 14) | 127.8 ± 3.8 μrad |

The instrument parameter on the spatial resolution in the along-track direction is the scan period. Table 2-14 shows the scan period which is specified so as to meet the spatial resolution described in Table 2-7 when the spacecraft is crossing over the the equator with an altitude of 705 km.  The spatial resolution on the ground directly depends on the spacecraft velocity. Specified scan period corresponds to one line scan period for VNIR and SWIR bands and ten lines scan period for TIR bands.

Table 2-14  Scan Period

| | |
|---|---|
| VNIR  (1 - 3) | 2.199 ± 0.022 ms |
| SWIR band (4 - 9) | 4.398 ± 0.044 ms |
| TIR bands (10 - 14) | 131.94 ± 0.13 ms |

The band-to-band registration (BBR) requirements are ±0.2 pixels (3σ) in the same telescope and ±0.3 pixels of the coarser spatial resolution among different telescopes after necessary ground processing (Level-1 processing).

The VNIR and SWIR subsystems use electronically scanned linear detector arrays for each band to obtain one line data in the cross-track direction for each scan period.  In TIR subsystem ten detectors for each band are  arranged to obtain ten lines in the cross-track direction for each scan period.  The detector configuration accuracy is specified as shown in Table 2-15.  Only for TIR subsystem the deviation is defined as deviation from integer times of the nominal pixel size.

The bias is fixed deviation from the exact band-to-band registration and specified by considering the current state of the art. Except for TIR subsystem, the resampling is necessary for precise band-to-band registration even in the same telescope. The stability is specified so as to be kept within 0.2 pixels of each band during the life of instrument in order to assure a registration accuracy of 0.2 pixels in the same telescope by using only preflight parameters on the focal plane configuration. For VNIR subsystem the bias deviation in the along-track direction is specified severer than that in the cross-track direction to keep a registration accuracy of around 0.2 pixels without compensating the earth rotation.

Table 2-16 shows the jitter and stability requirements in the various time scales from 69.7 μsec to 480 sec. Table 2-17 shows the scientific meaning of these time scales. These are total jitter and stability requirements from instrument boresight to Spacecraft navigation base reference, including both of the instrument and spacecraft contributions. The spacecraft allocation is shown in Table 2-3.

The pointing function are specified by the Table 2-18. The specifications except for VNIR range are applied only for the range of ±8.55 degrees.

The repeatability and detection accuracy are important parameters for band-to-band registration among different telescopes and specified by considering the current state of the art. The repeatability and the accuracy specified correspond to 41 and 6.1 pixels of a VNIR resolution of 15 m, respectively. Therefore, new parameters for band-to-band registration among different telescopes must be searched by ground processing such as correlation when the pointing mode is changed, though the searching range can be reduced by the accuracy or the repeatability.

When the pointing is kept in the same mode, band-to-band registration accuracy among different telescope is decided by the stability. The stability from the interface is specified so as to be kept within 0.1 pixels of each band during 8 minutes .

There is no specification for boresight-to-boresight stability due to spacecraft deformation. However, the performance is under calculation using FEM of the engineering model. The real performance might have to wait until the initial checkout period.

Table 2-15  Accuracy of Detector Configuration

| Subsystem | Bias | | Stability |
|---|---|---|---|
| | Along-track | Cross-track | (3σ) |
| VNIR | ≤ 3 pixels | ≤ 6 pixels | ≤ ±0.2 pixels |
| SWIR | ≤ 420 pixels | ≤ 0.2 pixels | ≤ ±0.2 pixels |
| TIR | ≤ 0.05 pixels | ≤ 0.05 pixels | N/A |

Table 2-16 Jitter and Stability Requirements

(Unit; arcsec-$3\sigma$, Peak-to-Peak)

| Time Scale | VNIR | | | SWIR | | | TIR | | | Note |
|---|---|---|---|---|---|---|---|---|---|---|
| | Roll | Pitch | Yaw | Roll | Pitch | Yaw | Roll | Pitch | Yaw | |
| 69.7 μs | - | - | - | - | - | - | 9.0 | 9.0 | 23.4 | MTF |
| 2.2 ms | 1.5 | 1.5 | 3.9 | - | - | - | - | - | - | MTF |
| 4.4 ms | - | - | - | 3.0 | 3.0 | 7.8 | - | - | - | MTF |
| 6.6 ms | 1.7 | 1.7 | 4.5 | - | - | - | - | - | - | BBR |
| 15.8 ms | - | - | - | - | - | - | 10.5 | 10.5 | 27.3 | BBR |
| 1.0 s | - | - | - | 5.2 | 5.2 | 13.7 | 15.8 | 15.8 | 40.9 | ITR |
| 1.8 s | - | - | - | 3.5 | 3.5 | 9.1 | - | - | - | BBR |
| 9 s | 18 | 12 | 60 | - | - | - | - | - | - | DEM |
| 480 s | 26.4 | 26.4 | 68.6 | - | - | - | - | - | - | Geolocation |

Note 1) MTF; Modulation Transfer Function
Note 2) BBR; Band-to-Band Registration
Note 3) ITR; Inter-Telescope Registration
Note 4) DEM; Digital Elevation Model

Table 2-17 Scientific Meaning of Time Scale for Jitter Stability Requirements

| Time Scale | Required from | Scientific Requirements | Note |
|---|---|---|---|
| 69.7 μs | TIR | 5% MTF degradation (Roll/Pitch)<br>1.25% MTF degradation (Yaw) | Time to image 1 pixel |
| 2.2 ms | VNIR | 5% MTF degradation (Roll/Pitch)<br>1.25% MTF degradation (Yaw) | Time to image 1 pixel |
| 4.4 ms | SWIR | 5% MTF degradation (Roll/Pitch)<br>1.25% MTF degradation (Yaw) | Time to image 1 pixel |
| 6.6 ms | VNIR | Within ±0.2 pixels from BBR (Roll/Pitch)<br>Within ±0.1 pixels from BBR (Yaw) | Time to image all VNIR bands |
| 15.8 ms | TIR | Within ±0.2 pixels from BBR (Roll/Pitch)<br>Within ±0.1 pixels from BBR (Yaw) | Time to image all TIR bands |
| 1.0 s | VNIR SWIR TIR | Within ± 0.3 pixels from ITR (Roll/Pitch)<br>Within ± 0.15 pixels from ITR (Yaw) | Registration between VNIR/SWIR and SWIR/TIR |
| 1.8 s | SWIR | Within ±0.2 pixels from BBR (Roll/Pitch)<br>Within ±0.1 pixels from BBR (Yaw) | Time to image all SWIR bands |
| 9 s | VNIR | Identify the elevation difference of ± 25 m (DEM accuracy) | Data acquisition time for 1 scene |
| 480 s | VNIR | Within ±3 pixels from geolocation (Roll/Pitch)<br>Within ±1.5 pixels from geolocation (Yaw) | Maximum data acquisition time for 1 orbit |

Table 2-18 Pointing Functions

| Items | | VNIR | SWIR | TIR |
|---|---|---|---|---|
| Range | | ≥ ±24˚ | ≥ ±8.55˚ | |
| Accuracy of pointing axis | | ≤ ±360 arcsec from X axis | | |
| Setting resolution | | ≤ ±45 arcsec | | |
| Repeatability (3σ) | | ≤ ±180 arcsec | | |
| Detecting resolution | | ≤ ±20 arcsec | | |
| Detection accuracy (3σ) | | ≤ ±27 arcsec | | |
| Variable frequency | | ≥ 20,000 | | ≥200,000 |
| Pointing time | | ≤ 60 sec | | |
| Stability | Roll | ≤ ±0.44 arcsec | ≤ ±0.88 arcsec | ≤ ±2.6 arcsec |
| (3σ values in | Pitch | ≤ ±0.44 arcsec | ≤ ±0.88 arcsec | ≤ ±2.6 arcsec |
| 8 minutes) | Yaw | ≤ ±2.2 arcsec | ≤ ±4.5 arcsec | ≤ ±13.4 arcsec |

Tables 2-19, 2-20, and 2-21 show the pointing performance of VNIR, SWIR, and TIR, respectively. The design values are those for the Proto Flight Model provided at PQR. For the dynamic error, only roll component of the knowledge is better than the accuracy, because an encoder is used for the cross-track pointing angle detection of each subsystem.

Table 2-19 Pointing Performance of VNIR

| | Specification | Design Values | | | | | |
|---|---|---|---|---|---|---|---|
| | | Dynamic Error | | | Static Error | | |
| | | Roll | Pitch | Yaw | Roll | Pitch | Yaw |
| Pointing knowledge (arcsec, 3σ) | ±60 (Each Axis) | ±14 | ±11 | ±11 | ±30 | ±29 | ±29 |
| Pointing accuracy (arcsec, 3σ) | ±225 (Each Axis) | ±26 | ±25 | ±11 | ±113 | ±75 | ±71 |

Table 2-20 Pointing Performance of SWIR

| | Specification | Design Values | | | | | |
|---|---|---|---|---|---|---|---|
| | | Dynamic Error | | | Static Error | | |
| | | Roll | Pitch | Yaw | Roll | Pitch | Yaw |
| Pointing knowledge (arcsec, 3σ) | Roll ±60 Pitch ±60 Yaw ±348 | ±28 | ±21 | ±12 | ±32 | ±34 | ±333 |
| Pointing accuracy (arcsec, 3σ) | Roll ±225 Pitch ±225 Yaw ±520 | ±111 | ±21 | ±12 | ±48 | ±36 | ±335 |

Table 2-21  Pointing Performance of TIR

| | Specification | Design Values | | | | | |
| | | Dynamic Error | | | Static Error | | |
| | | Roll | Pitch | Yaw | Roll | Pitch | Yaw |
|---|---|---|---|---|---|---|---|
| Pointing knowledge (arcsec, 3σ) | Roll ±60 Pitch ±60 Yaw ±348 | ±11 | ±15 | ±11 | ±49 | ±41 | ±40 |
| Pointing accuracy (arcsec, 3σ) | Roll ±225 Pitch ±225 Yaw ±520 | ±28 | ±23 | ±22 | ±132 | ±262 | ±315 |

Table 2-22 shows the relative pointing knowledge among different telescopes which is important for the inter-telescope registration.  The distance errors on the earth surface are calculated by using a spacecraft altitude of 705 km for the roll and the pitch directions and a maximum instrument off-nadir distance of 136 km for yaw direction.  After removal of the static error during the initial checkout period, only the dynamic component will be the system correction accuracy for the inter-telescope registration.

Table 2-22  Relative Pointing Knowledge among Different Telescopes

| | Unit | Design Values | | | | | |
| | | Dynamic Error | | | Static Error | | |
| | | Roll | Pitch | Yaw | Roll | Pitch | Yaw |
|---|---|---|---|---|---|---|---|
| VNIR - SWIR | arcsec, 3σ | ±31 | ±24 | ±16 | ±44 | ±45 | ±334 |
| | m, 3σ | ±106 | ±82 | ±11 | ±150 | ±154 | ±220 |
| VNIR - TIR | arcsec, 3σ | ±17 | ±19 | ±17 | ±57 | ±50 | ±49 |
| | m, 3σ | ±58 | ±65 | ±11 | ±194 | ±170 | ±32 |
| SWIR - TIR | arcsec, 3σ | ±30 | ±26 | ±16 | ±56 | ±53 | ±335 |
| | m, 3σ | ±102 | ±89 | ±11 | ±190 | ±181 | ±221 |

Table 23 shows the pointing stability performance of each subsystem for 480 seconds time span at PQR.  The instrument boresight stability is specified so as to be kept within ±0.1 pixels for each band during 8 minutes (0.2 pixels for peak-to-peak) as shown in Table 2-18.  The sources of the stability are a thermal distortion and a jitter.  For SWIR and TIR major stability disturbance is caused by the high frequency jitter due to self cryocooler.

Table 2-23  Pointing Stability Performance of Each Subsystem for 480 seconds Time Span

(Unit: arcsec, 3σ, peak-to-peak)

| Subsystem | Specification | | | Design Values | | |
| | Roll | Pitch | Yaw | Roll | Pitch | Yaw |
|---|---|---|---|---|---|---|
| VNIR | 0.88 | 0.88 | 4.4 | 0.1 | 0.12 | 0.01 |
| SWIR | 1.76 | 1.76 | 9.0 | 1.6 | 2.0 | 7.4 |
| TIR | 5.2 | 5.2 | 26.8 | 1 | 0.2 | 0.2 |

Table 24 shows the pixel geolocation knowledge at PQR considering both the spacecraft and the instrument contributions. Total ASTER pixel geolocation knowledge is decided by the spacecraft position knowledge, the spacecraft pointing knowledge and ASTER pointing knowledge. Only the pixel geolocation knowledge of VNIR is considered, since the SWIR and TIR bands will be coregistered to VNIR band 2 as a reference band in the Level-1 processing.

Only dynamic component is important, since the static component can be removed during the initial checkout period.

Table 2-24  Pixel Geolocation Knowledge

|  |  | Specification | Dynamic Error (3$\sigma$) | Static Error (3$\sigma$) |
|---|---|---|---|---|
| Along-track(m) | Spacecraft[1] | ±342 | ±28 | ±111 |
|  | ASTER/VNIR | ±205 | ±38 | ±99 |
|  | Total | ±431[2] | ±47 | ±149 |
| Cross-track (m) | Spacecraft[1] | ±342 | ±25 | ±148 |
|  | ASTER/VNIR | ±205 | ±48 | ±103 |
|  | Total | ±437[2] | ±54 | ±180 |

[1]: Three non-optimal 9 minute TDRS contacts per orbit, GJM2 Geopotential ( 30 x 30), solar flux of 175, 5 % Cd error, TDRS ephemeris error of 75 meters. Two star trackers, rigid body/low frequency pointing knowledge error removed
[2]: Slightly larger than RSS of two values (Spacecraft and ASTER instrument), because of unallocated margin.

## 2.2.5. Sensor Geometric Model and Data Base

Figure 2-1 shows the sensor geometric model which includes detector configurations of each focal plane expressed by the foot print on the ground in relation to the spacecraft flight direction and the boresight of each telescope. The sizes on the focal planes are shown with the configuration, because the sizes on the ground depend on the spacecraft altitude. These sizes are designed so as to meet the base line requirement for the spatial resolution within the fabrication accuracy of the focal length when the spacecraft altitude is 705 km.

For VNIR and SWIR subsystems, one line image data of all bands in the cross-track direction are acquired simultaneously because of data sampling function of CCD detector arrays. For TIR subsystem, they are acquired time-sequentially in accordance to the scanning speed of the mirror because of the whiskbroom scanning method. A tilt angle of 0.3 degree is set for the compensation of the spacecraft movement during the scan period so as to align the swath line at the right angle to the spacecraft flight direction. All scan direction in the cross-track direction is designed to be at the right angle to the spacecraft flight direction.

The number of the detector for each band is as follows.

| | |
|---|---|
| VNIR bands 1, 2, 3N: | 4100 pixels |
| VNIR band 3B: | 5000 pixels |
| SWIR all bands: | 2048 pixels |
| TIR all bands: | 10 pixels |

The VNIR band 3B has extra detectors of 900 compared to other VNIR bands. The extra detectors are necessary to compensate the earth rotation. Only 4100 pixel data among 5000 will be sent to the ground. The selection of 4100 pixels will be automatically carried out by referring the spacecraft position data in the ancillary data and refreshed every 1.024 seconds.

Figure 2-2 shows the sensor geometric data base which consists of the following two kinds of parameters.

(1) A set of the line of sight (LOS) vectors for the nadir cross-track pointing position toward NBR.

(2) The pointing drive axis vector toward the NBR.

The line of sight vectors are defined toward the Navigation Base Reference (Spacecraft Reference Axes). The spacecraft's attitude control system attempts to align the Navigation Reference Axes with the Orbital Reference Coordinate Frame. The error between two axes will be provided as the attitude information in the spacecraft ancillary data. Therefore, the pointing direction of each detector can be expressed toward the Orbital Reference Coordinate Frame by using the geometric data base and the pointing information of the spacecraft provided as the ancillary data.

At first stage the geometric data base shall be preliminarily prepared based on the preflight measurement. Then it shall be evaluated using acquired image data during the in-flight initial checkout period and tuned up for the operational use. The geometric data base may be updated based on the quality evaluation of the acquired image data during the life of the mission. The detail plan is descrbed in Chapter 4.
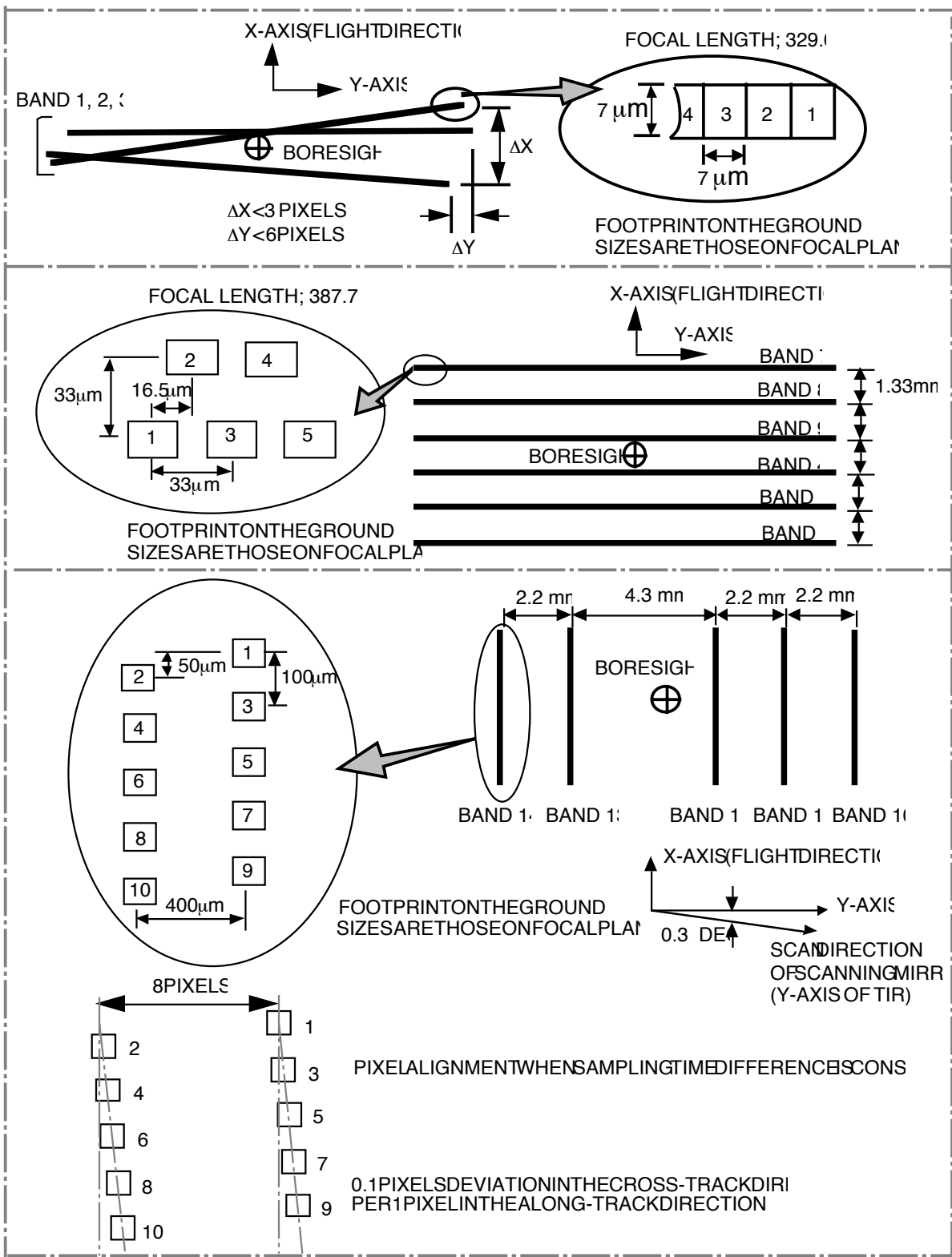
Figure 2-1  Sensor Geometric Model

VNIRGEOMETRICCORRECTIONDATABASE

LINEOFSIGHTVECTORSOFEACHDETECT
ATNADIRPOINTINGPOSITION

V/G-DE

4100 X 3 + 5000 X 1 DETEC
3 DATA/DETECTOR
4 BYTES/DATA

POINTINGDRIVEAXISVECT

3 DATA
4 BYTES/DAT

SWIRGEOMETRICCORRECTIONDATABASE

LINEOFSIGHTVECTORSOFEACHDETECT
ATNADIRPOINTINGPOSITION

S/G-DE

2048 X 6  DETECT
3DATA/DETECTOR
4 BYTES/DATA

POINTINGDRIVEAXISVECT

3 DATA
4 BYTES/DAT

TIRGEOMETRICCORRECTIONDATABASE

LINEOFSIGHTVECTORSOFEACHDETEC
ATNADIRPOINTINGPOSITION

T/G-DE

10 X 5 DETECTO
3DATA/DETECTO
4 BYTES/DATA

POINTINGDRIVEAXISVECT

3 DATA
4 BYTES/DAT

Figure 2-2  Sensor Geometric Correction Data Base

## 2.2.6. Sensor Radiometric Model and Data Base

Figure 2-3 shows the radiometric model of the ASTER instrument. Reflected or emitted radiation from the Earth goes through the optics, reaches the detectors and is converted into electric current. For VNIR and SWIR the current is integrated in detector itself during sampling period to convert to the electric charge. The current or the electric charge is then converted into t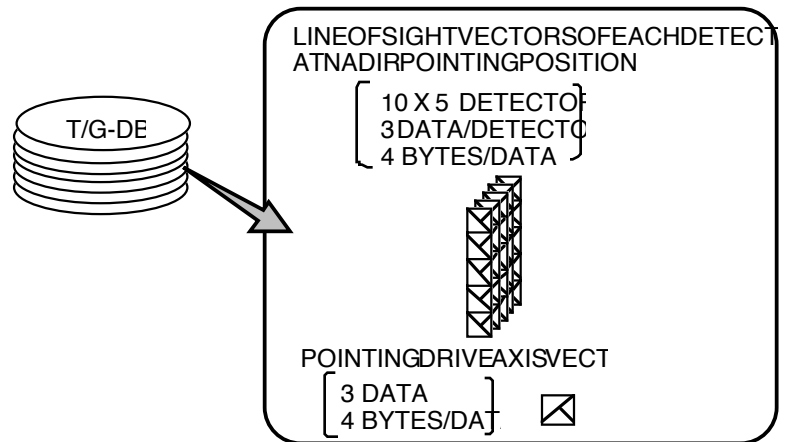he voltage, followed by amplification with variable gain and then digitization by AD converters. For TIR a large offset voltage from the photo-conductive type detector is eliminated prior to the amplification.

As for VNIR and SWIR, since the linearity of CCD detectors are basically excellent, the relation between input radiance L and output signal $V$ can be expressed by following equation.

$$V = A_L L + D_L$$

or $$L = A_V V + D_V$$

Here $A_V$ and $D_V$ are the radiometric correction coefficients (RCCs) which are used to calculate the input radiance from the instrument output. $D_L$ is the offset signal without radiation and $A_L$ is the gain. The total system can basically be considered to be linear with a excellent accuracy.

The sensitivities are defined for each detector under the normal gain setting. For other than the normal gain setting the sensitivities are modified by multiplying the gain factors. The offsets are defined for each detector and each gain setting.

Both the offset and the sensitivity coefficients slightly depend on the detector temperature for VNIR, and the detector temperature and the dewar temperature for SWIR. These dependences are evaluated during the preflight test period and accomodated in the radiometric data bases as the predetermined parameters.

For TIR, mercury cadmium telluride detectors are used in photo-conductive mode, so the detectors generally have the nonlinearity. But as the input radiance level is small, the nonlinearity is anticipated to be small. The relation between input radiance and output signal can be expressed as follows.

$$L = C_0 + C_1 V + C_2 V^2$$

where $C_0$ is the offset, and $C_1$ and $C_2$ are gain coefficients of first and second powers for output vs. radiance curve, respectively. TIR will receive the background radiation inside the TIR optics and the structure. This effect will be evaluated before launch by changing the temperature distribution inside the TIR and accommodated in the radiometric data base as the temperature depencence coefficients as the predetermined parameters

The contents of the radiometric correction data base files for VNIR, SWIR and TIR bands are shown in Figure 2-4. The radiometric correction data base will be prepared from the prelaunch data, the inflight on-board calibration data and the vicarious calibration data. All information which is necessary for the radiometric coefficients generation during Level-1A processing must be included in the radiometric data base

More details will be described in Chapter 5 for the radiometric data base preparation and in Section 3.4 for the radiometric coefficients generation by using the data base.
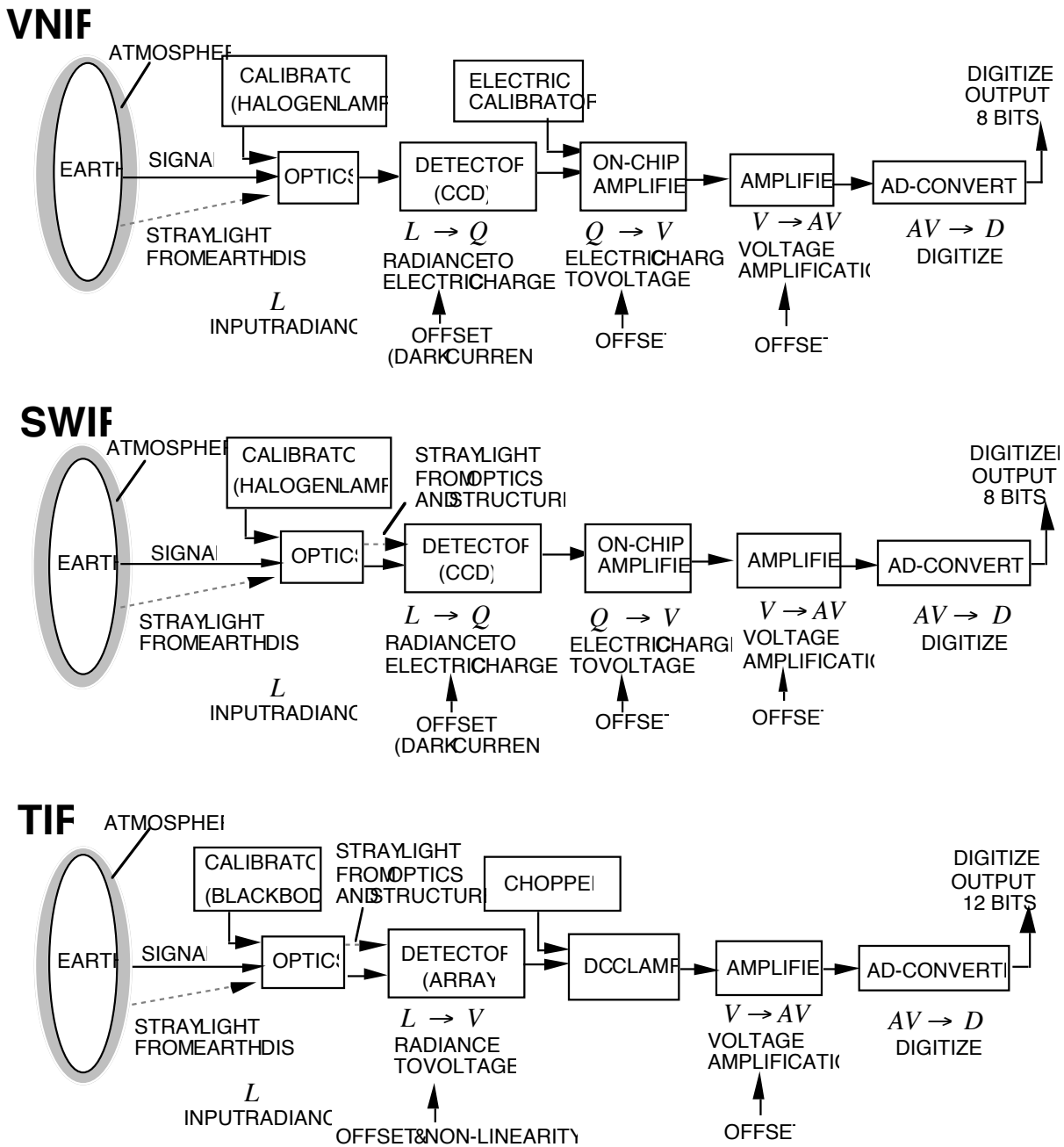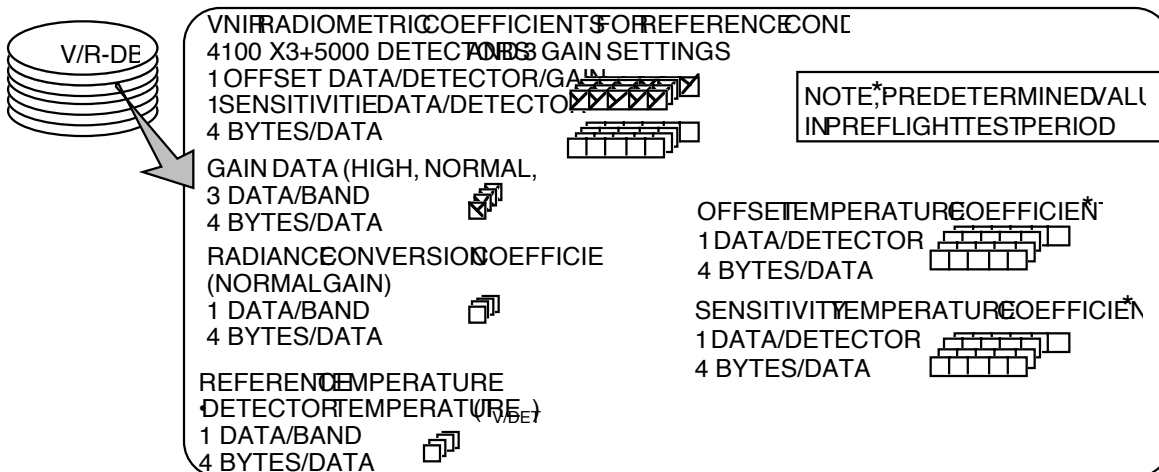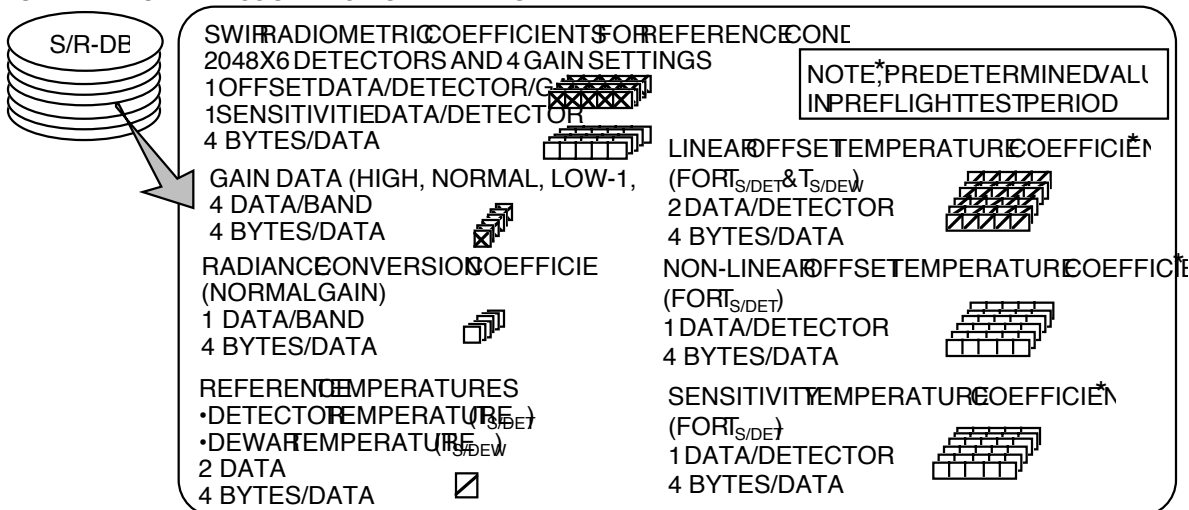
## VNIF



## SWIF



## TIF



Figure 2-3  Sensor Radiometric Model

VNIR RADIOMETRIC CORRECTION DATABASE

V/R-DB

VNIR RADIOMETRIC COEFFICIENTS FOR REFERENCE CONDITION
4100 X3+5000 DETECTORS AND 3 GAIN SETTINGS
1 OFFSET DATA/DETECTOR/GAIN
1 SENSITIVITIES DATA/DETECTOR
4 BYTES/DATA

NOTE*; PREDETERMINED VALUE
IN PREFLIGHT TEST PERIOD

GAIN DATA (HIGH, NORMAL,
3 DATA/BAND
4 BYTES/DATA

RADIANCE CONVERSION COEFFICIENT
(NORMAL GAIN)
1 DATA/BAND
4 BYTES/DATA

OFFSET TEMPERATURE COEFFICIENT*
1 DATA/DETECTOR
4 BYTES/DATA

SENSITIVITY TEMPERATURE COEFFICIENT*
1 DATA/DETECTOR
4 BYTES/DATA

REFERENCE TEMPERATURE
•DETECTOR TEMPERATURE ($T_{V/DET}$)
1 DATA/BAND
4 BYTES/DATA

SWIR RADIOMETRIC CORRECTION DATABASE

S/R-DB

SWIR RADIOMETRIC COEFFICIENTS FOR REFERENCE CONDITION
2048X6 DETECTORS AND 4 GAIN SETTINGS
1 OFFSET DATA/DETECTOR/GAIN
1 SENSITIVITIES DATA/DETECTOR
4 BYTES/DATA

NOTE*; PREDETERMINED VALUE
IN PREFLIGHT TEST PERIOD

GAIN DATA (HIGH, NORMAL, LOW-1,
4 DATA/BAND
4 BYTES/DATA

RADIANCE CONVERSION COEFFICIENT
(NORMAL GAIN)
1 DATA/BAND
4 BYTES/DATA

LINEAR OFFSET TEMPERATURE COEFFICIENT*
(FOR $T_{S/DET}$ & $T_{S/DEW}$)
2 DATA/DETECTOR
4 BYTES/DATA

NON-LINEAR OFFSET TEMPERATURE COEFFICIENT*
(FOR $T_{S/DET}$)
1 DATA/DETECTOR
4 BYTES/DATA

REFERENCE TEMPERATURES
•DETECTOR TEMPERATURE ($T_{S/DET}$)
•DEWAR TEMPERATURE ($T_{S/DEW}$)
2 DATA
4 BYTES/DATA

SENSITIVITY TEMPERATURE COEFFICIENT*
(FOR $T_{S/DET}$)
1 DATA/DETECTOR
4 BYTES/DATA

TIR RADIOMETRIC CORRECTION DATABASE

TIR/DB

TIR RADIOMETRIC COEFFICIENT
10X5 DETECTORS
1 OFFSET DATA/DETECTOR
2 SENSITIVITIES DATA/DETECT
4 BYTES/DATA

NOTE*; PREDETERMINED VALUE
IN PREFLIGHT TEST PERIOD

OFFSET TEMPERATURE COEFFICIENT*
($T_{T/CHP}$, $T_{T/TEL}$ AND $T_{T/LNS}$)
3 DATA/BAND
4 BYTES/DATA

REFERENCE TEMPERATURES
•DETECTOR TEMPERATURE ($T_{T/DET}$)
•CHOPPER TEMPERATURE ($T_{T/CHP}$)
•TELESCOPE TEMPERATURE ($T_{T/TEL}$)
•LENS TEMPERATURE ($T_{T/LNS}$)
4 DATA, 4 BYTES/DATA

LINEAR SENSITIVITY TEMPERATURE COEFFICIENT*
(FOR $T_{T/DET}$)
1 DATA/BAND
4 BYTES/DATA

RADIANCE CONVERSION COEFFICIENT
1 DATA/BAND
4 BYTES/DATA

NON-LINEAR SENSITIVITY TEMPERATURE COEFFICIENT*
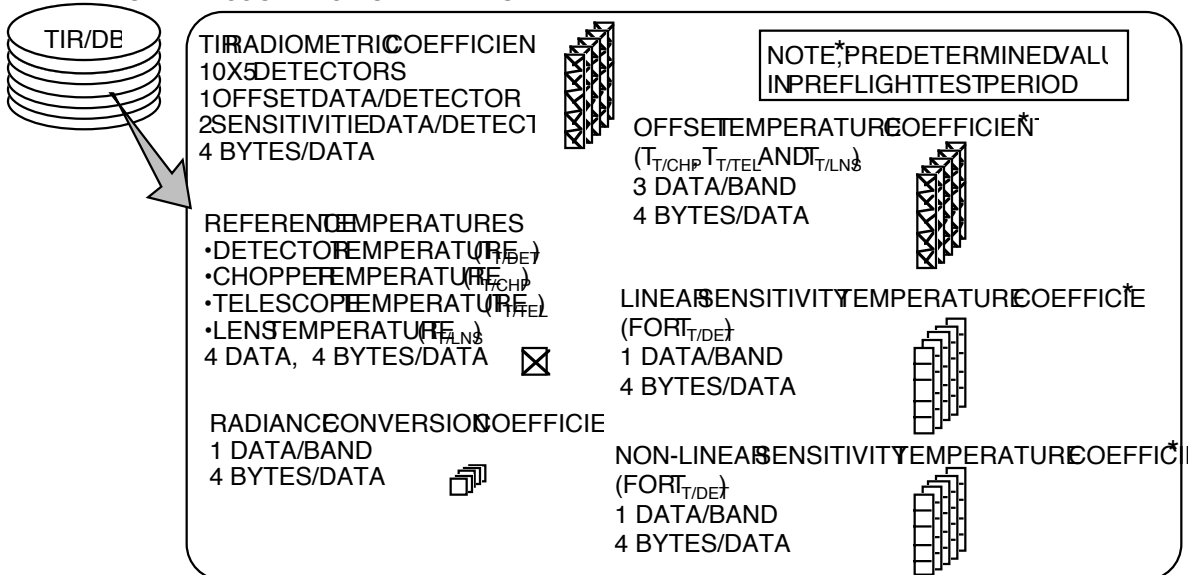(FOR $T_{T/DET}$)
1 DATA/BAND
4 BYTES/DATA

Figure 2-4   Sensor Radiometric Correction Data Base

## 2.2.7. Supplement Data

ASTER Level-0 data include supplement data of each subsystem which contain various engineering information such as temperatures and pointing angles. Tables 25, 26 and 27 list the supplement data of VNIR, SWIR and TIR subsystems, respectively.

Table 2-25  VNIR Supplement Data

| No. | Byte | Content |
|-----|------|---------|
| 1 | 1 | Band 1 detector temperature |
| 2 | 1 | Band 2 detector temperature |
| 3 | 1 | Band 3N detector temperature |
| 4 | 1 | Band 3B detector temperature |
| 5 | 1 | Calibration lamp A temperature |
| 6 | 1 | Calibration lamp B temperature |
| 7 | 1 | Monitor amp. temperature |
| 8 | 1 | Photodiode 1 temperature |
| 9 | 1 | Photodiode 2A temperature |
| 10 | 1 | Photodiode 2B temperature |
| 11 | 1 | VSP 1 temperature |
| 12 | 1 | VSP 2 temperature |
| 13 | 1 | VEL base plate temperature |
| 14 | 1 | Nadir telescope temperature 1 |
| 15 | 1 | Nadir telescope temperature 2 |
| 16 | 1 | Nadir telescope temperature 3 |
| 17 | 1 | Backward telescope temperature 1 |
| 18 | 1 | Backward telescope temperature 2 |
| 19 | 1 | Backward telescope temperature 3 |
| 20 | 1 | VPS lamp power supply Voltage |
| 21 | 1 | Photodiode 1A output |
| 22 | 1 | Photodiode 1B output |
| 23 | 1 | Photodiode 2A output |
| 24 | 1 | Photodiode 2B output |
| 25 | 1 | Electric calibration Voltage.1 |
| 26 | 1 | Electric calibration Voltage.2 |
| 27 | 1 | Electric calibration Voltage.3 |
| 28 | 1 | Electric calibration Voltage.4 |
| 29 | 1 | VSP1 APS Vol +10V |
| 30 | 1 | VSP1 APS Vol -10V |
| 31 | 1 | Pointing angle 1 |
| 32 | 1 | Pointing angle 2 |
| 33 | 1 | Initial extract address 1 |
| 34 | 1 | Initial extract address 2 |
| 35 | 1 | Spare |
| 36 | 1 | Spare |

Table 2-25  VNIR Supplement Data (continued)

| No. | Byte | Content |
|---|---|---|
| 37 | 1 | Band 1 normal/high gain selection |
| | | Band 1 normal/low gain selection |
| | | Band 2 normal/high gain selection |
| | | Band 2 normal/low gain selection |
| | | Band 3 normal/high gain selection |
| | | Band 3 normal/low gain selection |
| | | Band 3 A/B selection |
| | | OPE. optical/electric calibration selection |
| 38 | 1 | Calibration lamp A/B selection |
| | | PS1 on/off |
| | | PS3 on/off |
| | | Table cancel on/off |
| | | PS4 on/off |
| | | Spare |
| | | Spare |
| | | Spare |
| 39-50 | 12 | Spare |

Table 2-26  SWIR Supplement Data

| No. | Byte | Output Frequency /Frame | Content |
|---|---|---|---|
| 1 | 1 | 1 | Optics monitor voltage A |
| 2 | 1 | 1 | Optics monitor voltage B |
| 3 | 1 | 1 | Cooler current 1 |
| 4 | 1 | 1 | Cooler current 2 |
| 5 | 1 | 1 | Cooler current 3 |
| 6 | 1 | 1 | Cooler current 4 |
| 7 | 1 | 1 | Detector temperature (Narrow) |
| 8 | 1 | 1 | TLM/CMD circuit reference voltage 1 |
| 9 | 1 | 1 | TLM/CMD circuit reference voltage 2 |
| 10 | 1 | 1 | TLM/CMD circuit reference voltage 3 |
| 11 | 1 | 1/4 | A/D reference voltage (Band 4) |
| 12 | 1 | 1/4 | A/D reference voltage (Band 5) |
| 13 | 1 | 1/4 | A/D reference voltage (Band 6) |
| 14 | 1 | 1/4 | A/D reference voltage (Band 7) |
| 15 | 1 | 1/4 | A/D reference voltage (Band 8) |
| 16 | 1 | 1/4 | A/D reference voltage (Band 9) |
| 17 | 1 | 1/4 | Calibration lamp voltage A |
| 18 | 1 | 1/4 | Calibration lamp voltage B |
| 19 | 1 | 1/4 | Detector temperature (Wide) |
| 20 | 1 | 1/4 | Motor amplitude |
| 21 | 1 | 1/4 | Detector dewar temperature |
| 22 | 1 | 1/4 | Radiator temperature (Inner ring) |
| 23 | 1 | 1/4 | Radiator temperature A |

Table 2-26 SWIR Supplement Data (continued)

| No. | Byte | Output Frequency/ Frame | Content |
|---|---|---|---|
| 24 | 1 | 1/4 | Structure cover temperature 2A (-x) |
| 25 | 1 | 1/4 | Structure cover temperature 1A (+x) |
| 26 | 1 | 1/4 | Structure cover temperature 3A (+z) |
| 27 | 1 | 1/4 | Barrel structure temperature |
| 28 | 1 | 1/4 | Kinematic mount temperature |
| 29 | 1 | 1/4 | Electrical circuit 1 temperature |
| 30 | 1 | 1/4 | Electrical circuit 2 temperature |
| 31 | 1 | 1/4 | Pointing mechanism temperature 1 (Motor) |
| 32 | 1 | 1/4 | Calibration lamp temperature |
| 33 | 1 | 1/4 | Collector module temperature 1 |
| 34 | 1 | 1/4 | Collector module temperature 2 |
| 35 | 1 | 1/4 | Detector preamp/dewar temperature A |
| 36 | 1 | 1/4 | Pointing mechanism temperature 2 (Bearing) |
| 37 | 1 | 1/4 | Cooler temperature 1 A (Compressor) |
| 38 | 1 | 1/4 | Cooler temperature 2 A (Cold finger) |
| 39 | 1 | 1/4 | Electric circuit 1 temperature 1 (Driver) |
| 40 | 1 | 1/4 | Electric circuit 1 temperature 2 (Processor amp) |
| 41 | 1 | 1/4 | Electric circuit 1 temperature 3 A (TLM/CMD cir) |
| 42 | 1 | 1/4 | Electric circuit 1 temperature 4 (Cal. cir) |
| 43 | 1 | 1/4 | Optics monitor temperature A |
| 44 | 1 | 1/4 | Optics monitor temperature B |
| 45-47 | 2 + 1/8 | 1 | Pointing mirror encoder |
| 48 | 1 | 1 | Drive pulse width |
| 49-50 | 2 | 1/4 | Drive pulse number |
| 51 | 2/8 | 1/4 | Band 4 gain status |
| 52 | 2/8 | 1/4 | Band 5 gain status |
| 53 | 2/8 | 1/4 | Band 6 gain status |
| 54 | 2/8 | 1/4 | Band 7 gain status |
| 55 | 2/8 | 1/4 | Band 8 gain status |
| 56 | 2/8 | 1/4 | Band 9 gain status |
| 57 | 1/8 | 1/4 | Digital signal processor circuit power on/off |
| 58 | 1/8 | 1/4 | TLM/CMD power on/off |
| 59 | 1/8 | 1/4 | Analog circuit power on/off |
| 60 | 1/8 | 1/4 | Pointing control circuit power on/off |
| 61 | 1/8 | 1/4 | Calibration lamp power on/off |
| 62 | 1/8 | 1/4 | Calibration lamp A/B selection |
| 63 | 1/8 | 1/4 | Thermal control circuit on/off |
| 64 | 1/8 | 1/4 | Heater 3 on/off |
| 65 | 1/8 | 1/4 | Heater 4 on/off |
| 66 | 1/8 | 1/4 | Heater 5 on/off |
| 67 | 2/8 | 1/4 | CLR motor amplitude status |
| 68 | 2/8 | 1/4 | Detector temperature set status |
| 69 | 2/8 | 1 | Pointing motor excitation status 1 |
| 70 | 2/8 | 1/4 | Pointing motor excitation status 2 |
| 71 | 1/8 | 1/4 | Parity flag status |

Table 2-26  SWIR Supplement Data (continued)

| No. | Byte | Output Frequency/ Frame | Content |
|---|---|---|---|
| 72 | 5/8 | 1/4 | Error CMD distinctive status |
| 73 | 1/8 | 1 | Mirror position limit status |
| 74 | 1/8 | 1 | Limit ENA/DISA |
| 75 | 1/8 | 1 | Pointing motor ENA/DISA |
| 76 | 1/8 | 1 | Encoder on/off |
| 77 | 1/8 | 1 | Motor rotation CW/CCW |

Table 2-27  TIR Supplement Data

| No. | Byte | Content |
|---|---|---|
| 1 | 8000 | Chopper data |
| 2 | 4 | Detector temperatures |
| 3 | 4 | Black body temperature 1 |
| 4 | 4 | Black body temperature 2 |
| 5 | 4 | Black body temperature 3 |
| 6 | 4 | Black body temperature 4 |
| 7 | 4 | Black body temperature 5 |
| 8 | 4 | Chopper temperature 1 |
| 9 | 4 | Chopper temperature 2 |
| 10 | 4 | Chopper temperature 3 |
| 11 | 4 | Telescope temperature |
| 12 | 4 | Lens temperature |
| 13 | 1870 | Scanning angle |

# 3. ALGORITHM DESCRIPTION

## 3.1. Overview of End-to-End Processing Flow

Figure 3-1 shows the Level-1 data processing end-to-end flow. The Level-0 data which are sent from EDOS are packetized in the CCSDS format. These packets shall be classified into four groups of data according to APID (Application Process Identification) in the primary header of each packet. The group 1 data contain the data for VNIR bands 1 and 2. The group 2 data contain the data for VNIR bands 3N and 3B. The group 3 data contain the data for all SWIR bands. The group 4 data contain the data for all TIR bands. Each group data include science image data, instrument supplement data and spcecraft ancillary data. The groups 1 and 2 contain the common supplement data. All groups contain common ancillary data.

The packets of each group shall be depacketized and aligned to recover the unpacketized instrument source data by using sequential counter and flags in the primary header, and time tag in the secondary header of the packet. In the instrument source data the spectral band information are multiplexed with the BIP (Band Interleaved by Pixel) format.

Then the instrument source data shall be demultiplexed to separate image data every spectral band with BSQ (Band Sequential) format. For SWIR and TIR image data the Level-0 pixel addresses shall be realigned the order to correct stagger alignment among pixels in a same swath line as shown in Figure 2-1. This realignment process is carried out not only to have the more exactly aligned image data without resampling for image matching process but also to simplify subsequent processes.

Here, we have the data rearranged in three groups, that is, the VNIR data group, the SWIR data group and the TIR data group. The each group data consists of the image data of each spectral band, the common supplement data for the group and the common ancillary data for all group. Only for TIR data group the short term calibration data which will be obtained at the biginning and the end of each observation is included. The supplement data are necessary for all of the group data to make it possible to process independently. In this stage the image data will not be divided into scenes but kept in each continuous observation unit, that is, a long strip image data unit for more flexible scene selection. This data set is defined as Level-0A data which is a tentative product being effective only during processing. The processing between Level-0 and Level-0A is named the front-end processing as a whole.

The geometric system correction, which mainly consists of the coordinate transformation of the line of sight vector by using the ancillary information from the spacecraft and the supplement information from the instrument, shall be carried out to identify the observing point in the latitude/longitude coordinate on the earth surface defined by the earth model.

Strip unit or scene specific radiometric coefficients shall be generated from radiometric coefficients in the radiometric data base, which are the coefficients under reference temperature conditions such as the detector temperature, by using real temperature values in the instrument supplement data.

The Level-0B data, which is also a tentative product being effective only during processing, consist of the Level-0A data, the geometric system correction data and the radiometric correction data. The Level-0B data products are used for the image matching and the cloud coveragecalculation.
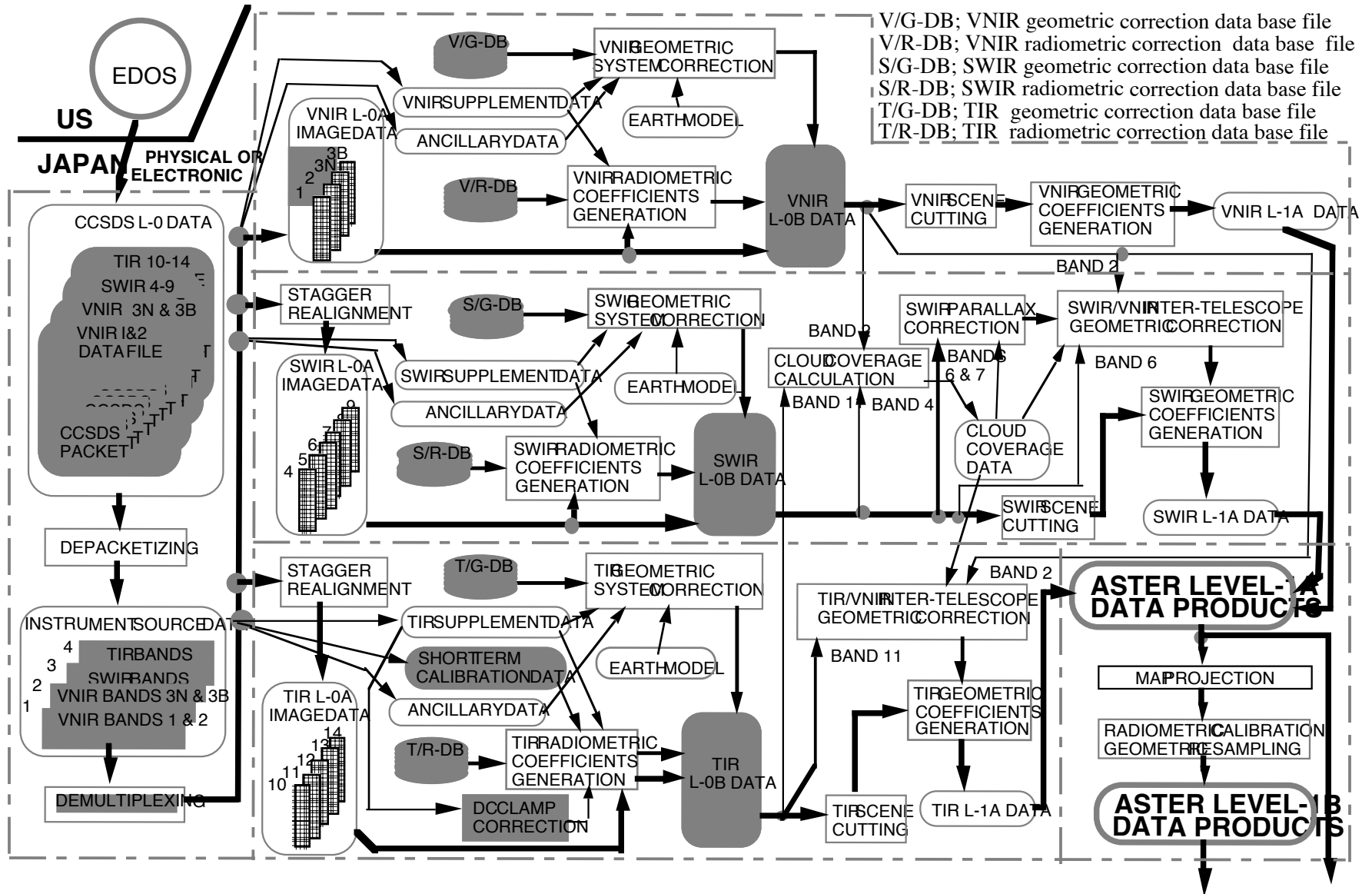
Figure 3-1   Level-1 Data Processing End-to-End Flow

V/G-DB; VNIR geometric correction data base file
V/R-DB; VNIR radiometric correction  data base  file
S/G-DB; SWIR geometric correction data base file
S/R-DB; SWIR radiometric correction data base file
T/G-DB; TIR  geometric correction data base file
T/R-DB; TIR  radiometric correction data base file

For SWIR bands the parallax error correction are carried out with the image matching techniques or the coarse DEM data base depending on cloud coverage by using Level-0B data. The parallax error is caused by the offset in detector alignment in the along-track direction and depends on the distance between the spacecraft and the observing earth surface. A distance evaluation error of 1750 m gives rise to 1 pixel registration error (that is, ± 1 pixel for 3500 m) for the worst combination between bands 6 and 7 with the maximum offset. Therefore, this correction will be at most ± 1 pixel except for extremely high elevation larger than 3500 m.

For SWIR and TIR bands the inter-telescope registration correction shall be carried out for VNIR band 2. The correction coefficient is evaluated by the image matching between bands 2 and 6 for SWIR bands and between bands 2 and 11 for TIR bands. There is a strong possibility to omit the image matching process between VNIR and TIR, since the system correction seems to be better than the image matching accuracy judging from the pointing knowledge of each boresight described in Section 2.2.4 and the image matching accuracy described in Section 8.2.5. An initial checkout result after launch will be necessary for final decision.

The scene cutting shall be carried out from Level-0B data according to the predetermined World Reference System (WRS). Each group data shall be divided into scenes every 60 km for the along-track direction. One scene size shall be 63 km including an overlap of 5 % with neighboring scenes except for band 3B. For band 3B the scene size shall be 69 km including an additional overlap of 6 km to compensate the terrain error contribution, that is, 7.5 km overlap with the previous scene and 1.5 km overlap with the next scene. This scene cutting is necessary for granularizing the Level-1A and the Level-1B data products. It does not necessarily mean that the scene position is rigidly predetermined. It is still possible to revert the scenes to Level-0B data for a different scene cutting.

All geometric correction processes and scene cutting process shall be followed by a set of geolocation data generation for each scene. All geometric information is consolidated to generate a set of the geolocation data every block which is expressed in the latitude/longitude.

The Level-1A data product consists of the image data, the radiometric coefficients, the geolocation data and the auxiliary data. The Level-1B data product can be generated by applying these data for radiometric calibration and geometric resampling.


## 3.2.  Front-End  Processing  Flow
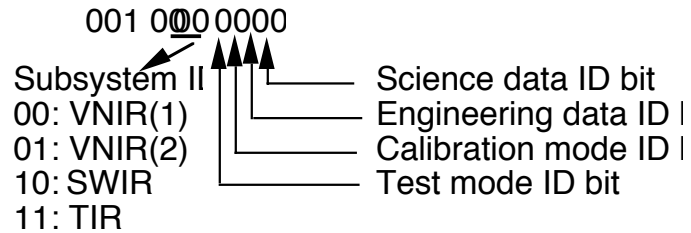
### 3.2.1.  Level-0  Production  Data  Set

The Level-0 data which are sent from EDOS are packetized in the CCSDS format as shown in Figure 3-2. These packets shall be classified into four groups of data according to APID (Application Process Identification) in the primary header of each packet. The group 1 data contain the data for VNIR bands 1 and 2. The group 2 data contain the data for VNIR bands 3N and 3B. The group 3 data contain the data for all SWIR bands. The group 4 data contain the data for all TIR bands. Each group data include science image data, instrument supplement data and spacecraft ancillary data as shown in Figure 3-3.

The ASTER is allocated the 64 APIDs that lie within the decimal equivalent range of 256 - 319 in UIID. Table 3-1 shows the APIDs allocated for each category of data. Different APIDs are allocated for each group of data and for each operation mode.

The data set generation at EDOS is based on multiple APID.    Each data file from EDOS which is called the Level-0 Production Data Set (PDS) contains the packet with multiple APIDs which belong to the same VCID as shown in Table 3-1.  The packets are sorted out with the

time tag data in the secondary header and then sorted out in the order of the image data, the combined data and the engineering data with different APID as shown in Table 3-1. Only TIR has the engineering packets. In a group with the same APID the packets are sorted out in the order of sequential counter data in the primary header.

Table 3-1 APID Allocation

001 0000 0000

Subsystem II
00: VNIR(1)
01: VNIR(2)
10: SWIR
11: TIR

Science data ID bit
Engineering data ID I
Calibration mode ID I
Test mode ID bit

| | VCID | Data Content | Observation Modes | Calibration Mode | Test Mode |
|---|---|---|---|---|---|
| VNIR(1) | 01 0001 | Science | 001 0000 0001 | 001 0000 0101 | 001 0000 1001 |
| | | Sci.+ Eng. | 001 0000 0011 | 001 0000 0111 | 001 0000 1011 |
| VNIR(2) | 01 1110 | Science | 001 0001 0001 | 001 0001 0101 | 001 0001 1001 |
| | | Sci.+ Eng. | 001 0001 0011 | 001 0001 0111 | 001 0001 1011 |
| SWIR | 01 0010 | Science | 001 0010 0001 | 001 0010 0101 | 001 0010 1001 |
| | | Sci.+ Eng. | 001 0010 0011 | 001 0010 0111 | 001 0010 1011 |
| TIR | 01 0111 | Science | 001 0011 0001 | 001 0011 0101 | 001 0011 1001 |
| | | Sci.+ Eng. | 001 0011 0011 | 001 0011 0111 | 001 0011 1011 |
| | | Engineering | 001 0011 0010 | 001 0011 0110 | 001 0011 1010 |
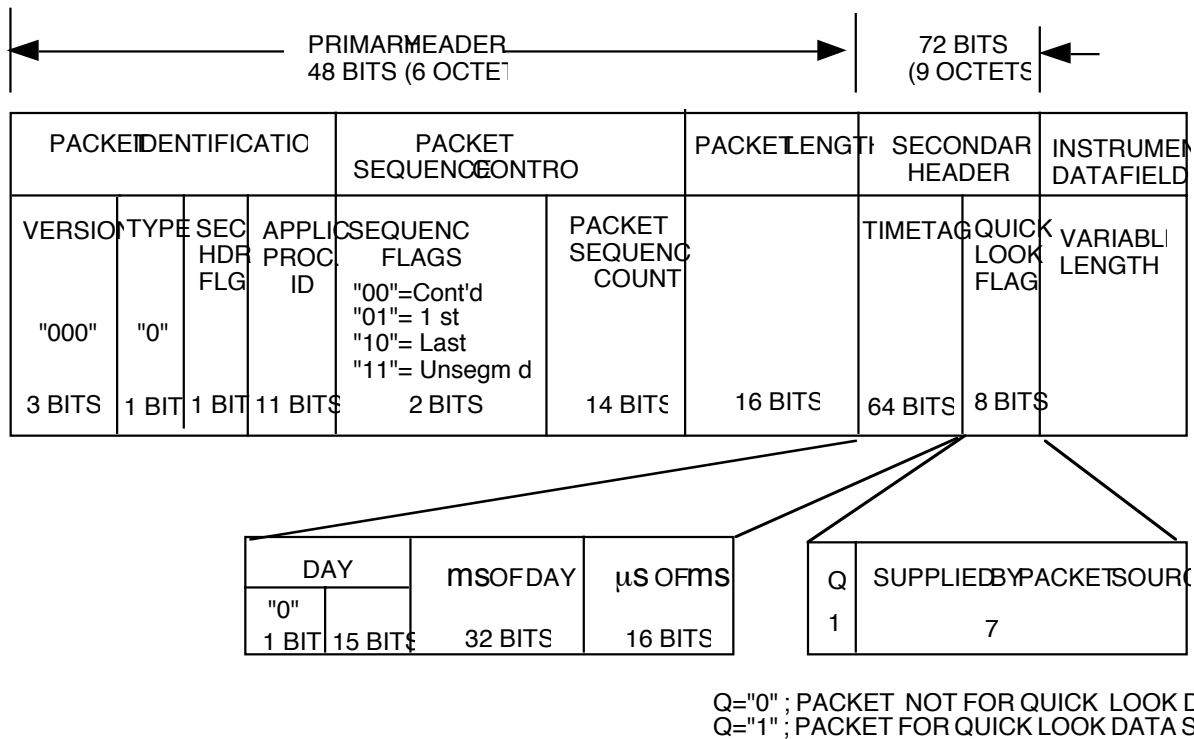
Figure 3-2  CCSDS Level-0 Data Packet Format

## 3.2.2.  Depacketizing of CCSDS Level-0 Data

The packets of each group shall be depacketized and aligned to recover the unpacketized instrument source data by using sequential counter, flags in the primary header and time tag in the secondary header. In the instrument source data the spectral band information are multiplexed with the BIP (Band Interleaved by Pixel) format as shown in Figure 3-3. Each swath line image data is appended by the specific engineering data for the line.



Figure 3-3  Instrument Source Data Format

### 3.2.3. Demultiplexing Instrument Source Data

Then the instrument source data shall be demultiplexed to separate image data every spectral band with BSQ (Band Sequential) format.  Here, we have the data rearranged in three groups, that is, the VNIR data group, the SWIR data group and the TIR data group. The each group data consists of the image data of each spectral band, the common supplement data for the group and the common ancillary data for all group.  Only for TIR data group the short term calibration data which will be obtained at the biginning and the end of each observation is included.  The supplement data are necessary for all of the group data to make it possible to process independently.  In this stage the image data will not be divided into scenes but kept in each continuous observation unit, that is, a long strip image data unit for more flexible scene selection.  This data set is defined as Level-0A data which is a tentative product being effective only during processing.

### 3.2.4. Image Data Stagger Realignment

For SWIR and TIR image data the Level-0 pixel addresses shall be realigned the order to correct stagger alignment among pixels in a same swath line as shown in Figure 2-1. This realignment process is carried out not only to have the more exactly aligned image data without resampling for image matching process but also to simplify subsequent processes.

The SWIR subsystems use electronically scanned linear detector arrays for each band to obtain one line data simultaneously in the cross-track direction for each scan period.  These detector arrays are separated for odd and even number of detectors with stagger configuration as shown in Figure 2-1.  The realignment for SWIR pixel addresses shall be carried out to compensate the difference from the center line between the odd and the even lines as shown in Figure 3-4.  The stagger offset value to the center line can be set to ±1 pixel with a good approximation.
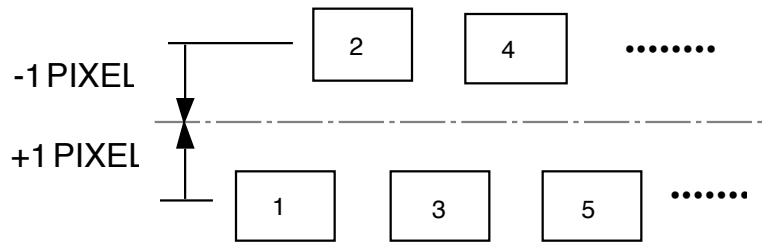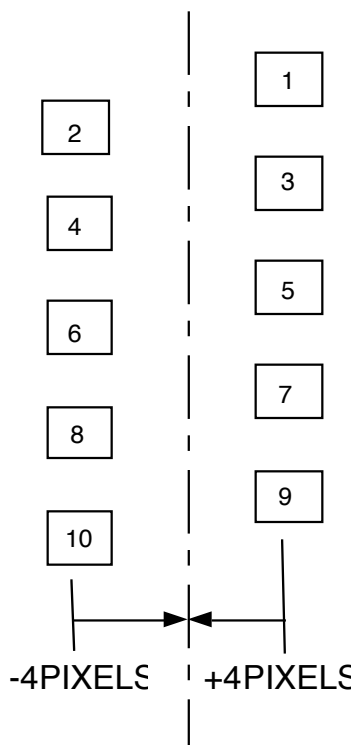
Figure 3-4  Stagger Realignment Position of All SWIR Pixels

TIR images are obtained by mechanical scanning with 10 detectors for each spectral band, that is, 50 detectors in total.  Ten detectors for each band are arranged with the stagger configuration in the cross-track direction as shown in Figure 2-1.  The realignment for TIR pixel addresses shall be carried out to compensate the difference from the center line between the odd and the even lines as shown in Figure 3-5.  The stagger offset value to the center line can be set to ±4 pixels with a good approximation.

Figure 3-5  Stagger Realignment Position of All TIR Pixels

## 3.3.  Geometric  System  Correction

The geometric system correction is the rotation and the coordinates transformation from the line of sight vectors of detectors to the earth Greenwich Coordinate by using only the engineering information from the instrument and the spacecraft to identify the observing points by the detectors. The observation point on the surface is identified from cross-point between the earth surface and an extension line of the vector  The engineering information from the instrument and the spacecraft is called the supplement data and the ancillary data, respectively.  The geometric system correction is almost common to three subsystems, except for selected numbers of vectors to be transformed.  Figures 3-6, 3-7 and 3-8 show the geometric system correction flows of VNIR, SWIR and TIR, respectively.

One observation point shall be divided into blocks for both of the cross-track and the along-track directions.  The block sizes are as follows.

| | |
|---|---|
| VNIR bands 1, 2, 3N: | 410 x 400 pixels |
| VNIR band 3B: | 500 x 400 pixels |
| SWIR all bands: | 20 x 20 pixels |
| TIR all bands: | 72 x 70 pixels |

These values are decided by considering a distortion of optical images on the focal plane in the cross-track direction and a spacecraft stability in the along-track direction.  The coordinates transformations are carried out only for the line of sight vectors of selected detectors.  The numbers of the selected detectors are 11, 104 and 11 for VNIR, SWIR and TIR bands, respectively, which correspond to number of corner points (number of block + 1) for each block of Level-0 images in the cross-track direction.  Dummy detectors will have to be

introduced to compensate a fraction and then to completely define the block at the end of the cross-track direction.

The geometric system correction is divided into several parts as follows:

(1) The pointing correction--The line of sight vectors in the geometric data base are those for the reference pointing angles (nominal nadir direction). The line of sight vectors shall be changed using the pointing position and knowledge data from the supplement data. The pointing axes information in the geometric data base shall be used for the transformation of the line of sight vectors due to the pointing position change.

(2) The coordinates transformation from the spacecraft coordinates (Spacecraft Reference Axes or Navigation Base Reference) to the orbit coordinates (Orbital Reference Coordinate Frame)--The spacecraft coordinates slightly different from the orbit coordinates. The difference is originated from a spacecraft attitude control accuracy and provided as the attitude angle data in the spacecraft ancillary information. The orbit coordinates is right-handed and orthogonal. The +z-axis is a line from the spacecraft center of mass to the center of the earth. The +y-axis is a line normal to the z-axis and the spacecraft instantaneous velocity vector (negative orbit normal direction). The x-axis completes the right hand set. This process shall be carried out by using attitude angles and attitude rates in the ancillary data.

(3) The coordinates transformation from the orbit coordinates to the earth inertial coordinates--This process is the coordinates transformation to the earth centered coordinates in the inertial space. Two dimensional array vectors can be obtained by this transformation according to the spacecraft movement. The array dimension depends on each observation period. This process shall be carried out by using positions, and velocities information in the ancillary data.

(4) The coordinates transformation from the earth inertial coordinates to the earth Greenwich coordinates--This process is the coordinates transformation to the earth centered and earth fixed coordinates, and shall be carried out by using the earth rotation values calculated from the time information in the ancillary data.

(5) The observation point shall be identified by calculating a cross-point between the earth surface and an extended line of the vector. The WGS-84 shall be used as the earth surface model.
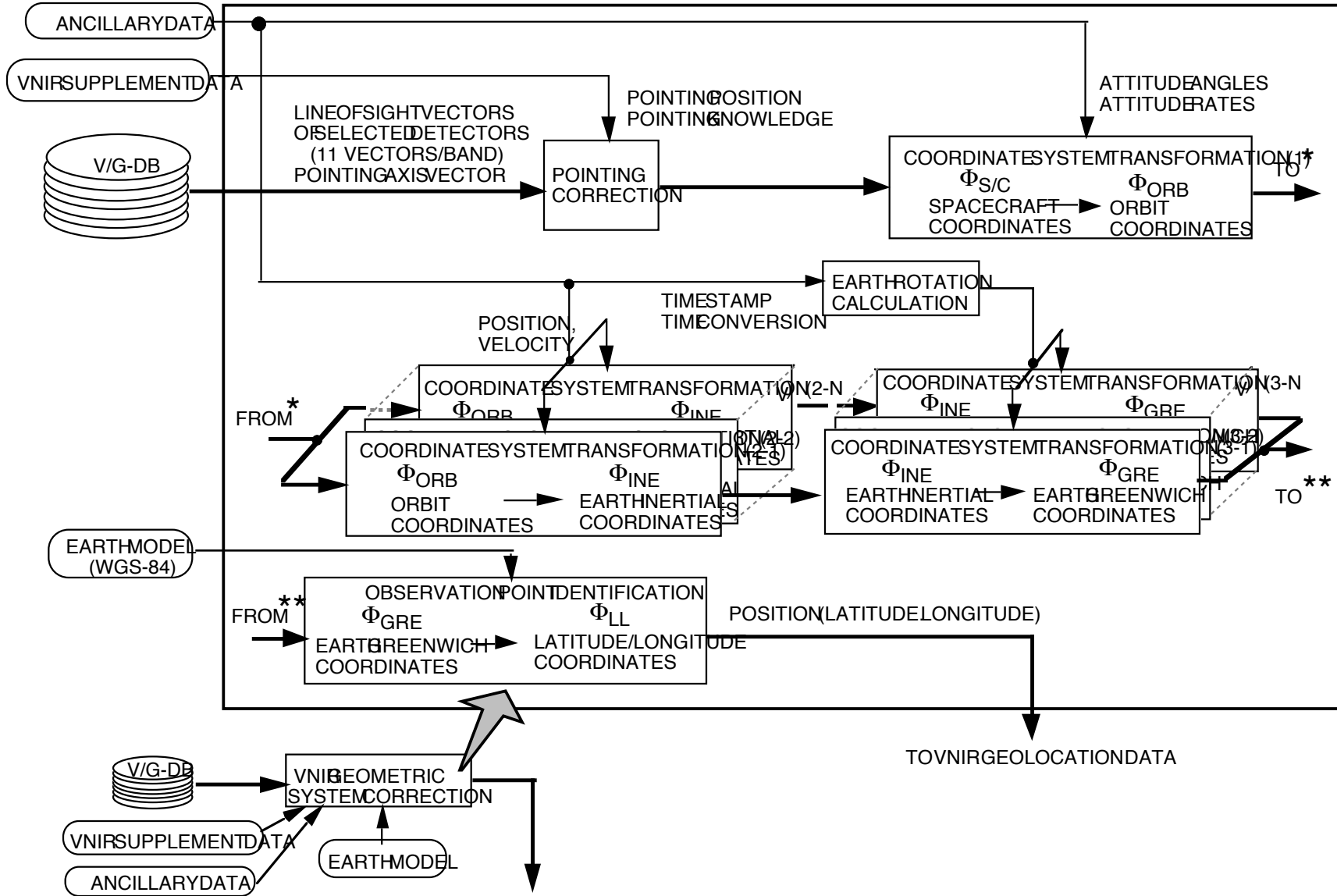
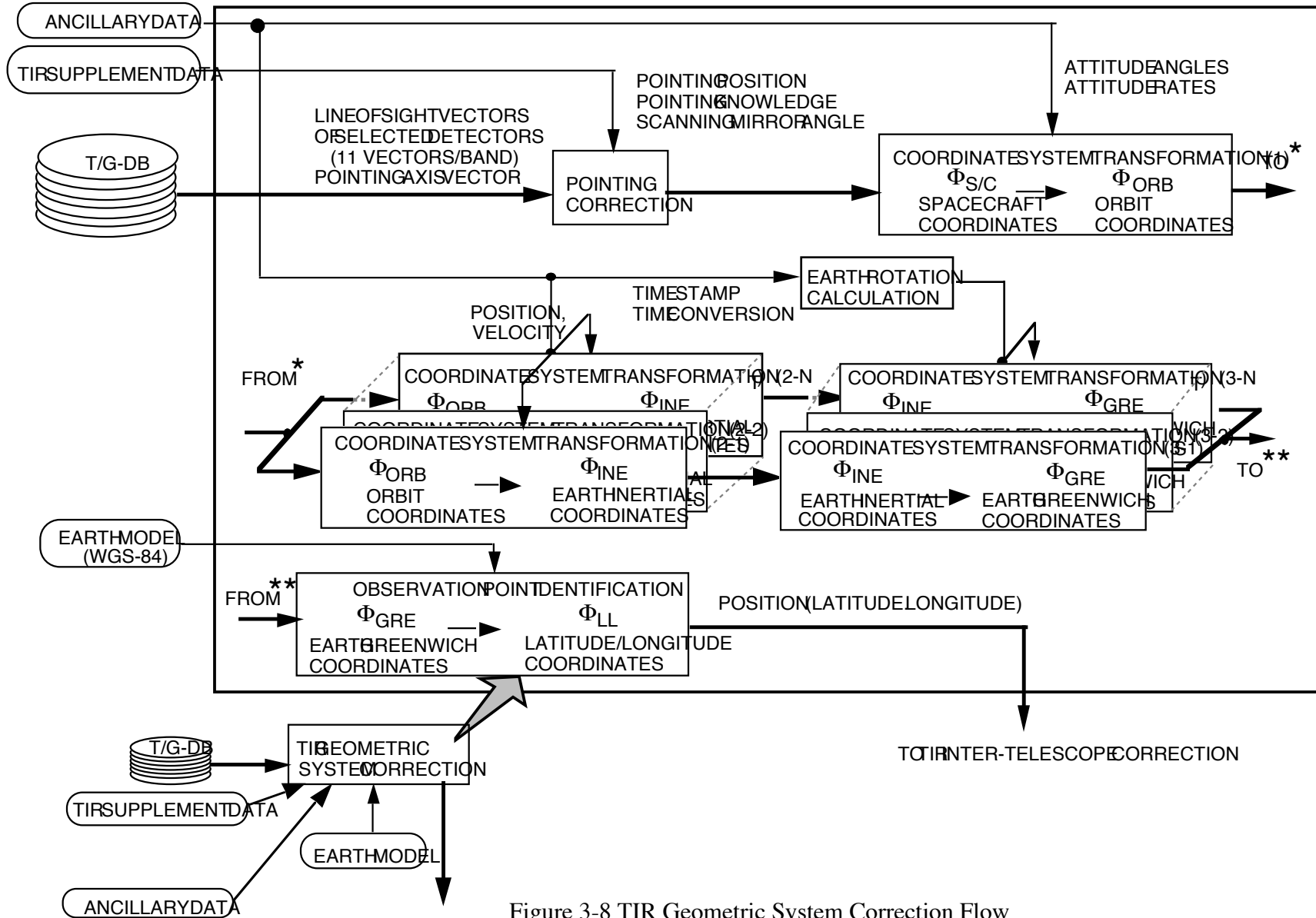Figure 3-6  VNIR Geometric System Correction Flow

Figure 3-7  SWIR Geometric System Correction Flow

Figure 3-8 TIR Geometric System Correction Flow

## 3.4. Radiometric Coefficients Generation

Observation unit or scene specific radiometric coefficients shall be generated by using reference temperature data in each subsystem supplement data and the geometric data bases which contain the radiometric coefficients for the reference temperature and temperature dependence coefficients, since the radiometric coefficients in the data base are values under a reference condition such as detector and dewar temperatures. One set of offset and sensitivity data are necessary for VNIR and SWIR bands. While one set of offset, linear sensitivity and nonlinear sensitivity data are necessary for TIR bands.

The radiometric coefficients for the reference temperatures shall be evaluated during the preflight test period at first stage, followed by a regular evaluation during the inflight period and then updated if necessary. All temperature dependence coefficients shall be prepared during the preflight test period and used throughout the mission period.

### 3.4.1. VNIR Radiometric Coefficients Generation

Figure 3-9 shows the VNIR radiometric coefficients generation flow. Only detector temperature is the reference parameter by which the radiometric coefficients (offset and sensitivity) have to be corrected for a specific observation unit data. Under a normal operation condition within the designed temperature range this correction process will not be necessary to execute, since the correction value is expected to be very small. This process is entirely prepared for an abnormal operation beyond the designed range but still within a range of the practical use.

VNIR Destriping parameters shall be generated from the VNIR image data. The details are TBD.



Figue 3-9  VNIR Radiometric Coefficients Generation

## 3.4.2. SWIR Radiometric Coefficients Generation

Figure 3-10 shows the SWIR radiometric coefficients generation flow. Detector temperature and dewar temperature are the reference parameters by which the radiometric coefficients (offset and sensitivity) have to be corrected for a specific observation unit data. Under a normal operation condition the detector temperature is controlled very precisely within ±0.2 K around 77 K. Therefore the correction process for the detector temperature will not be necessary to execute as long as the SWIR is operating normally . This process is entirely prepared for an abnormal operation beyond the designed range but still within a range of the practical use.

The dewar temperature correction, which is necessary for compensating a thermal radiation from it, shall be applied only to the offset, since SWIR detector has a sensitivity for the room temperature thermal radiation up to 5 μm and the band pass filter can not completely cut the out-of-band radiation. The dewar temperature shall be used as a representative value for the internal thermal radiation. This process shall always be executed even for the normal operation condition.

SWIR Destriping parameters shall be generated from the SWIR image data. The details are TBD.
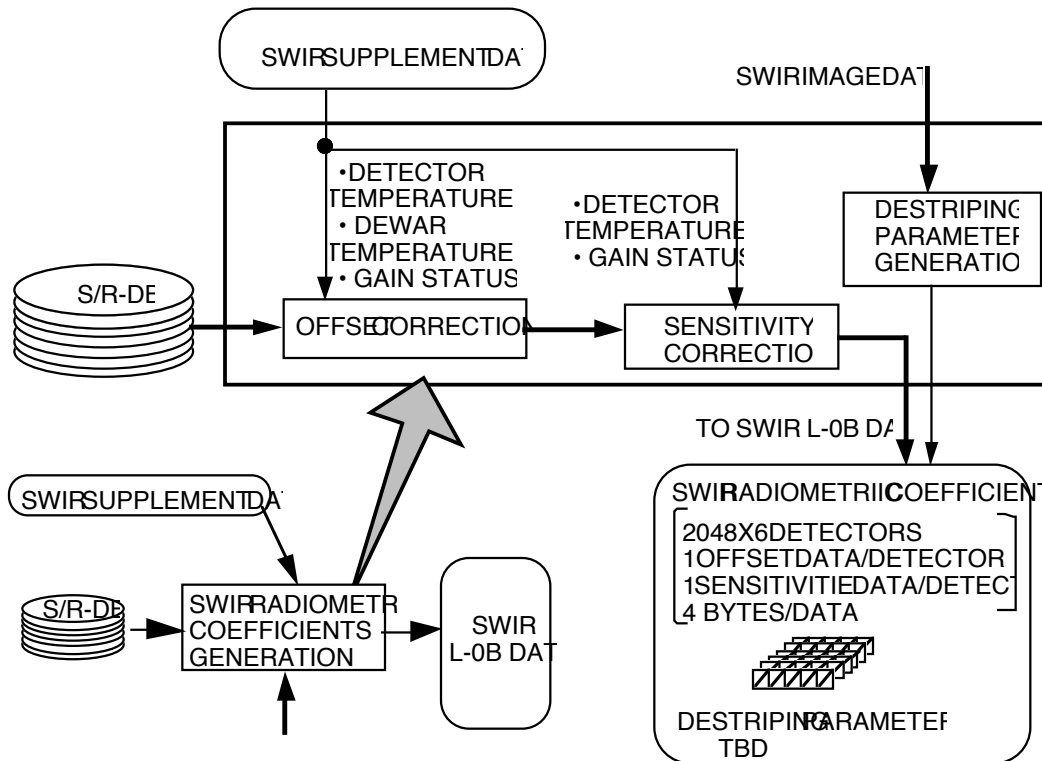


Figue 3-10  SWIR Radiometric Coefficients Generation

### 3.4.3. TIR Radiometric Coefficients Generation

Two kinds of processing flows, the baseline processing and the optional processing, are prepared for TIR radiometric coefficients generation. The baseline flow shall be applied if the short term calibration data at the beginning of each observation are available. While the optional flow shall be applied to the case without the short term calibration data. The former is the normal processing.

Figure 3-11(a) shows the baseline TIR radiometric coefficients generation flow. The linear and the non-linear sensitivities coefficients in the data base shall be corrected only by the detector temperature. Under a normal operation condition the detector temperature is controlled very precisely within ±0.2 K around 80 K. Therefore, the correction process for the detector temperature will not be necessary to execute as long as TIR is operating normally. This process is entirely prepared for an abnormal operation beyond the designed range but still within a range of the practical use.

For the baseline processing the offset data, which is the common data throughout the observation unit, shall be generated from the short term calibration data at the beginning of each observation by referring the blackbody temperature in the TIR supplement data. The predetermined offset data in the radiometric data base shall not be used in the baseline processing.

The chopper temperature correction data for the offset data shall be calculated using the chopper temperature changes from the short term calibration period. The chopper temperature correction shall be carried out for the DN value correction of the TIR L-0A image data with the DC clamp correction. This correction will be possible for each scan data (each ten line data in the along-track direction), since the chopper temperature data is included every scanning in the supplement data.

This image data correction will result slightly different TIR L-0B image data DN value from Level-0 data. The Level-0 data is digitized by 12 bits. The LSB (Least Significant Bit) value of L-0B image data is very small compared to NEΔT (below one third at 300 K target signal). Therefore, this difference will not give rise to any significant round error.

TIR Destriping parameters shall be generated from the TIR image data. The details are TBD.
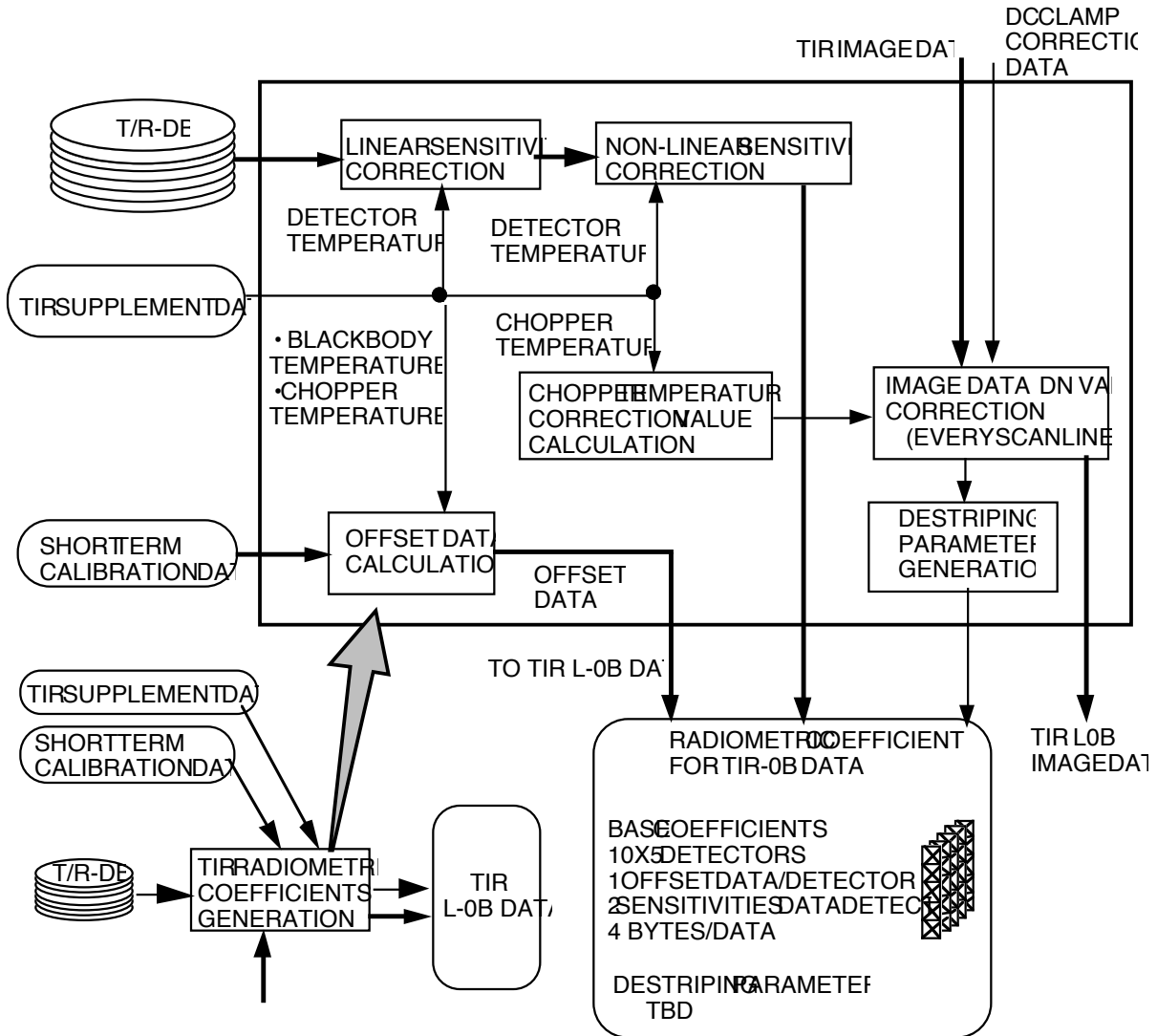
Note
A/T-LATTICE POINT: Lattice point in along-track direction

Figure 3-11(a)  Baseline TIR Radiometric Coefficients Generation
(Baseline Process with Short Term Calibration)

Figure 3-11(b) shows the optional TIR radiometric coefficients generation flow. Sometimes only some limited numbers of scenes in an observation unit will be sent electronically from EDOS as the Expedited Data Set (EDS) for quick processing without the short term calibration data. In such a case the optional flow shall be applied to prepare the tentative Level-1 data product with less radiometric accuracy.

The linear and the non-linear sensitivities coefficients in the data base shall be corrected only by the detector temperature in the same method as the baseline processing. The offset data in the radiometric data base shall be used as the base data and then corrected by the chopper temperature, the lens temperature and the telescope temperature in the TIR supplement data. These temperatures dependence coefficients are accommodated in the radiometric data base as predetermined parameters in the preflight test period.

The chopper temperature is the most important parameter for the offset correction, since the majority radiation comes from the chopper at the timing when the detectors see the chopper and the DC clamp is set. On the other hand the lens temperature and the telescope temperature are less important parameters than the chopper temperature. If these temperature effects are identified to be very small by the preflight evaluation, this correction process will be more simplified.

TIR Destriping parameters shall be generated from the TIR image data. The details are TBD.
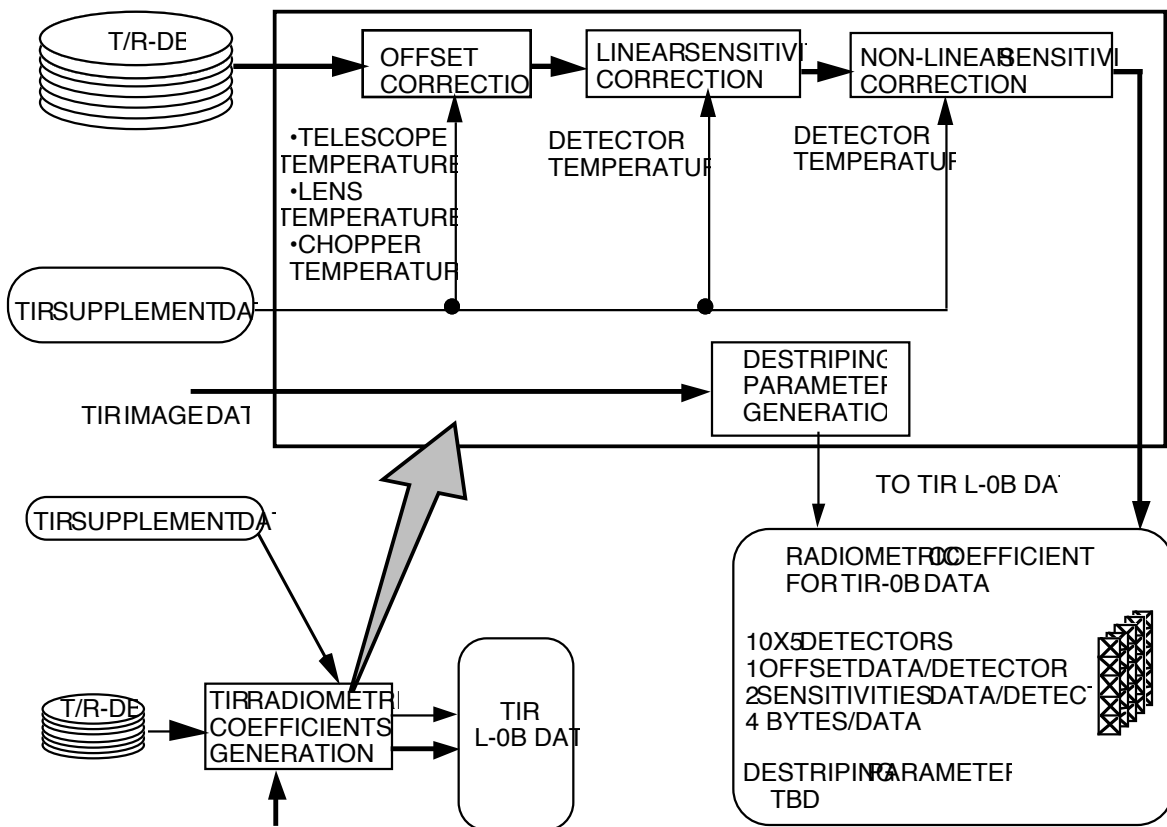


Figure 3-11(b)  Optional TIR Radiometric Coefficients Generation
(Optional Process without Short Term Calibration)Å

## 3.5. TIR DC Clamp Correction

TIR output voltage is clamped at -1.4 V $\pm$ $\Delta V_n$ for the bands 10-12 and -0.9 V$\pm$ $\Delta V_n$ for the bands 13, 14 when the chopper plate is observed by the detectores every scan. The small voltate $\Delta V_n$ is the noise voltage at a moment of the clamp which changes at random evey sacn and must be corrected to set up the clamp voltage exactly.

Figure 3-12 shows the TIR DC clamp correction flow. The exact clamped output (DN values) is accommodated in the TIR supplement data as the chopper data. The chopper data in the one previous scan shall be used for the correction. The one scan chopper data with 100 sampled data shall be averaged to have the value without including the noise component, followed by the DC clamp error calculation which corresponds to $\pm$ $\Delta V_n$ . This clamp error shall be subtracted from the TIR L-0A image data to generate L-0B image data.
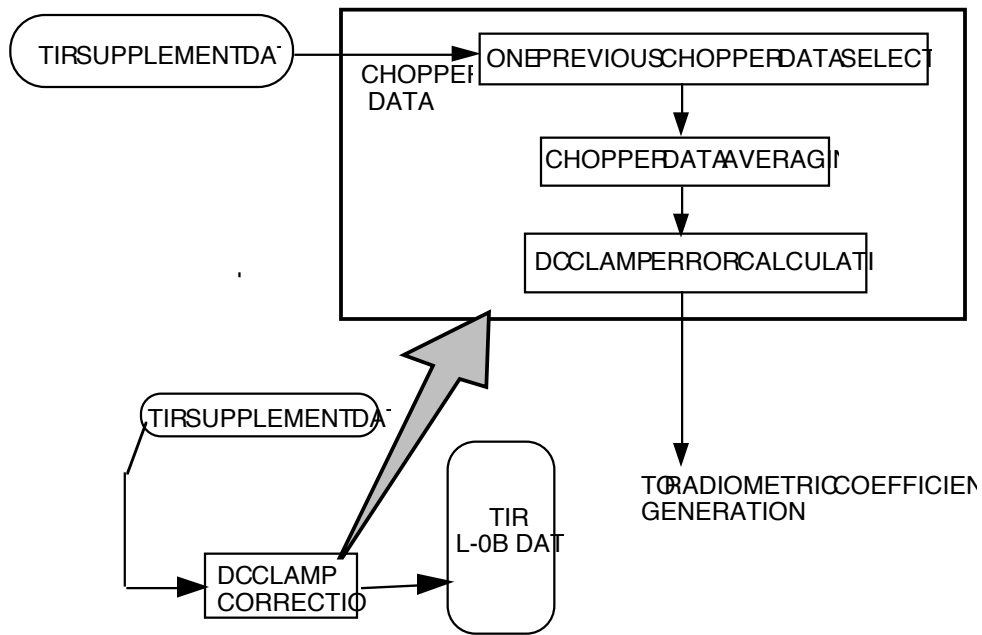


Figure 3-12  TIR DC Clamp Correction

## 3.6. SWIR Parallax Correction

The large offset among SWIR bands in the along-track direction gives rise to the parallax error for band-to-band registration depending on the distance between the instrument and the targeting ground. Figure 3-13 shows the parallax correction flow. In order to eliminate this band-to-band misregistration due to the parallax, the SWIR parallax correction process handles the image data as follows:

(1) Select band 7 as a moving window image and band 6 as a target image. The moving window shall be selected such that its center corresponds to the lattice point at which the geometric system correction is carried out. The target image shall be selected to cover the search area. The moving window image (band 7) size is 21 by 21 pixel.

(2) Select only cloud free windows for the correlation. Apply the coarse DEM data for cloudy window.

(3) Carry out the radiometric correction for the two window images

(4) Find correlation coefficients by moving the moving window in the pixel unit in the along-track direction.

$$\Delta (m,n) = \frac{\sum_{i=1}^{LY} \sum_{j=1}^{LX} [S(i,j) - \overline{S}] \times [D(i-m,j-n) - \overline{D}]}{\left( \sum_{i=1}^{LY} \sum_{j=1}^{LX} [S(i,j) - \overline{S}]^2 \times \sum_{i=1}^{LY} \sum_{j=1}^{LX} [D(i-m,j-n) - \overline{D}]^2 \right)^{1/2}}$$

where $\Delta$ is the correlation coefficient.
$m$ and $n$ are the along-track and the cross-track window numbers, respectively.
$i$ and $j$ are the along-track and the cross-track pixel numbers, respectively.
$S$ are $D$ are band 6 and band 7 images, respectively.

(5) Find the highest correlation point in sub-pixel unit by interpolating the correlation data calculated in the pixel unit.

(6) Evaluate the image matching quality. Criteria for the judgment are the correlation coefficient and the deviation from the predetermined value from the coase DEM data. The threshold value for the correlation coefficient is 0.7 (TBR). The threshold deviation for the predetermined value is 0.2 (TBR). Apply the coarse DEM data for the window with a bad quality.

(7) Evaluate the parallax error of all SWIR bands for the nadir direction.

The registration error due to the parallax shall be evaluated every the lattice point (the corner point of the block) and expressed with the pixel unit for the L-0B image data in the along-track direction.

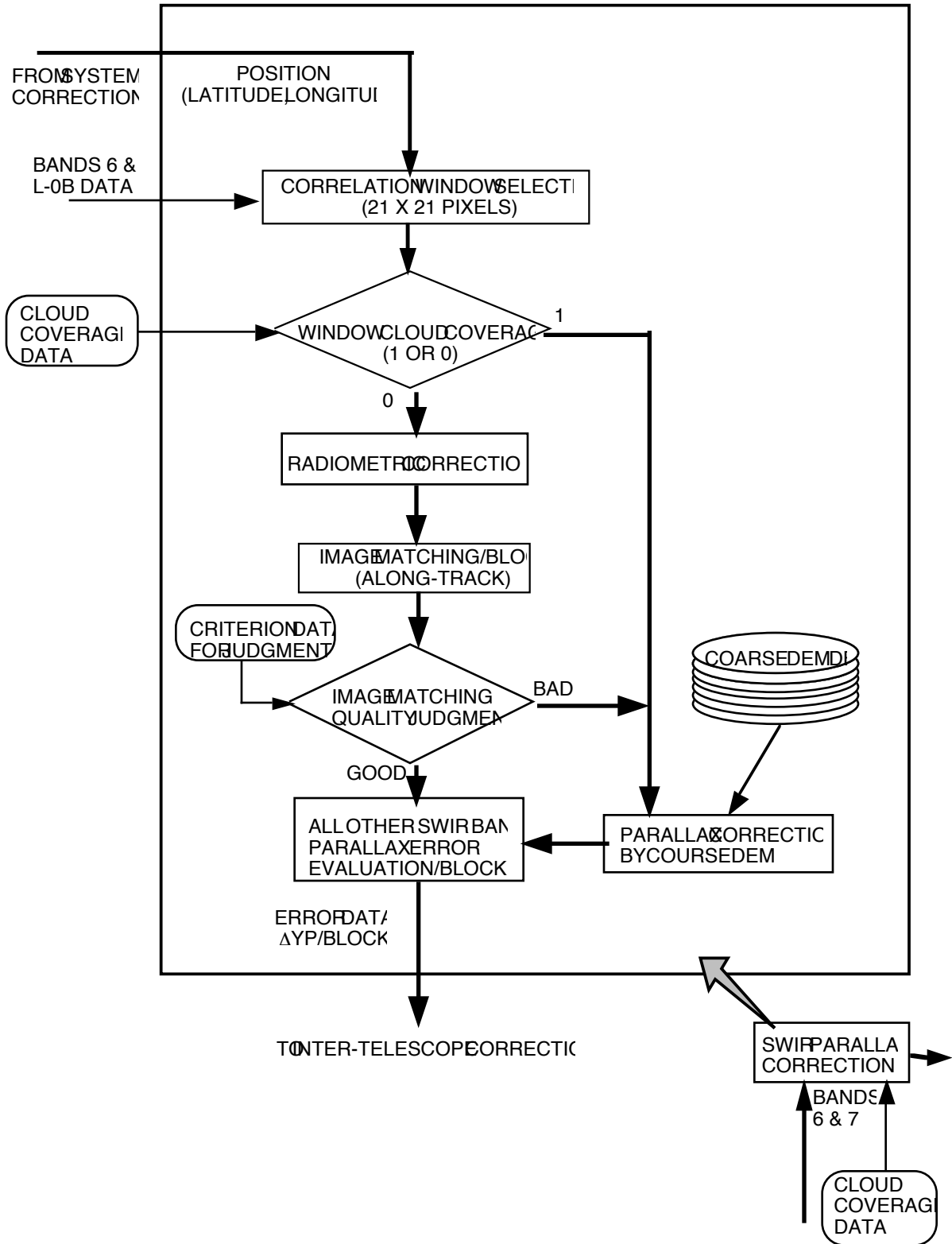ΔYP: Parallax error in pixel unit for along-track direction

FROM SYSTEM
CORRECTION
POSITION
(LATITUDE, LONGITUDE)

BANDS 6 &
L-0B DATA
→ CORRELATION WINDOW SELECTION
(21 X 21 PIXELS)

CLOUD
COVERAGE
DATA
→ WINDOW CLOUD COVERAGE
(1 OR 0)

1

0

RADIOMETRIC CORRECTION

IMAGE MATCHING/BLOCK
(ALONG-TRACK)

CRITERION DATA
FOR JUDGMENT
→ IMAGE MATCHING
QUALITY JUDGMENT
BAD →

COARSE DEM DB

GOOD

ALL OTHER SWIR BANDS
PARALLAX ERROR
EVALUATION/BLOCK
← PARALLAX CORRECTION
BY COURSE DEM

ERROR DATA
ΔYP/BLOCK

TO INTER-TELESCOPE CORRECTION

SWIR PARALLAX
CORRECTION
→

BANDS
6 & 7

CLOUD
COVERAGE
DATA

Figure 3-13  SWIR Parallax Correction Flow

### 3.7. Inter-telescope Geometric Correction

The ASTER instrument configuration with the multi-telescopes leads to necessity of routine processing for the inter-telescope band-to-band registration on the ground, unless the boresights are stable enough during the mission life to keep the initial state after launch. The pointing change mechanism is also a source of the disturbance because of a limited accuracy for the pointing position knowledge.

The relative pointing knowledge, which is important for the inter-telescope band-to-band registration, is described in Table 2-22. Judging from the knowledge, the system geometric correction will not give enough accuracy, even if the static error is removed during the initial checkout period. Image matching techniques will be inevitable for the inter-telescope registration.

The VNIR band 2 shall be used as the reference band for the inter-telescope registration by the reason described later in Chapter 8. Therefore, the inter-telescope registration process consists of two parts. One is the correction parameter generation between SWIR and VNIR. Another is the correction parameter generation between TIR and VNIR.

The important feature to be stressed here for the inter-telescope registration is that a set of the correction parameters will be valid and can be applied all images as long as the pointing is kept at the same position and the elapsed time since previous parameter setting is short enough for the boresight stability. The inter-telescope registration correction will be carried out every the observation unit.

### 3.7.1. SWIR/VNIR Inter-telescope Geometric Correction

Figures 3-14 shows the SWIR inter-telescope geometric correction flows for VNIR band 2. This correction process shall be carried out as follows.

(1) Start the registration error calculation at the beginning of each observation unit only for the full mode observation.

(2) Select band 2 as a moving window image and band 6 as a target image. The moving window shall be selected such that its center corresponds to the lattice point at which the geometric correction is carried out. The target image shall be selected to cover the search area. The moving window image size is 41 x 41 pixels. The target window size shall be larger than the moving window to cover the search area.

(3) Select a cloud free window for the correlation by repeating the previous item (2).

(4) Carry out the radiometric correction for the cloud free images

(5) Find correlation coefficients by moving the moving window in the pixel unit in both along-track and the cross-track directions.

$$\Delta (m,n) = \frac{\sum_{i=1}^{LY} \sum_{j=1}^{LX} [S(i,j) - \overline{S}] \times [D(i-m,j-n) - \overline{D}]}{\left( \sum_{i=1}^{LY} \sum_{j=1}^{LX} [S(i,j) - \overline{S}]^2 \times \sum_{i=1}^{LY} \sum_{j=1}^{LX} [D(i-m,j-n) - \overline{D}]^2 \right)^{1/2}}$$

where $\Delta$ is the correlation coefficient.

*m* and *n* are the along-track and the cross-track window numbers, respectively.
*i* and *j* are the along-track and the cross-track pixel numbers, respectively.
*S* are *D* are band 2 and band 6 images, respectively.

(6) Find the highest correlation point in sub-pixel unit by interpolating the correlation data calculation in the pixel unit.

(7) Evaluate the image matching quality. Criteria for the judgment are the correlation coefficient. The threshold value for the correlation coefficient is 0.7 (TBR).

(8) Repeat the process from item (2) to item (7) until the preset number of the effective error data is obtained. The preset numbers are a minimum of 100 and a maximum of 200.

(9) If the preset number error data can not be obtained in the observation unit, the zero error data shall be applied for this unit and the failed information shall be output.

(10) Exclude the error data which deviate over 3σ value from the average.

(11) The obtained number of the effective error data shall be averaged to generate a set of final error data.
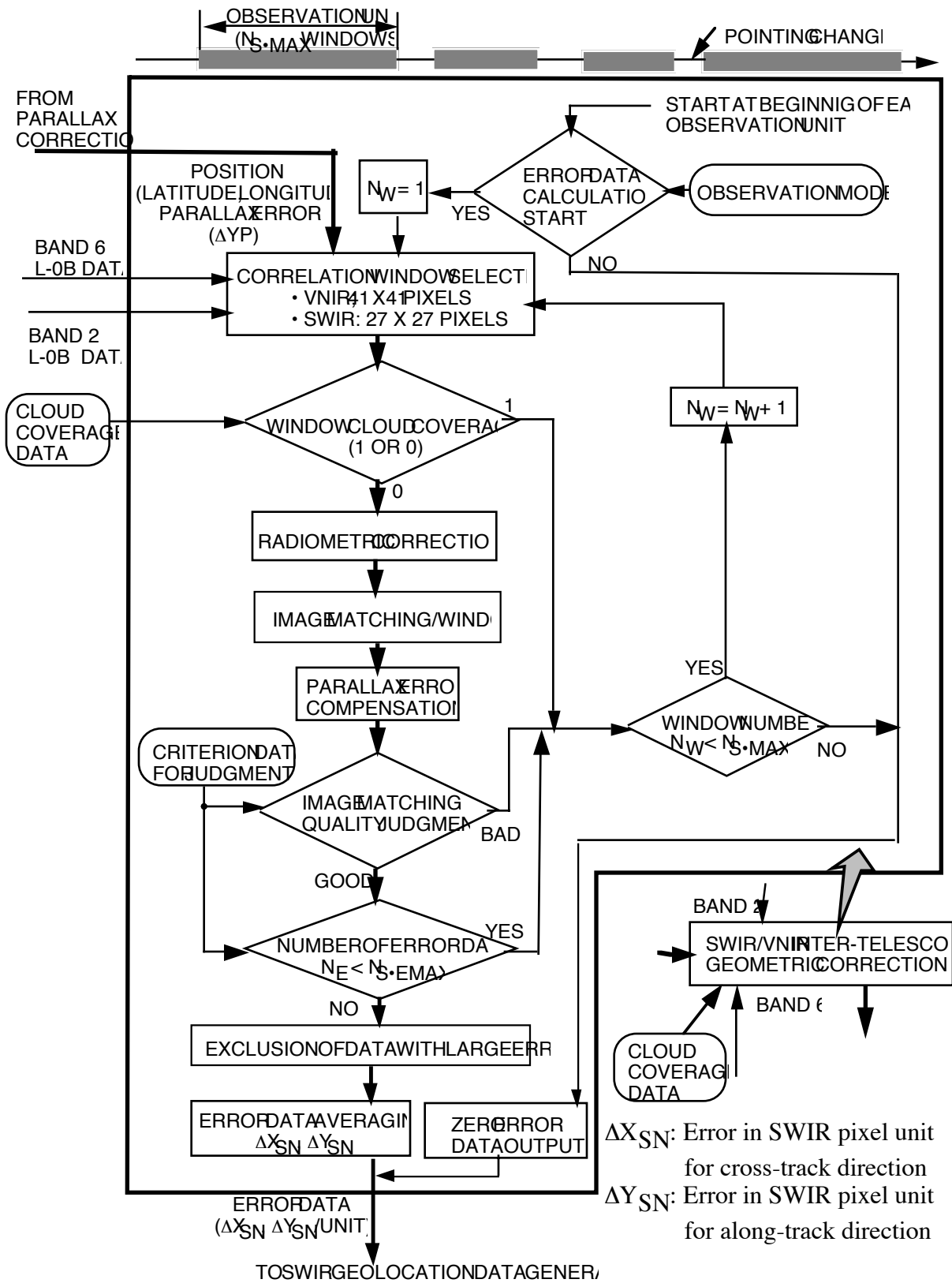
(12) Calculate 3σ value to evaluate the accuracy.

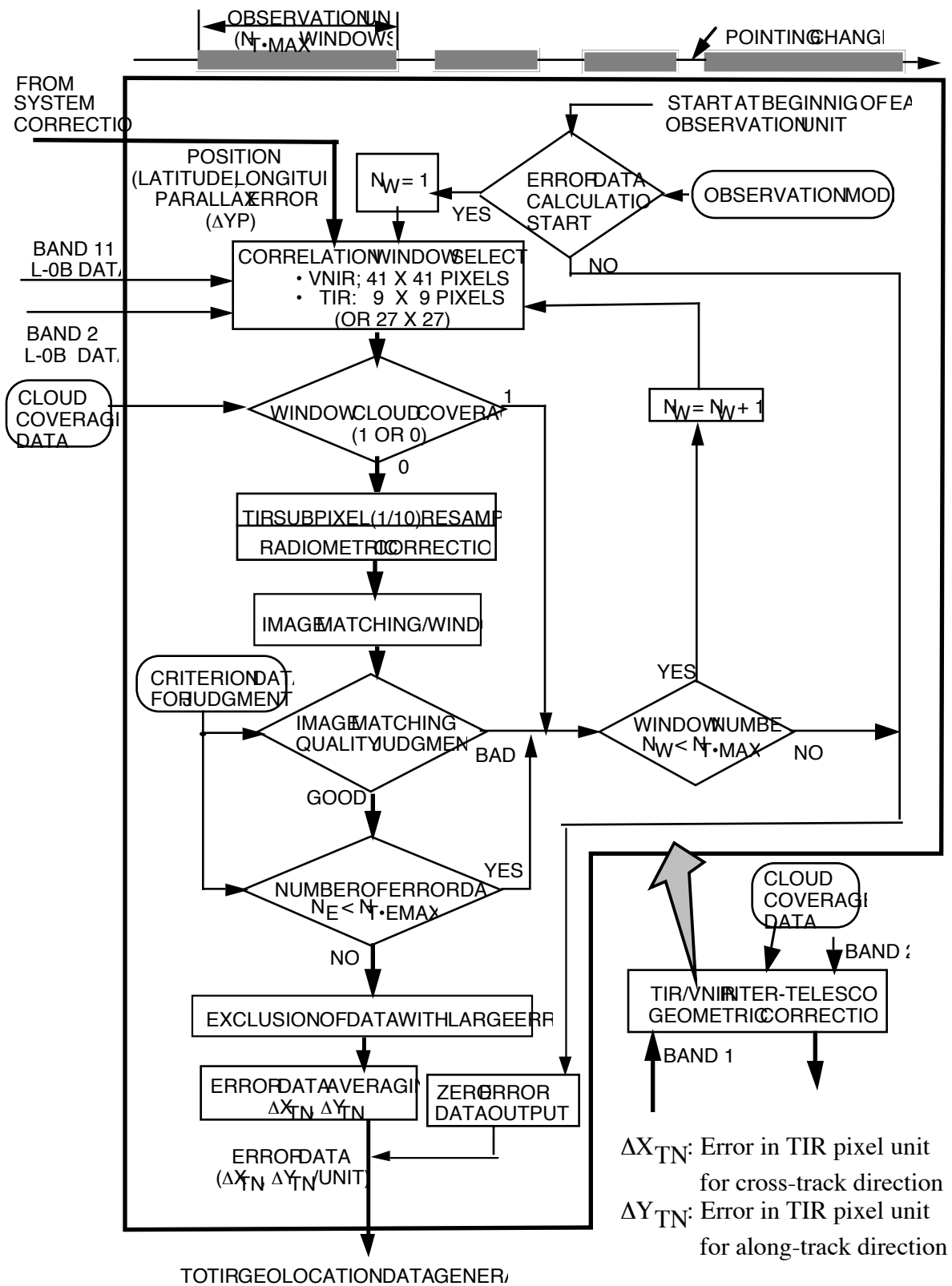## 3.7.2. TIR/VNIR  Inter-telescope  Geometric  Correction

Figures 3-15 shows the TIR inter-telescope geometric correction flows for VNIR band 2. This correction process shall be carried out as follows.

(1) Start the registration error calculation at the beginning of each observation unit, only if one of the conditions shown below is satisfied for the full mode observation.
• The pointing was changed after the previous observation.
• The elapsed time since the previous error data setting exceeds 16 minutes (TBR).
For the observation mode other than the full mode, skip the new error data calulation process.

(2) Select band 2 as a moving window image and band 11 as a target image. The moving window shall be selected such that its center corresponds to the lattice point at which the geometric correction is carried out. The target image shall be selected to cover the search area. The moving window image size is 41 x 41 (or 121 x 121) pixels. The target window size shall be larger than the moving window to cover the search area.

(3) Select a cloud free window for the correlation by repeating the previous item (2).

(4) Carry out the radiometric correction for the cloud free images. For band 11 image the 1/10 pixel time delay shall be compensated by 1/10 sub-pixel resampling.

(5) Find correlation coefficients by moving the moving window in the pixel unit in both along-track and the cross-track directions.

$$\Delta\,(m,n) = \frac{\displaystyle\sum_{i=1}^{LY}\sum_{j=1}^{LX}[S(i,j) - \overline{S}] \times [D(i\text{-}m,j\text{-}n) - \overline{D}]}{\left(\displaystyle\sum_{i=1}^{LY}\sum_{j=1}^{LX}[S(i,j) - \overline{S}]^2 \times \sum_{i=1}^{LY}\sum_{j=1}^{LX}[D(i\text{-}m,j\text{-}n) - \overline{D}]^2\right)^{1/2}}$$

where $\Delta$ is the correlation coefficient.

$m$ and $n$ are the along-track and the cross-track window numbers, respectively.

$i$ and $j$ are the along-track and the cross-track pixel numbers, respectively.

$S$ are $D$ are band 2 and band 11 images, respectively.

(6) Find the highest correlation point in sub-pixel unit by interpolating the correlation data calculation in the pixel unit.

(7) Evaluate the image matching quality. Criteria for the judgment are the correlation coefficient. The threshold value for the correlation coefficient is 0.7 (TBR).

(8) Repeat the process from item (2) to item (7) until the preset number of the effective error data is obtained. The preset numbers are a minimum of 100 and a maximum of 200.

(9) If the preset number error data can not be obtained in the observation unit, the zero error data shall be applied for this unit and the failed information shall be output.

(10) Exclude the error data which deviate over $3\sigma$ value from the average.

(11) The obtained number of the effective error data shall be averaged to generate a set of final error data.(12) Calculate $3\sigma$ value to evaluate the accuracy.

Figure 3-14  SWIR/VNIR Inter-telescope Geometric Correction Flow

POINTING CHANGE

FROM SYSTEM CORRECTION

START AT BEGINNING OF EACH OBSERVATION UNIT

POSITION
(LATITUDE, LONGITUDE)
PARALLAX ERROR
($\Delta$YP)

$N_W = 1$

ERROR DATA CALCULATION START

OBSERVATION MODE

YES

NO

BAND 11
L-0B DATA

CORRELATION WINDOWS SELECT
• VNIR; 41 X 41 PIXELS
• TIR: 9 X 9 PIXELS
(OR 27 X 27)

BAND 2
L-0B DATA

CLOUD COVERAGE DATA

WINDOW CLOUD COVERAGE
(1 OR 0)

$N_W = N_W + 1$

0

1

TIR SUBPIXEL (1/10) RESAMPLE
RADIOMETRIC CORRECTION

IMAGE MATCHING/WINDOW

CRITERION DATA FOR JUDGMENT

IMAGE MATCHING QUALITY JUDGMENT

BAD

GOOD

YES

WINDOW NUMBER
$N_W < N_T·MAX$

NO

NUMBER OF ERROR DATA
$N_E < N_T·EMAX$

YES

NO

EXCLUSION OF DATA WITH LARGE ERROR

ERROR DATA AVERAGING
$\Delta X_{TN}$, $\Delta Y_{TN}$

ZERO ERROR DATA OUTPUT

ERROR DATA
($\Delta X_{TN}$, $\Delta Y_{TN}$/UNIT)

CLOUD COVERAGE DATA

BAND 2

TIR/VNIR INTER-TELESCOPE GEOMETRIC CORRECTION

BAND 1

$\Delta X_{TN}$: Error in TIR pixel unit
for cross-track direction
$\Delta Y_{TN}$: Error in TIR pixel unit
for along-track direction

TO TIR GEOLOCATION DATA GENERATION

Figure 3-15  TIR/VNIR Inter-telescope Geometric Correction Flow

## 3.8. Scene Cutting

The scene cutting shall be carried out from Level-0B data according to the predetermined World Reference System (WRS). Each group data shall be divided into scenes every 60 km for the along-track direction. One scene size shall be 63 km including an overlap of 5 % with neighboring scenes except for band 3B. For band 3B the scene size shall be 69 km including an additional overlap of 6 km to compensate the terrain error contribution, that is, 7.5 km overlap with the previous scene and 1.5 km overlap with the next scene. This scene cutting is necessary for granularizing the Level-1A and the Level-1B data products. It does not necessarily mean that the scene position is rigidly predetermined. It is still possible to revert the scenes to Level-0B data for a different scene cutting.

Since the radiometric correction coefficients are the observation unit specific parameters for the VNIR and the SWIR bands, the same coefficients shall be appended for all scenes which belong to the same unit. On the other hand, for the TIR bands, the offset component of the radiometric correction coefficients might be slightly depend on the position in the unit. In the L-0B data the chopper temperature dependence coefficients with the chopper data are accommodated by which the scene specific data can be calculated. The radiometric correction coefficients correspond to the scene center shall be calculated and appended as a part of the Level-1A data product.

## 3.9. Geometric Coefficients Generations

Figures 3-16, 3-17 and 3-18 show the geometric coefficients generations flows for VNIR, SWIR and TIR, respectively.

All registration error data which are calculated by the parallax correction and the inter-telescope geometric correction processes shall be consolidated and changed into the latitude/longitude from the pixel unit in the along- and cross-track directions. The latitude/longitude values at each lattice point, which are calculated by the geometric system correction, shall be corrected with the consolidated error data.

A set of positions expressed by the latitude and the longitude are adopted as the geolocation data for each lattice point.

Other parameters which are necessary for higher level product generations such as the Level-3 (the geocoded ortho images) data products and the Level-4 (DEM) data products are calculated or arranged in this module, and shall be appended to the Level-1A products. The detailed contents are defined in the separate document (the Level-1 Data Product Specification).
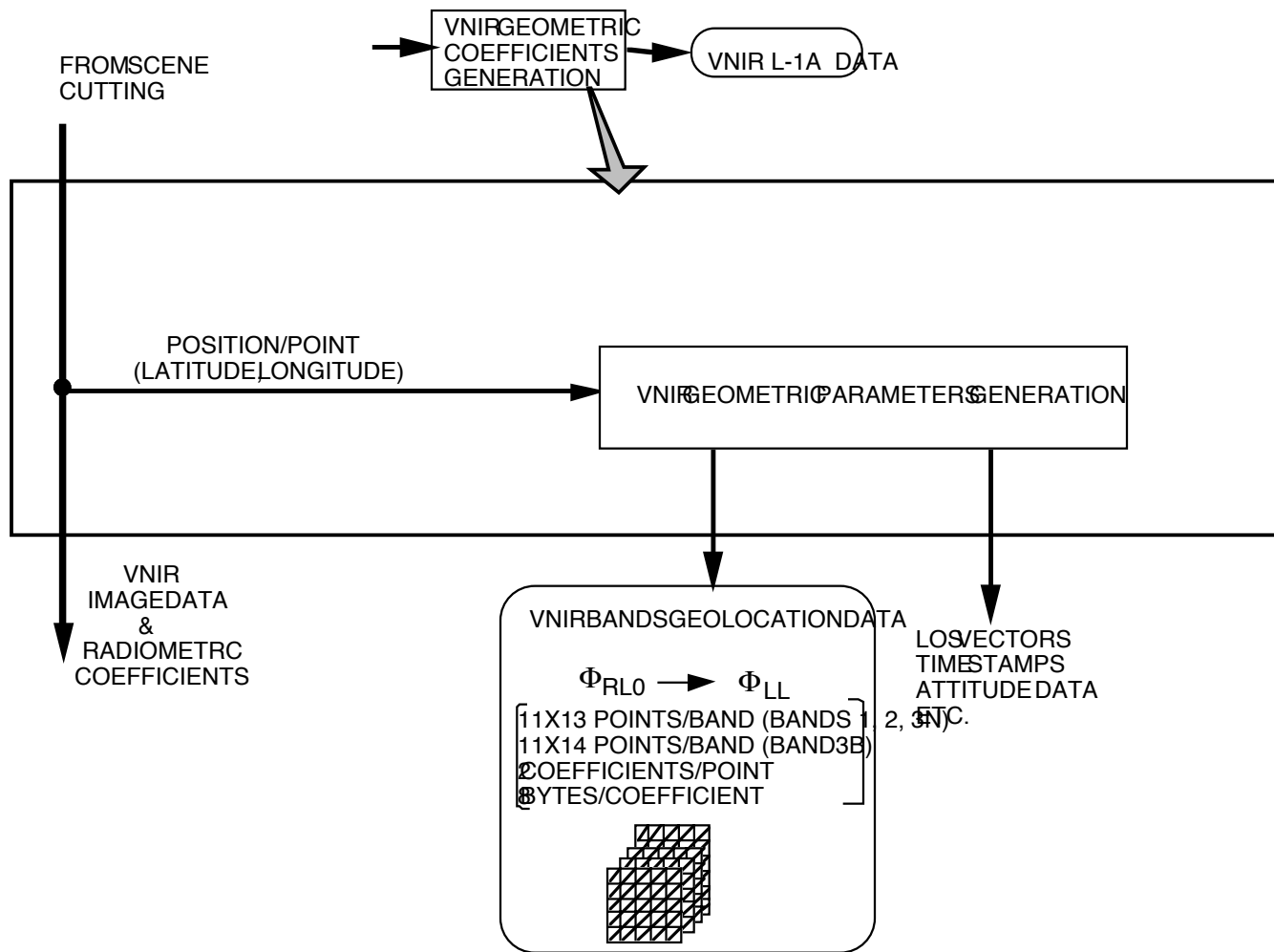
Figure 3-16 VNIR Geometric Coefficients Generation

FROM SCENE
CUTTING

FROM INTER-TELESCOPE
GEOMETRIC CORRECTION

PARALLAX ERROR
&
SWIR/VNIR
INTER-TELESCOPE
REGISTRATION ERROR

POSITION/POINT
(LATITUDE LONGITUDE)

CONSOLIDATION

(SYSTEM CORRECTION + PARALLAX CORRECTION + SWIR/VNIR INTER-TELESCOPE CORRECTION)

SWIR GEOMETRIC PARAMETERS GENERATION

SWIR GEOMETRIC
COEFFICIENTS
GENERATION

SWIR BANDS GEOLOCATION DATA

$$\Phi_{RL0} \longrightarrow \Phi_{LL}$$

99 X 110 POINTS/BAND
2 COEFFICIENTS/POINT
8 BYTES/COEFFICIENT

LOS VECTORS
TIME STAMPS
ATTITUDE DATA
ETC.

SWIR L-1A DATA

SWIR
IMAGE DATA
&
RADIOMETRC
COEFFICIENTS

Figure 3-17   SWIR Geometric Coefficients Generation

FROM SCENE
CUTTING

FROM INTER-TELESCOPE
GEOMETRIC CORRECTION

TIR/VNIR
INTER-TELESCOPE
REGISTRATION ERROR

POSITION/POINT
(LATITUDE,LONGITUDE)

CONSOLIDATION

(SYSTEM CORRECTION + TIR/VNIR INTER-TELESCOPE CORRECTION)

TIR GEOMETRIC PARAMETERS GENERATION

TIR GEOMETRIC
COEFFICIENTS
GENERATION

TIR L-1A DATA

TIR
IMAGE DATA
&
RADIOMETRC
COEFFICIENTS

TIR BANDS GEOLOCATION DATA

$\Phi_{RL0} \longrightarrow \Phi_{LL}$

11 X 13 POINTS/BAND
2 COEFFICIENTS/POINT
8 BYTES/COEFFICIENT

LOS VECTORS
TIME STAMPS
ATTITUDE DATA
ETC.

Figure 3-18 TIR Geometric Coefficients Generation

## 3.10. Level-1A Data Products

Figure 3-19 shows the contents of the Level-1A data products.
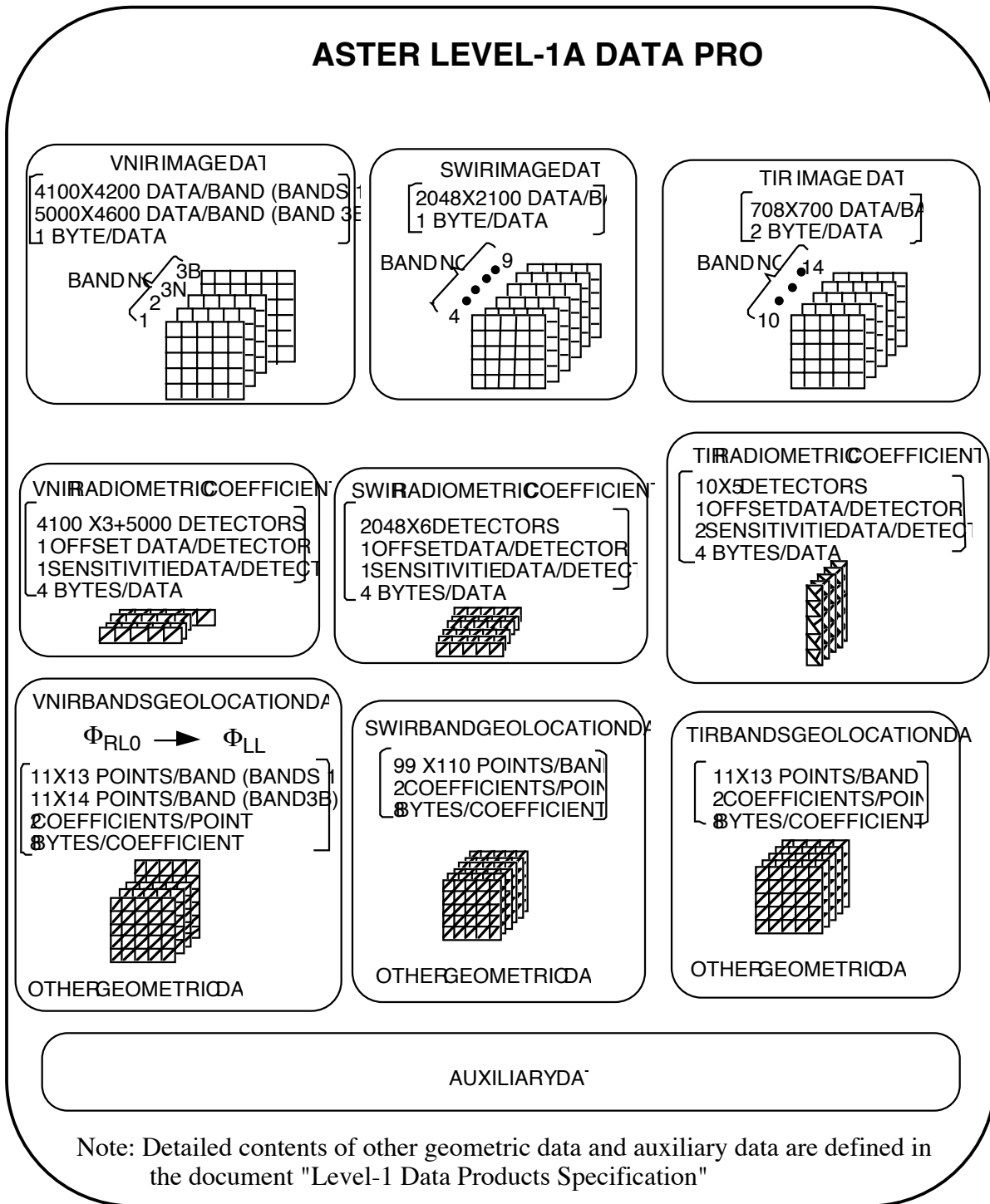


Figure 3-19 Contents of Level-1A

## 3.11. Cloud Coverage Calculation

The ASTER cloud cover assessment algorithm(ACCAA) is an algorithm which estimates the cloud cover fraction of one scene in order to determine whether the SWIR parallax correction process is carried out or skipped.

The ACCAA uses ASTER band 2(VNIR),4(SWIR) and 11(TIR) to determine whether image pixels are cloud contaminated or not. Since the data from all the three telescopes will be used, following consideration will be needed. At first step, image pixel data shall be subsampled so that final pixel number is 7 x 7 pixels for band 11. For band 2 data for corresponding point, shalll be averaged over 42 x 42 pixels and for band 4, over 21 x 21 pixels, considering the pixel size difference of VNIR, SWIR and TIR. Also, notice that this process should be done after the process of system correction of band to band registration. This set of data from bands 2,4 and 11 are called "subsampled pixel data".

At second step, each subsampled pixel data shall be thresholded against band 2 to determine that it is bright and then against band 11 to determine that it is cold. If this subsampled pixel is both highly bright and cold, it shall be assumed that this pixel is either a cloud or a snow/ice feature. At third step, the pixel is again thresholded in band 4 to determine whether it is a cloud or a snow/ice feature. In addition, the image pixel is further thresholded in bands 2 and 4 to determine whether it is an ice or a ice/snow feature.

Flow chart of ACCAA is shown in Figure 3-20. Threshold values are be derived from the experience of EOSAT and depend on sun elevation angle.
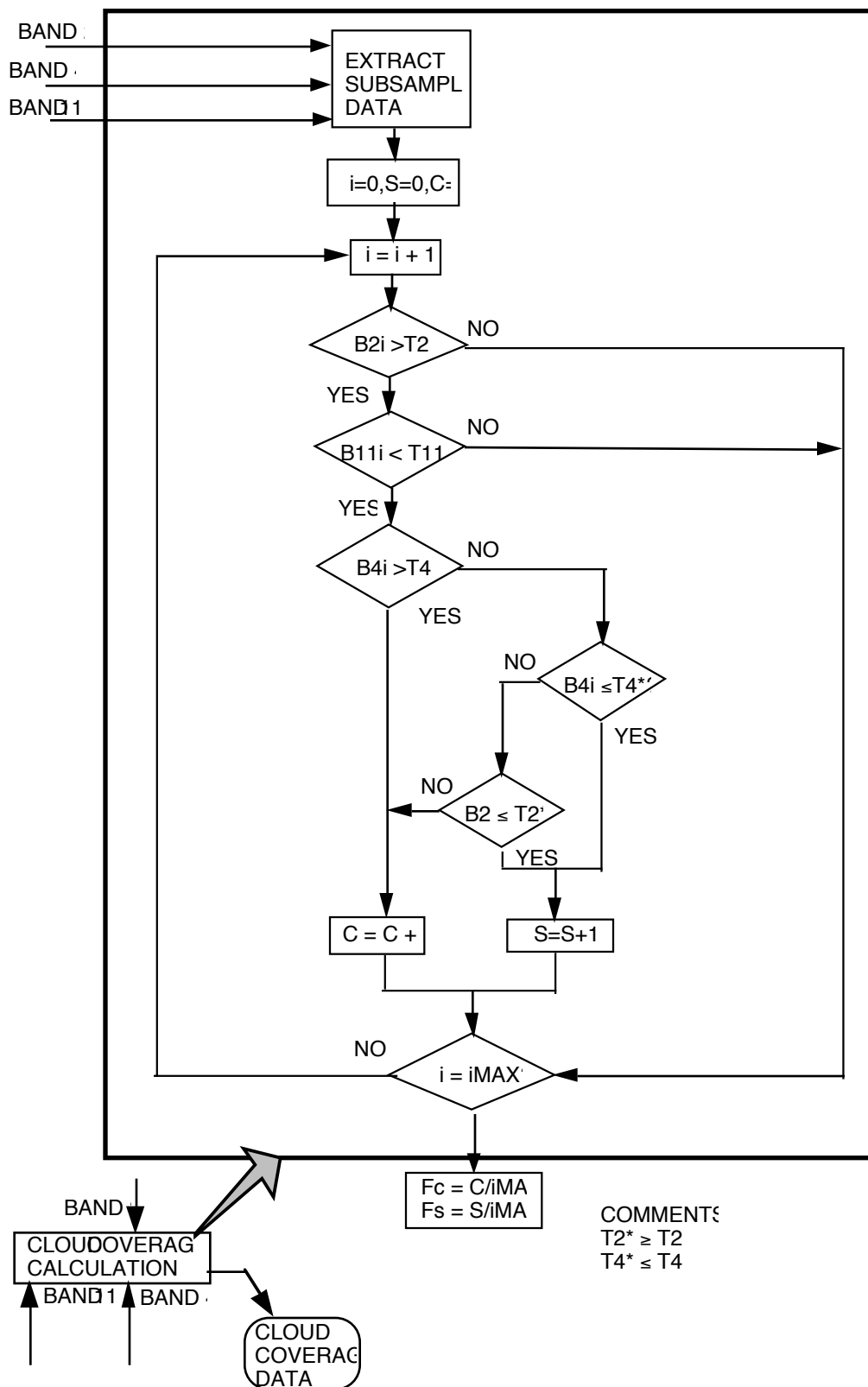
Figure 3-20    Flow Chart of ASTER Cloud and Snow Cover Assessment Algorithm

## 3.12. Level-1B Processing

The Level-1A data product consists of the image data, the radiometric coefficients, the geometric correction coefficients and the auxiliary data. The Level-1B data products will be generated by using these data for the requested map projection and the resampling method.

Figure 3-21 shows the psudo-affin coefficients generation flow for the map projections such as UTM, LCC, SOM, Mercator, Polar Stereo and Uniform Lat/Long. The coordinates transformation from the latitude/longitude to the selected map projection coordinates shall be followed by the coordinates transformation to the Level-1 coordinates expressed by the pixel size units of each band. The path oriented coordinates shall be used rather than the map oriented coordinates in order to keep the image quality as close to the Level-0 data as possible. The pixel sizes of Level-1 are 15 m for VNIR bands, 30 m for SWIR bands and 90 m for TIR bands on the standard lines for each map projection regardless of real pixel sizes which slightly depends on the spacecraft altitude and the pointing angle.

A set of the pseudo-affin transformation coefficients which consists of eight coefficients shall be generated for each block of the Level-1 coordinates by using the relation from the L-0B to the Level-1 coordinates according to the well-established usual procedure. The sizes of the block is the same as those of Level-0 coordinates.
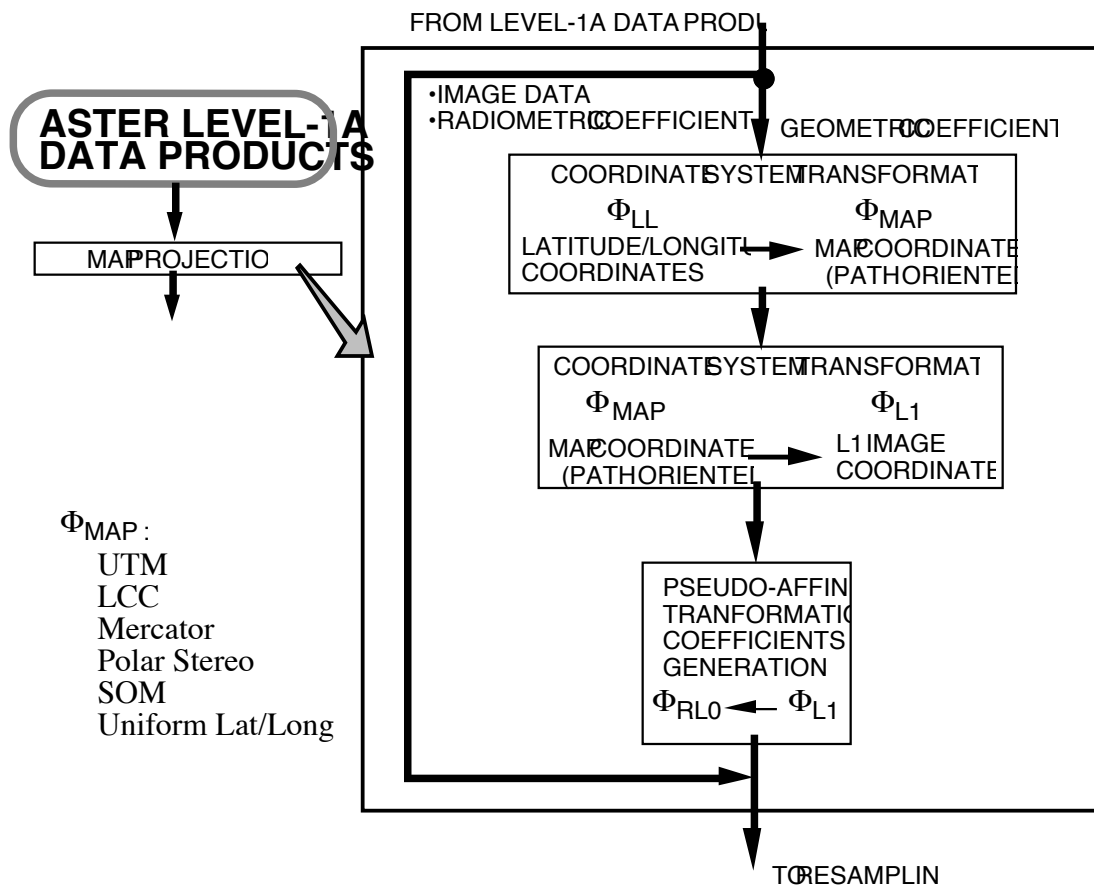


Figure 3-21 Map Projection

Figure 3-22 shows the geometric resampling. All pixel addresses in the Level-1 coordinate system shall be transformed into the realigned (stagger-corrected) L-0B coordinates by which corresponding one, four or sixteen pixel addresses depending on the resampling methods with weight functions are found for resampling. Prior to the resampling, DN values of the bad pixels shall be evaluated by the linear interpolation from the adjacent pixels, followed by the destriping correction for the DN values of the image data.

Resampling shall be carried out using the radiometric coefficients of detectors. The nearest neighbor (NN), the bi-linear (BL) and the cubic convolution methods are considered as types of the resampling. Finally the radiance shall be converted to the DN value using the radiance converdion coefficient of the normal gain and the gain factor which are accommodated in the radiometric data base file.
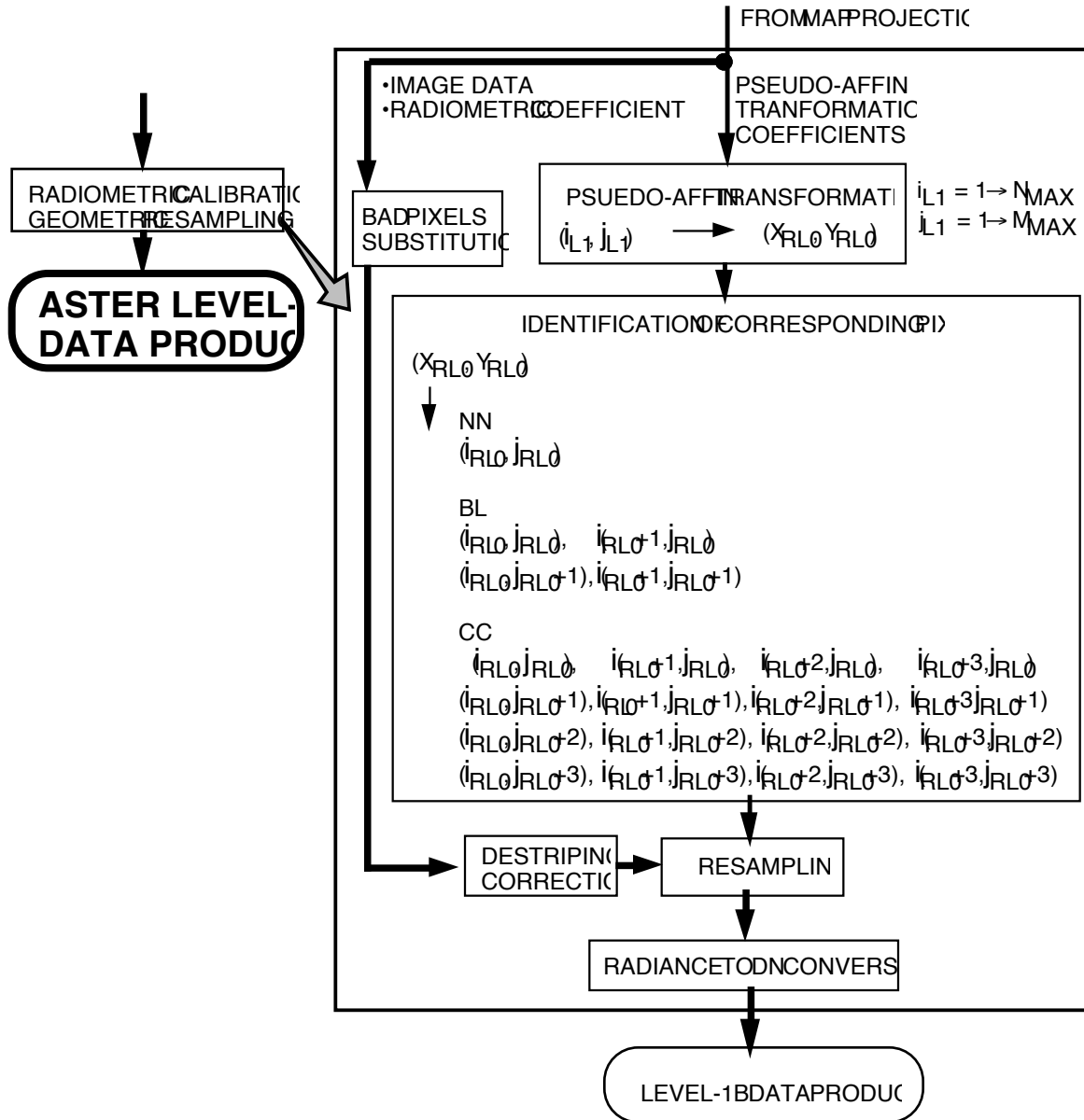


Figure 3-22  Geometric Resampling

### 3.13. Level-1B Data Products

Figure 3-23 shows the Level-1B data products which consist of the image data, the radiance conversion coefficients and the auxiliary data. The contents of the auxiliary data are defined in the document "Level-1 Data Products Specification".
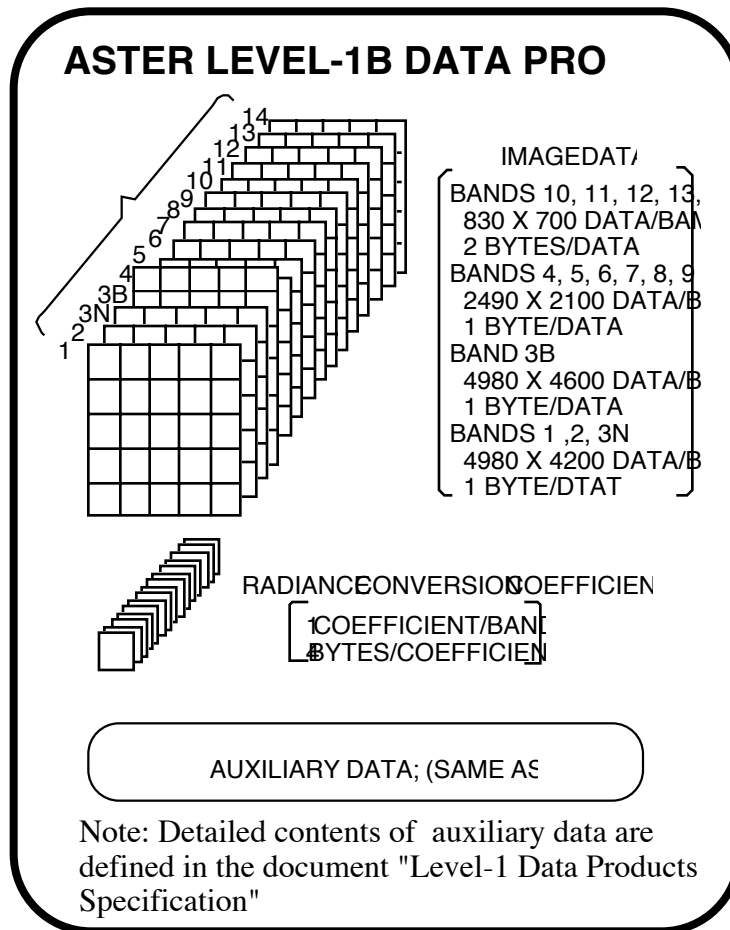


Figure 3-23  Level-1B Data Products

## 4. GEOMETRIC DATA BASE PREPARATION AND CORRECTION PLAN

The VNIR subsystem has two telescopes, that is, one nadir telescope and one backward telescope. While SWIR and TIR subsystems have one telescope for each. The boresight is defined for each telescope as an average direction of all detectors in the same telescope. For SWIR and TIR subsystems a optical path bending due to the pointing mirror shall be included in the boresight vector and the stagger alignment of detectors shall be realigned to the center position. The final products in the geometric data base are summarized in the following two kinds of parameters from which the LOS vectors toward the navigation base reference (NBR) can be calculated for an arbitrary pointing position.

(1) A set of the line of sight (LOS) vectors for the nadir cross-track pointing position toward NBR.

(2) The pointing drive axis vector toward the NBR.

## 4.1. Preflight Activity

## 4.1.1. Preflight Activity during Subsystem Test

During the subsystem preflight test the line of sight (LOS) vectors shall be evaluated toward the boresight coordinate frame of each telescope by using the collimator. The boresight coordinate frame is right-handed and orthogonal. The Z-axis is coaligned with the boresight vector. The Y-axis is a line normal to the Z-axis and to the pointing drive axis. The X-axis is perpendicular to both the Y-axis and the Z-axis to complete the right hand set. It should be noted that the boresight coordinate frame changes depending on the cross-track pointing position. Therefore, the coordinate transformation is necessary to identify the LOS vectors for an arbitrary pointing position. The evaluation process is as follows.

(1) The cross-track pointing shall be set to the predetermined nadir position, because the boresight changes the direction depending on the cross-track pointing position.

(2) The LOS vectors of selected detectors (number is currently TBD) shall be evaluated toward the body-fixed coordinate system of each subsystem at initial stage.

(3) The boresight vector for each telescope shall be calculated from the evaluated LOS vectors according to the definition of the boresight in which the boresight is an average direction of the all detectors. Then the boresight coordinate frame for the nadir pointing position shall be defined for each telescope.

(4) The exact direction of the pointing drive axis toward the boresight coordinate frame shall also be evaluated.

(5) Then, the measured LOS vectors shall be expressed with the boresight coordinate frame by coordinates transformation from the body-fixed to the boresight coordinates

(6) For SWIR and TIR telescopes the stagger configuration of detectors shall be realigned to the center position between the odd and the even alignment lines.

## 4.1.2. Preflight Activity during I & T on Spacecraft

During the integration and test on the spacecraft the nadir boresight coordinates (the boresight coordinates for the nadir position of the cross-track pointing) for each subsystem is aligned to the Spacecraft Reference Axes (Navigation Base Reference) as exactly as possible except for TIR subsystem, which is rotated by 0.3 degree on Z-axis from the exactly coincided position as shown in Figure 2-1. For VNIR subsystem the boresight coordinates shall be represented by the nadir telescope. A small alignment error between each subsystem and the spacecraft can be evaluated by using the instrument cube of each subsystem and the spacecraft cube. Then the LOS vectors and the boresight vectors toward Navigation Base Reference (NBR) can be obtained with the coordinate transformation by an alignment error between two coordinate system. The boresight shall be as close to the Z-axis of NBR as possible.

The final product during the preflight test is the preliminary geometric data base (Version 0) which contains a set of the LOS vectors toward the NBR as shown in Figures 4-1. The cross-track pointing axis which is expressed toward the NBR is also a part of the geometric data base.

## 4.2. In-Flight Initial Checkout Activity

The LOS vectors measurements with the collimator during the preflight test may not be accurately enough for the precise band-to-band registration. Real image data are indispensable for it. However, It is not possible to have focused image data during the preflight test activity on the ground. Therefore, a fine tune-up process based on acquired image data will be necessary for the preparation of the geometric data base with an accuracy for the operational use. This process shall be carried out during the in-flight initial checkout period which is scheduled for three months just after the launch. The special Level-1B products without the SWIR parallax and the inter-telescope corrections shall be used for this purpose.

In addition, there is a strong possibility to enhance the pixel geolocation knowledge (PGK) by evaluating a static error of the pointing information by comparing an acquired image with GCP (Ground Control Point). A specified value of PGK is 437 m which can be evaluated from a position knowledge of 150 m and a boresight pointing knowledge of 120 arcsec. By considering that these design values of the knowledge for the flight model is much better than the specified values and that the majority part of the pointing knowledge is static, a PGK of about 50 m may be anticipated, if the static error is removed.

The initial checkout activity for the geometric data base consists of three parts, that is, an intra-telescope registration error correction, an inter-telescope registration error correction and a geolocation error correction. The correction process flow is shown in Figure 4-2.

### 4.2.1. Intra-telescope Registration Correction

The intra-telescope registration error detection shall be carried out for all bands relative to the reference band of each subsystem, that is, band 2 for VNIR, band 4 for SWIR and band 11 for TIR. The image matching techniques shall be used for the error detection relative to the reference band. An elevation information of the target subscene for the image matching is necessary for compensating the parallax error of SWIR. Therefore, the scenes for this purpose shall be same as those specially prepared for the geolocation correction described in Section 4.2.3. The correction procedure is as follows. The special Level-1B products without the SWIR parallax and the inter-telescope corrections shall be used for this purpose.

   (1) Several subscenes with GCP information are selected in a scene as correlation windows of which sizes are tentatively set to 42 x 42 pixel for VNIR, 21 x 21 pixels of SWIR and 7 x 7 pixels for TIR.

(2) Matching error components in both the along-track (X-axis) and the cross-track (Y-axis) directions are evaluated for each subscene. Subpixel resampling may be carried out if necessary.

(3) For SWIR the parallax error is calculated from the elevation information of GCP and subtracted from the image matching error in the along-track direction to evaluate alignment error only.

(4) The error is applied to one closest detector correspond to the center of each subscene.

(5) The LOS vector errors for roll, pitch and yaw components of these selected detectors can be evaluated from these error data.

(6) The LOS vectors of other detectors can be evaluated with the linear interpolation method.

This correction will be very small and a few arcseconds at most judging from the accuracy of the preflight measurements. This intra-telescope registration correction will be necessary only for the in-flight initial checkout period, because the detector alignment in the same telescope is considered to be very stable. This stability is specified within ±0.2 pixels during the life of the instrument as shown in Table 2-15.

## 4.2.2. Inter-telescope Registration Correction

The inter-telescope registration error detection shall be carried out for band 6 for SWIR and band 11 for TIR relative to the reference band 2. The image matching techniques shall be used for the error detection relative to the reference band. The parallax error among the reference bands is very small. Therefore, the scenes for this purpose will not be necessarily same as those specially prepared for the geolocation correction including GCP information but be preferable to be same as those for consistency throughout the geometric correction process. The correction procedure is as follows.

(1) Several subscenes for the image matching are selected in a scene as correlation windows of which sizes are tentatively set to 42 x 42 pixel for VNIR, 21 x 21 pixels of SWIR and 7 x 7 pixels for TIR.

(2) Matching error components in both the along-track (X-axis) and the cross-track (Y-axis) directions are evaluated for each subscene. Subpixel resampling may be carried out if necessary.

(3) The error is applied to one closest detector correspond to the center of each subscene.

(4) The LOS vector errors for roll, pitch and yaw components of these selected detectors can be evaluated from these error data.

(5) All LOS vectors of bands 4 and 11 can be evaluated with the linear interpolation method.

(6) The same LOS vector errors as bands 4 and 11 are applied to all other SWIR and TIR bands.

In this correction process pixel size adjustment among different telescopes is most important and will be kept in the same value during the mission life. At the same time a static component of the misalignment among different telescopes can be evaluated in the flight condition. Therefore, only dynamic part of the misalignment including the pointing knowledge in the cross-track direction is necessary to be corrected by the image matching during the normal operation phase

### 4.2.3. Geolocation Correction

The geolocation error detection shall be carried out only for band 2. The geolocation accuracy for other bands may be guaranteed through intra- and inter-bands registration processes. The special GCP file is planned to be prepared for the this geolocation error detection using JERS-1 data with a spatial resolution of 18 m. About 30 scenes with 10 - 20 GCPs will be prepared throuout the world. At least 30 data will be necessary for statistically evaluating the static pointing error. Considering the cloud coverage probability about 300 GCP will be prepared for this purpose. The correction procedure is as follows.

(1) The scenes of VNIR band 2 which include the specially prepared GCP chips for this purpose are selected.

(2) Matching error components with GCP chips in both the along-track (X-axis) and the cross-track (Y-axis) directions are evaluated for each subscene.

(3) The LOS vector error based on the spacecraft position and the boresight pointing errors can be evaluated from these image matching error data for each scene with GCPs.

(4) The error correction for band 2 shall be applied to all LOS vectors of all bands

A major purpose of this correction process is to evaluate a static pointing error as a whole including the spacecraft and the instrument. The static error shall be finally determined from a lot of error data during the initial checkout period and will probably be kept in the same value during the mission life. The static error correction shall be applied to all LOS vectors of all bands.

The final product during the in-flight initial checkout period is to prepare the geometric data base for the normal operational use by tuning up the preliminary data base. The initial data base for the normal operation is named the data base (Ver. 1).

### 4.3. In-Flight Verification Activity

As described in the previous section the intra-telescope band-to-band registration will be kept in the same condition throughout the mission life as the initial checkout period. The inter-telescope band-to-band registration is to be carried out routinely in the Level-1 processing by the image matching to compensate a dynamic part of the pointing stability as described in the Section 3.6. Therefore, a special verification activity by the science team will not be necessary for the geometric data base correction regarding the band-to-band registration. Usual quality check of the data products will be enough to keep it

Although the geolocation knowledge is also considered to be kept in the enhanced value throughout the mission life after a removal of the static pointing error during the initial checkout period, a special verification activity will be important on the geolocation knowledge, because it can not be done by the usual quality check of the data products. This activity will also be useful to monitor instrument pointing behavior as a whole including both instrument and the spacecraft.

This verification activity is planned to be carried out whenever the instrument acquires the good image data of the scenes with a lot of GCPs which is specially prepared for this activity. The GCP file is same as that prepared for the initial checkout activity. Figure 4-3 shows the verification activity flow for the geometric data base during the normal operation which is basically same as the geolocation correction part of the initial checkout period. Judgment will

be done for the data base update if an average pointing error during TBD operation period (tentatively 3 months) exceeds some threshold value.


## 4.4.  GCP  Preparation  Plan

The GCP preparation is planned for the absolute calibration of the line of sight vectors and the pointing axes of each telescope.  This calibration activity is important to keep the geolocation accuracy and will have to be carried out intensively during the initial checkout period. Even in the normal operation period the prepared GCPs will be used for routine verification activity of the geolocation accuracy.  The geometric data base shall be updated considering the results if necessary.  The planned GCPs are shown below.

(1) Standard GCP
   Purpose: absolute calibration of the LOS vectors of band 2
   Accuracy: ±15 m or better for X and Y components,  ±50 m or better for Z component
   Location: Within ± 26 km from the nominal orbit
   Number: About 300 points at launch for initial checkout activity and TBD points for
        verification activity during normal operation period
   Position determination : digitized using maps with a scale of 1/24,000 or 1/25,000.

(2) High Quality GCP
   Purpose: absolute calibration of the pointing axis direction
   Accuracy: ±1.5 m (TBR) or better for X and Y components, ±2.5 m (TBR) or better for
        Z component
   Location: about 100 km away from the nominal orbit
   Number: 20 - 30  points at launch for initial checkout activity and TBD points for
        verification activity during normal operation period
   Position determination : measured with differential type GPS.

Table 4-1 shows  the candidate of Landsat scenes to prepare the GCPs, specifically for the initial checkout activity.  About 10 GCPs will be selected for each scene.  Additional GCPs are planned to prepare for verification activity during the normal operation period, although the details are TBD in current stage.

Table 4-1  Selected Landsat Scenes for GCP Preparation

| Area | Path/Row No | Average Cloud Coverage (%) | | |
|---|---|---|---|---|
| | | July | August | September |
| U.S.A. | 015/032 - 035 | 53 - 57 | 55 | 47 - 53 |
| | 026/033 - 036 | 34 - 39 | 39 - 43 | 39 - 46 |
| Australia | 091/076 - 078 | 27 - 33 | 24 - 29 | 21 - 27 |
| | 092/077 - 079 | 24 - 27 | 21 - 24 | 21 |
| | 092/084 - 086 | 34 - 49 | 32 - 48 | 21 - 48 |
| | 090/089 - 090 | 56 - 64 | 57 - 66 | 61 - 68 |
| Thailand | 129/047 - 049 | 82 - 85 | 85 - 87 | 71 - 80 |
| | 130/048 - 050 | 87 - 89 | 87 - 91 | 71 - 80 |
| France | 199/027 - 029 | 38 - 47 | 42 - 51 | 40 - 47 |
| Japan | 107/029 - 036 | 66 - 76 | 53 - 73 | 61 - 72 |
| | 108/035 | 68 | 53 | 68 |
| | 110/035 | 73 | 57 | 72 |
| | 112/037 | 68 | 56 | 67 |
| | 113/037 | 68 | 56 | 67 |

PREFLIGHT ACTIVITY

Note
LOS; Line of Sight Vector
NBR; Navigation Base Reference
(Spacecraft Reference Axes)

EVALUATION DURING
SUBSYSTEM TEST

MISALIGNMENT OF BORESIGHT
COORDINATES FOR EACH
TELESCOPE TOWARD NBR
· VNIR NADIR TELESCOPE
· VNIR STEREO TELESCOPE
· SWIR TELESCOPE
· TIR TELESCOPE
(ROLL, PITCH, YAW)

EVALUATION DURING
INTEGRATION AND TEST
ON SPACECRAFT

VNIR NADIR BANDS LOS VECTORS
FOR SELECTED DETECTORS
TOWARD VNIR NADIR TELESCOPE
BORESIGHT COORDINATES
· TBD VECTORS/BAND
· 3 DATA/VECTOR

COORDINATE SYSTEM TRANSFORMATION
$\Phi_{VNIR \cdot NADIR}$     $\Phi_{S/C}$
VNIR NADIR TEL BORESIGHT COORDINATES → SPACECRAFT NBR COORDINATES

CALCULATION OF LOS VECTORS
FOR ALL VNIR NADIR BANDS
DETECTORS
(INTERPOLATION)

VNIR STEREO BAND LOS VECTORS
FOR SELECTED DETECTORS
TOWARD VNIR STEREO TELESCOPE
BORESIGHT COORDINATES
· TBD VECTORS/BAND
· 3 DATA/VECTOR

COORDINATE SYSTEM TRANSFORMATION
$\Phi_{VNIR \cdot STEREO}$     $\Phi_{S/C}$
VNIR STEREO TEL BORESIGHT COORDINATES → SPACECRAFT NBR COORDINATES

CALCULATION OF LOS VECTORS
FOR ALL VNIR STERO BAND
DETECTORS
(INTERPOLATION)

V/G-DB
(VER. 0)

SWIR BANDS LOS VECTORS
FOR SELECTED DETECTORS
TOWARD SWIR TELESCOPE
BORESIGHT COORDINATES
· TBD VECTORS/BAND
· 3 DATA/VECTOR

STAGGER REALIGNMENT

COORDINATE SYSTEM TRANSFORMATION
$\Phi_{SWIR}$     $\Phi_{S/C}$
SWIR TEL BORESIGHT COORDINATES → SPACECRAFT NBR COORDINATES

CALCULATION OF LOS VECTORS
FOR ALL SWIR BANDS
DETECTORS
(INTERPOLATION)

S/G-DB
(VER. 0)

TIR BANDS LOS VECTORS
FOR SELECTED DETECTORS
TOWARD TIR TELESCOPE
BORESIGHT COORDINATES
· TBD VECTORS/BAND
· 3 DATA/VECTOR

STAGGER REALIGNMENT

COORDINATE SYSTEM TRANSFORMATION
$\Phi_{TIR}$     $\Phi_{S/C}$
TIR TEL BORESIGHT COORDINATES → SPACECRAFT NBR COORDINATES

CALCULATION OF LOS VECTORS
FOR ALL TIR BANDS
DETECTORS
(INTERPOLATION)

T/G-DB
(VER. 0)

Figure 4-1  Preliminary Geometric Data Base Preparation  during Preflight Test Period

# IN-FLIGHT ACTIVITY
# (INITIAL CHECKOUT PERIOD)

V/G-DB (VER. 0)

S/G-DB (VER. 0)

T/G-DB (VER. 0)

VECTOR TRANSFORMATION BY MISALIGNMENT OF LOS VECTORS FOR ALL DETECTORS

V/G-DB (VER. 1)

S/G-DB (VER. 1)

T/G-DB (VER. 1)

Note
LOS; Line of Sight Vector
NBR; Navigation Base Reference
(Spacecraft Reference Axes)

OVERALL LOS VECTORS ERROR CALCULATION OF ALL BANDS
•ANGLE(ROLL,PITCH,YAW)

ALL BANDS

INTRA-TELESCOPE REGISTRATION ERROR DETECTION
•RELATIVE TO BAND 2 FOR VNIR
•RELATIVE TO BAND 6 FOR SWIR
•RELATIVE TO BAND 11 FOR TIR
(IMAGE MATCHING)

LOS VECTORS ERROR CALCULATION
•RELATIVE TO BAND 2 FOR VNIR
•RELATIVE TO BAND 6 FOR SWIR
•RELATIVE TO BAND 11 FOR TIR
(ROLL,PITCH,YAW)

LEVEL-1B DATA PRODUCTS WITHOUT SWIR PARALLAX AND INTER-TELESCOPE REGISTRATION CORRECTIONS

SELECTION OF SCENES WITH GCP INFORMATION FOR EVALUATION

BAND 2
BAND 6
BAND 11

INTER-TELESCOPE REGISTRATION ERROR DETECTION RELATIVE TO BAND 2
•TBD POINTS/SCENE
(IMAGE MATCHING)

LOS VECTORS ERROR CALCULATION RELATIVE TO BAND 2
(ROLL, PITCH, YAW)

BAND 2

GCP FILE

GEOLOCATION ERROR DETECTION OF BAND 2
•TBD POINTS/SCENE
(GCP MATCHING)

LOS VECTORS ERROR CALCULATION OF BAND 2
(ROLL, PITCH, YAW)

Figure 4-2 Tune-up Activity for Geometric Data Base during Initial Checkout Period

IN-FLIGHT ACTIVITY
(NORMAL OPERATION PERIOD)

Note
LOS; Line of Sight Vector
NBR; Navigation Base Reference
(Spacecraft Reference Axes)

V/G-DB (VER. N+1)
S/G-DB (VER. N+1)
T/G-DB (VER. N+1)

V/G-DB (VER. N)
S/G-DB (VER. N)
T/G-DB (VER. N)

VECTOR TRANSFORMATION BY MISALIGNMENT OF LOS VECTORS FOR ALL DETECTORS

JUDGMENT FOR REVISION    YES

LOS VECTORS ERROR CALCULATION OF BAND 2 (ROLL, PITCH, YAW)

GEOLOCATION ERROR DETECTION OF BAND 2
• TBD POINTS/SCENE
(GCR MATCHING)

SELECTION OF SCENES WITH BAND 2 GCP INFORMATION FOR EVALUATION

LEVEL-1B DATA PRODUCTS WITHOUT SWIR PARALLAX AND INTER-TELESCOPE REGISTRATION CORRECTIONS

GCF FILE

Figure 4-3  Verification Activity for Geometric Data Base during Normal Operation Period

# 5. RADIOMETRIC DATA BASE   PREPARATION AND CORRECTION PLAN

## 5.1   Preflight   Activity

### 5.1.1.   Preflight   Activity   Overview

Figures 5-1, 2 and 3 show activities for radiometric calibration coefficients determination for VNIR, SWIR and TIR, respectively, in the preflight phase.  Performances of gain, offset, non-linearity, stray light and bright target recovery are being measured for PFM.   Such performances have temperature depndence so that temperature dependence is also being measured and characterized.  These measured data are converted to Radiometric Calibration Coefficients(RCCs) and temperature coefficients which are contents of the radiometric correction data base files.

At an initial stage of the preflight activity VNIR will be calibrated against a working standard large integrating sphere source whose radiance is traceable to the primary standard copper-and-silver point blackbodies. The preflight radiometric correction coefficients(RCCs) will be determined together with the offset signal.  Bright target recovery and stray light effect will be measured and might be applied to the Level 1 processing, if necessary.

For SWIR, the preflight RCCs will be obtained by measurements of a working standard large integrating sphere source whose radiance is traceable to the primary standard zinc-, lead- and tin- point blackbodies.  The offset signal will be determined for a zero radiance input.  The silicon photodiodes that monitor the on-board calibrator lamp outputs will be calibrated with respect to the integrating sphere source by transfer through SWIR.

Radiance monitor data together with wavelength correction data, silicon photodetector temperature, dewar temperature, calibration circuit temperature and electronics temprature will also be gathered for SWIR.  These are to be used in Level 1 processing. Bright target recovery and stray light effect will also be measured for SWIR and might be applied in the Level 1 processing.

TIR will be calibrated in preflight against a standard blackbody in a vacuum chamber.  The temperature of the standard blackbody will be changed from 100 K to 370 K.  The calibration will be carried out at various chopper and lens temperatures.  The radiance will be transferred through TIR to the on-board blackbody.

Offset term of the radiometric calibration coefficnets is a function of detector temperature, ,optics temperature, barrel temperature and also chopper temperature so that these temperatures will be monitored for correction. For non-linearity,  a quadratic form of the relationship between input radiances and output voltage is to be determined as a prelaunch data while radiance-brightness temperature relationship will also be characterized.  Besides, stray light effect will be measured and might be applied in Level 1 processing in the prelaunch phase.

During the preflight calibration and characterization of the EOS-AM1 instruments, there will be a cross-calibration activity to compare the absolute radiometric calibrations of ASTER, MISR, MODIS and MOPITT.   This activity will involve the use of several ultra-stable transfer radiometers that will be used to compare the integrating sphere sources and blackbodies (where applicable) used to calibrate these instruments. The transfer radiometers will be provided and operated by personnel from GSFC/NIST, NRLM and UofA.  The cross-calibrations will be conducted in ambient for bands in the solar-reflective range and in vacuum for the thermal infrared. The measurements are to be conducted immediately before or after the final preflight calibrations of the ASTER.

The results of these cross-calibrations will be analized to determine the magnitude of any systematic differences between the absolute calibrations of the preflight calibraion source. Any such differences may be used to modify the preflight calibration coefficients of the instrument.

PRELAUNCH ACTIVITIES(VNIR)
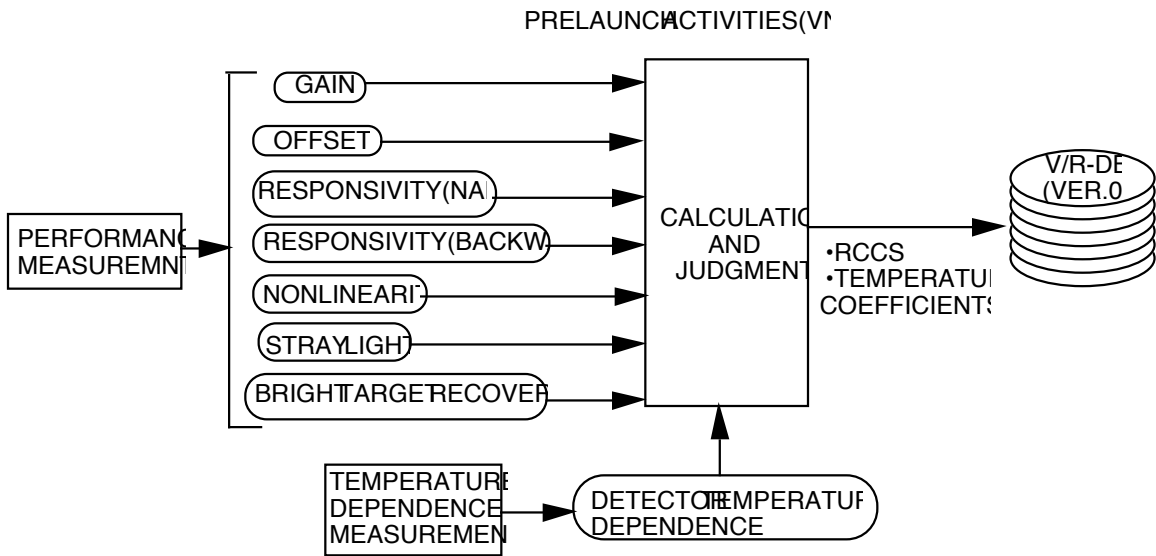
Figure.5-1  Prelaunch Calibration Activities for VNIR

PRELAUNCH ACTIVITIES(SWIR)
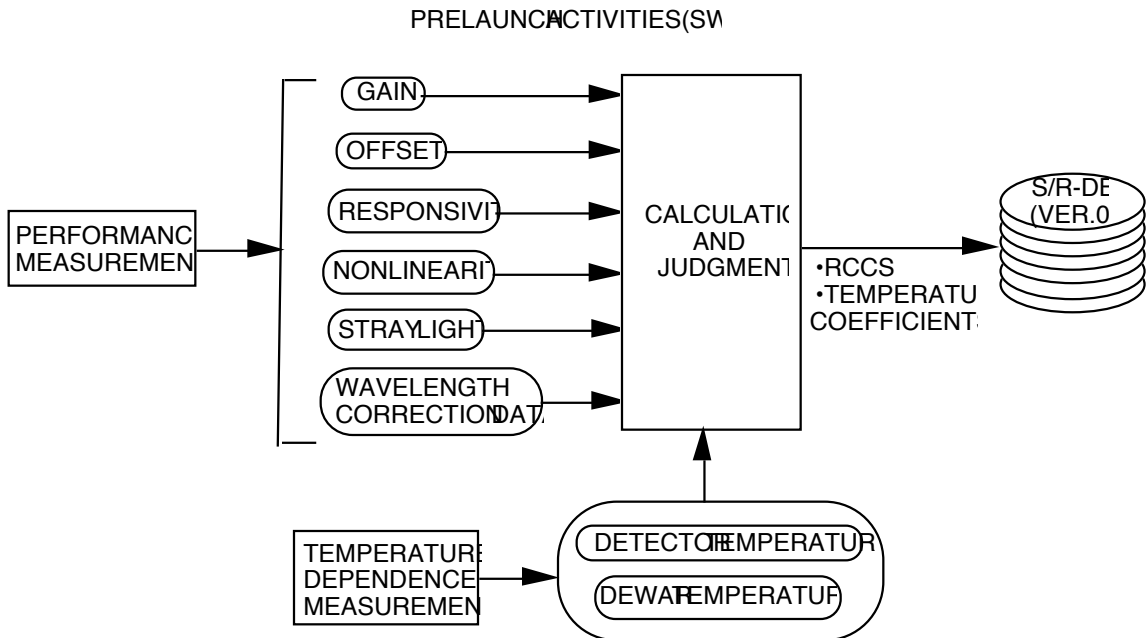
Figure 5-2  Prelaunch Calibration Activities for SWIR
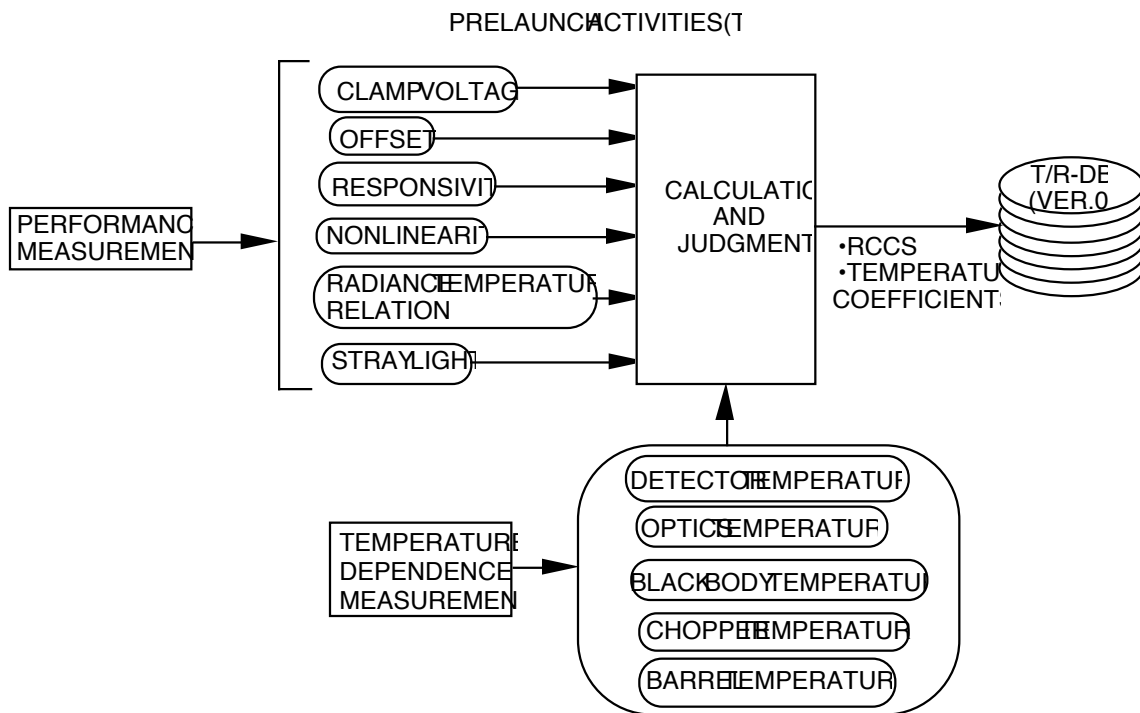
Figure 5-3  Preflight Calibration Activities for TIR

## 5.1.2.  More Detailed Preflight Activity

More detailed preflight activity are shown below for the case of VNIR as examples.  Similar activities are considered for SWIR and TIR, although they are not completely same as VNIR.

(1) Before Thermal Vacuum Chamber (TVC) test

- Calibration against a large integrating sphere (LIS) for all elements of Bands 1 to 3 nadir (3n) and 3 backward (3b) at ambient temperature and ambient pressure (ATP).

- Measurement of each on-board lamp (OBL) for all elements of Bands 1 to 3n at ATP just after the LIS calibration. Transfer of the calibrated value of 1) to each OBL.

(2) At TVC test
- Calibration against an LIS for center elements of Bands 1 to 3n and 3b at a TVC. Comparison of calibration data between ATP and TVC test.  This is for the measurement of the vacuum shift of the radiometer and ambient temperature influence test.

- Measurement of each OBL for all elements of Bands 1 to 3n at TVC just after the LIS calibration.  Transfer of the calibrated value of 1) to each OBL.  Comparison of calibration data between ATP and TVC test.  This is for the measurement of the vacuum shift of the OBL and ambient temperature influence test.

(3) After TVC test and before integration to ASTER system
- Calibration against an LIS for all elements of Bands 1 to 3n and 3b at ATP. Comparison of calibration data with previous results.

- Measurement of each OBL for all elements of Bands 1 to 3n at ATP just after LIS calibration. Transfer of the calibrated value of 1) to each OBL.  Comparison of calibration data from previous results.

- A review meeting will be held at this stage to determine the final prelaunch radiometric coefficients.

- The result will be reported in English to Joint ASTER team after PSR.

(4) After ASTER system integration and before shipment to U.S.A. (ASTER System Level Test)
  - Calibration against each OBL for all elements of Bands 1 to 3n at ATP and at TVC. Check of the stability of the calibrated value of (3).

(5) At USA before integration to EOS AM-1 (Bench Acceptance Test)
  - Calibration against each OBL for all elements of Bands 1 to 3n at ATP. Check of the stability of the calibrated value of (3).

(6) At USA after integration to EOS AM-1 (EOS AM-1 System Level Test)
  - Calibration against each OBL for all elements of Bands 1 to 3n at ATP and TVC. Check of the stability of the calibrated value of (3).

  - A review meeting will be held at this stage.

(7) Launch Site Test
  - Calibration against each OBL for all elements of Bands 1 to 3n at ATP. Check of the stability of the calibrated value of (3).

(8) Prelaunch Cross-Calibration

| | |
|---|---|
| Purpose | Check the preflight calibration of the calibration source of the each instrument of EOS AM-1 |
| Method | Cross-calibration using round-robin radiometers |
| Participants | NRLM, U. of Arizona, NIST and NASA GSFC |
| Instruments | ASTER VNIR, MODIS and MISR |
| Dates | First one for ASTER VNIR: February 21-22 in 1995 at NEC. First one for MODIS: Later than May in 1996. Second one for ASTER VNIR and SWIR: Later than May in 1996. Thermal round-robin by NIST in 1997. |
| Uncertainty | 2 % (TBR) |
| Note | If the agreement is worse than 3 % (TBR), the prelaunch calibration system will be reviewed severely. However the correction of coefficients using cross-calibration data will not be done. |

## 5.2.  Initial  Checkout  Activity

### 5.2.1.  Initial  Checkout  Activity  Overview

The inital in-flight calibration will be carried out during the three-month activation and elevation phase.  Using the earth images at night for the offset signal and the on-board lamp calibration data, the first in-flight RCCs will be obtained and compared to the preflight data.  Figures 5-4, 5-5 and 5-6 show activities for radiometric correction coefficients confirmation and refinement for VNIR, SWIR and TIR, respectively in initial checkout phase.

Calibration offset, electric calibration and optical calibration data are used for refinement of the coefficients for offset, responsivity(Nadir), responsivity(Backward) for VNIR.  As the results, VNIR radiometric data base file will be updated from Ver.0 to Ver.1.

On the other hand, calibration offset data of SWIR and optical calibration data are used for refinement of the coeffiecients for offset, responsivity.  In this connection, optical calibration data are to be corrected with radiance monitor output and calibration lamp voltage.  Then SWIR radiometric data base file will also be updated from Ver.0 to Ver.1.

Meanwhile, 270 K of the brackbody onboard on TIR will be used for the refinement of the correction coefficients of the offset. 270 K of brackbody temperature is observed in both before and after the observation.  Together with the difference between chopper and clamp temperature, offset term will be determined.  Four temperature of the onboard brackbody with the range of 270 K to 340 K will be used for refinement of the correction coefficients of the responsibity and the offset terms.  TIR ratiometric data base file will be updated from Ver.0 to Ver. 1.
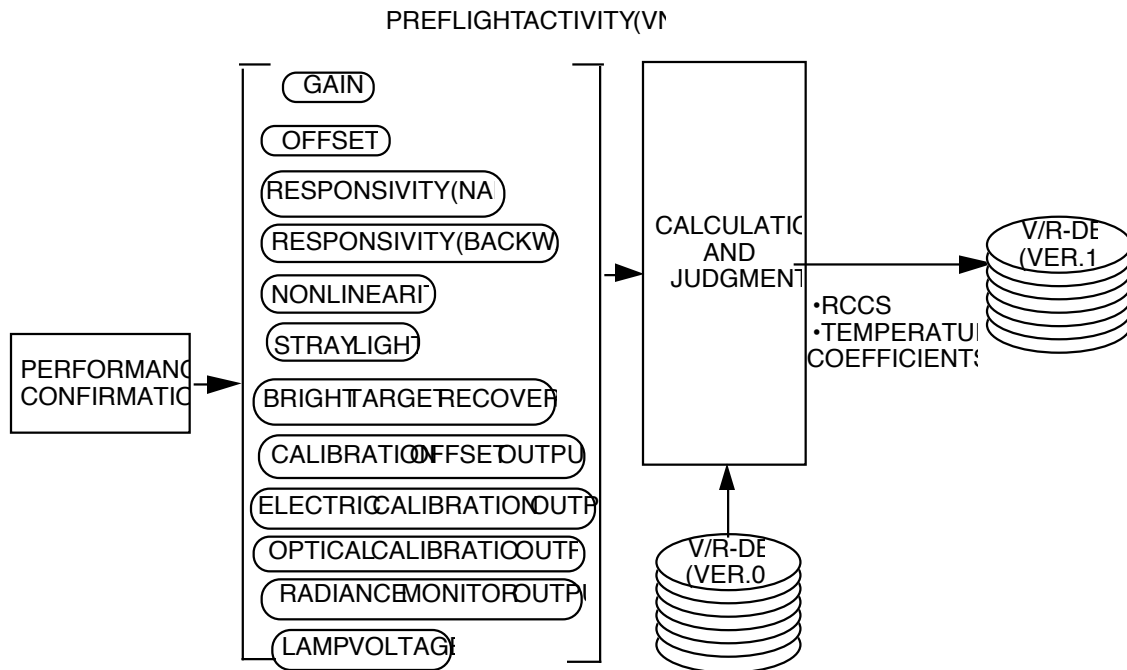


Figure 5-4  Initial Checkout Activity for VNIR

**PERFORMANC CONFIRMATIC**

- GAIN
- OFFSET
- RESPONSIVIT
- NONLINEARI
- STRAYLIGHT
- WAVELENGTH CORRECTION DAT
- CALIBRATION OFFSET OUTP
- OPTICAL CALIBRATION OUTP
- RADIANCE MONITOR OUTP
- LAMP VOLTAG

**CALCULATIO AND JUDGMENT**

•RCCS
•TEMPERATU
COEFFICIENTS

S/R-DE (VER.1

S/R-DE (VER.0
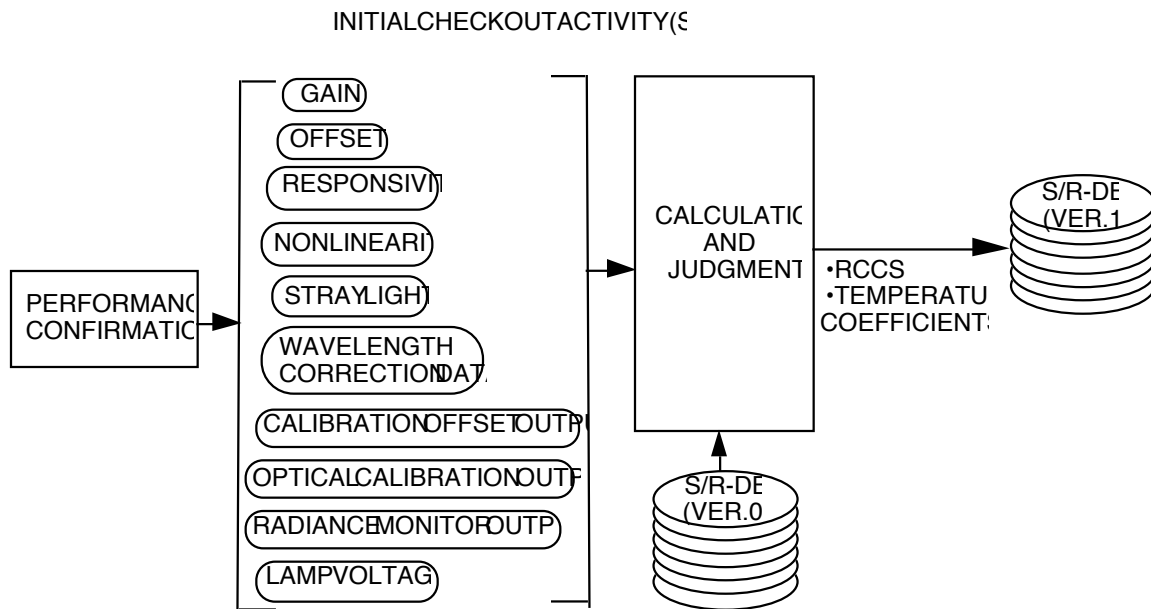
Figure 5-5  Initial Checkout Activity for SWIR

**PERFORMANC CONFIRMATIC**

- CLAMP VOLTAG
- OFFSET
- RESPONSIVIT
- NONLINEARI
- RADIANCE TEMPERATUI RELATION
- STRAYLIGHT
- 270K BLACKBODY TEMPERATI
- 270-340K BLACKBODY TEMPERA

**CALCULATIO AND JUDGMENT**

•RCCS
•TEMPERATU
COEFFICIENTS

T/R-DE (VER.1

T/R-DE (VER.0
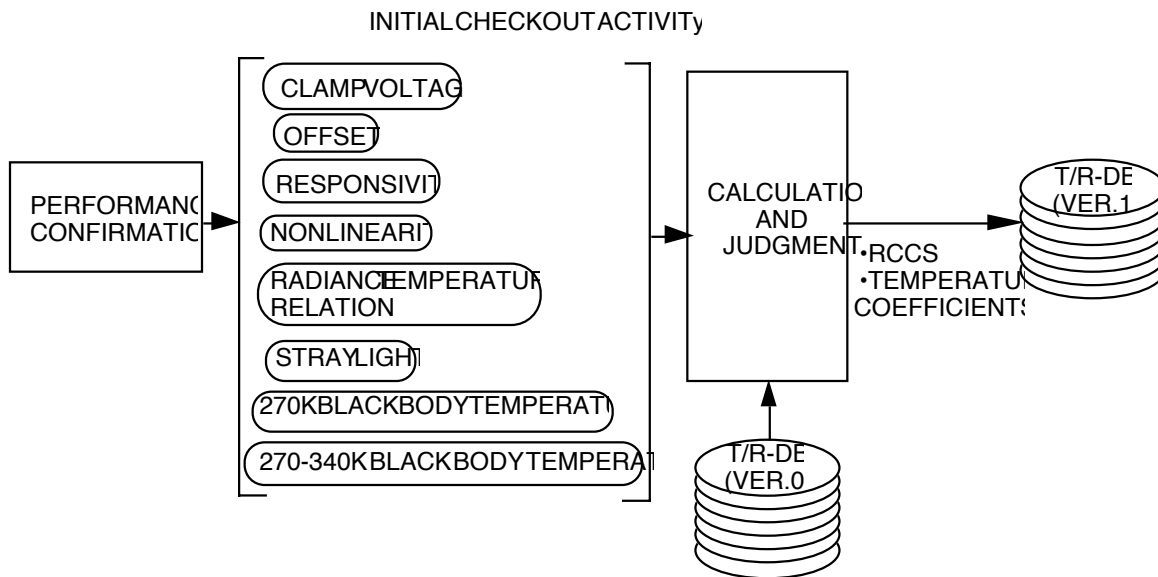
Figure 5-6  Initial Checkout Activity for TIR

## 5.2.2. On-board Calibration during Initial Checkout Period

Calibration against each on-boad calibration lamps for all elements of Bands 1 to 3n is carried out as follows.  Monitor output will be checked if the VNIR output show some change.  A proposal for the frequency of OBL calibration is as follows.

| Frequency | Repeatedtimes | Subtotal |
|---|---|---|
| Once Every Day | Four times | 4 Days |
| Every Two Days | Four times | 8 Days |
| Every Four Days | Two times | 8 Days |
| Every Eight Days | Two times | 16 Days |
| Total | 12times | 36 Days |

## 5.2.3. Vicarious Calibration Activity during Initial Checkout Period

Two kinds of the vicarious calibrations are planned.  The vicarious calibration 1 will be carried out at Deserts as follows.

Cross-Calibration at Deserts

| | |
|---|---|
| Testsite | Deserts in Saudi Arabia and other areas (Non occupant areas) |
| Method | Using uniform image data and averaging |
| Frequency | Every sixteen days, three times |
| Precision | 2.8 % (TBR) |
| Purpose 1 | Calibration of all elements of Band 3b |
| 2 | Uniformity Calibration among all elements in Bands 1 to3n and 3b |
| Note | The time difference of image acquisitions between Bands 3n and 3b is only 55 sec. The roughness of desert seen at different angles might influence through shadow effect on the accuracy of the cross calibration between them. |

The vicarious Calibration 2 will be carried out as follows.

Purpose   Calibration of center elements of Bands 1 to 3n and 3b

| Institute | Airborne | Testsite | Frequency |
|---|---|---|---|
| U. of A. | Helicopter | White Sands | Five times ? |
| JPL | AVIRIS | Lunar Lake etc. | Once (Three test site)? |
| GSJ | | Tsukuba, Nemuro | |
| Saga U | | Ariake Bay | |
| USGS/NAu | | | |
| JPL | MAS | | |
| CNR | MIVIS | | |
| CSIRO | | Ocean north-west Tasmania | |
| MISR | | | |
| CNES | | | |
| S. Dakota State | | | |
| Canada | | | |
| ESA | | | |

## 5.2.4. Cross-Calibration during Intial Checkout Period

Cross-calibration is planned with MODIS as follows

Institute          JP, GSJ, Saga U, U of A, U of Wisconsin (MODIS), CSIRO
                   MISR, CNES, S. Dakota State, Canada, ESA, etc.

Cross-Calibrations with Landsat, SPOT and AVNIR are also planned.  Details are TBD.

## 5.2.5. Method for Initial Radiometric Calibration Coefficients Determination

Figure 5-7 shows the method for determination of Initial Radiometric Calibration Coefficients.
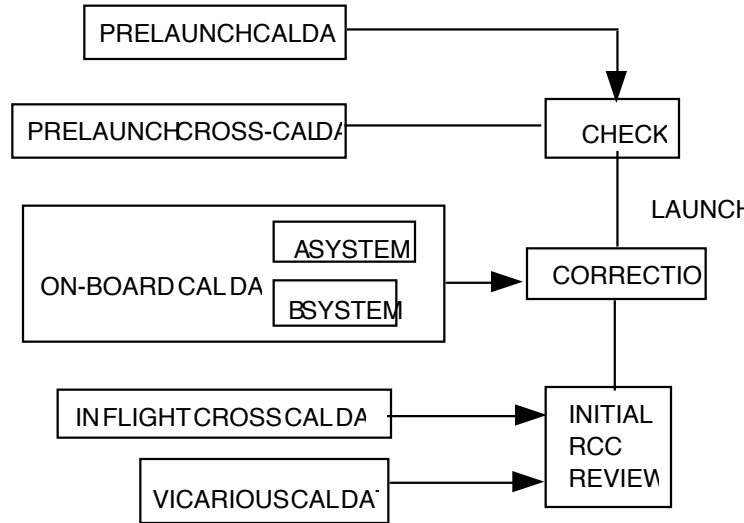


Figure 5-7  The method for Initial Radiometric Calibration Coefficients Determination.

Following Workshop for ASTER Cal/Val will be held for decision-making
Date                    Just after initial check-out period

Member                  Japanese coefficient review members, etc.
Language                English
Purpose                 For reviewing the Level 1 radiometric calibration coefficients
Review                  A review will be held at the end of the Workshop
Final Authority         Japanese ASTER Team Leader will owe the final responsivity of the
                        calibration coefficients generation.


## 5.3 In-flight Activity during Normal Operation Period

## 5.3.1. In-flight Calibration Activity Overview

Figures 5-8, 5-9 and 5-10 show activities for radiometric correction coefficients generation for VNIR, SWIR and TIR, respectively in the in-flight phase.  In this period, vicarious and cross calibration data are to be referred for RCCs revision based upon the strategy for the revision described in the Section 5.4.  The initial RCCs may be updated every 16 days (TBR) by new on-board calibration data, if necessary.
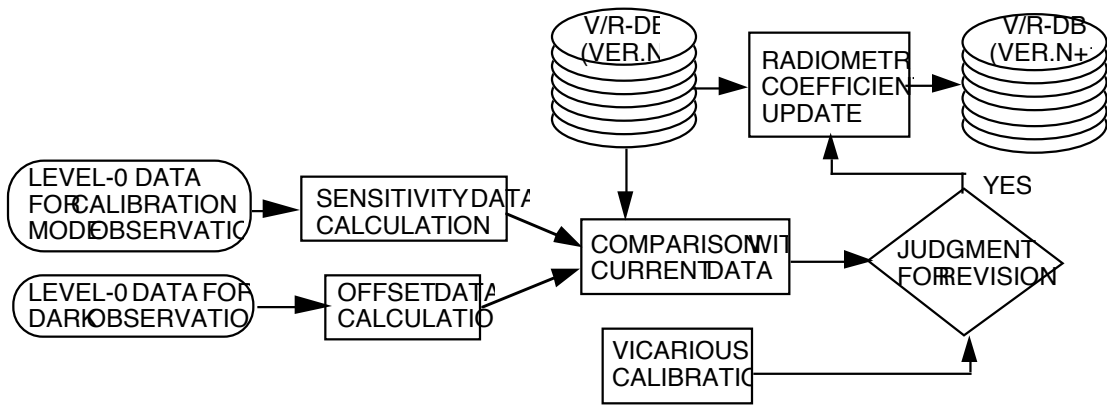
Figure 5-8  VNIR Radiometric Correction Data Update Flow
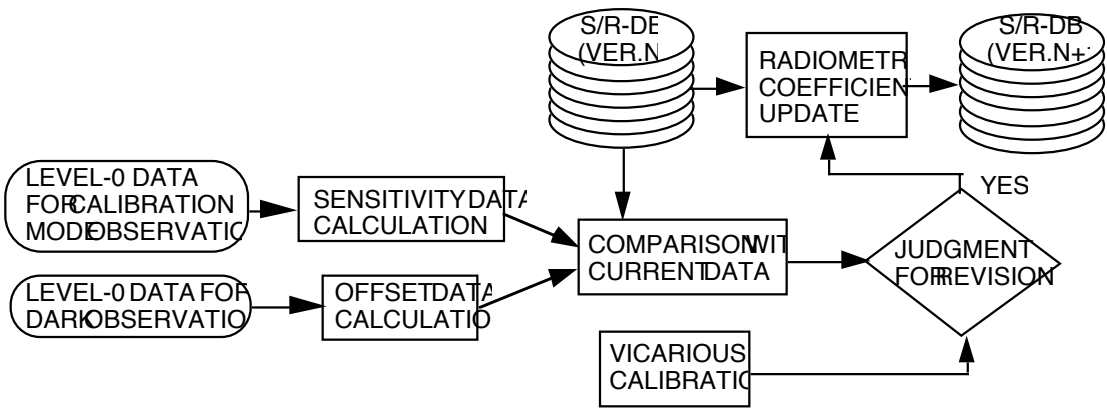


Figure 5-9  SWIR Radiometric Correction Data Base Update Flow
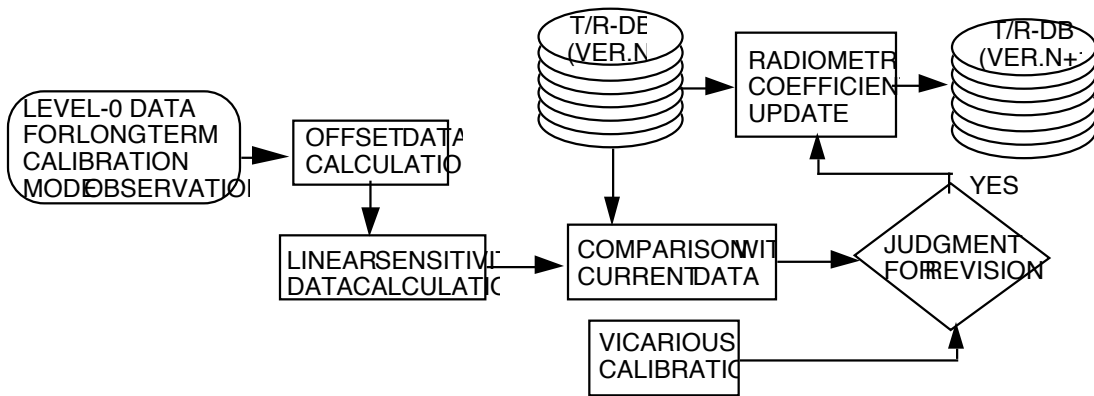


Figure 5-10  TIR Radiometric Correction Data Base Update Flow

## 5.3.2. On-board Calibration during Normal Operation Period

Key components of the VNIR On-board Calibrator(OBC) are a pair of halogen lamps and the electronic calibration source. The halogen lamps are for the total calibration of optics, the beam splitter, the detector arrays and and the electronics components. The electronic calibration source is for the calibration of the detector arrays and the electronics components. The reference source radiance from the two halogen lamps are monitored with a well qualified photodiode and are compensated with the photodiode temperature and the lamp voltage. While the electronic calibration reference voltages are compensated with the detector array temperature and the temperature of the electronics components.

Two halogen lamps are onboard as calibration sources for SWIR. The reference source radiances from the lamps are monitored with a well established photodiode and are compensated with a photodiode temperature, the temperature of the monitor electronics circuit and lamp voltages. Other than that, a gain and offset of the SWIR is compensated with detector array temperature and the temperature of the dewar.

TIR employs a well calibrated on-board blackbody of which temperature is changeable from 270 K to 340 K. Physical temperature of the blackbody is monitored with a set of well qualified Pt resistance thermometer. By using 270 K to 340 K of the blackbody temperature which are taken every 16 days, the gain and offset terms are calibrated and are compensated with the temperatures of the telescope barrel, the lens assembly and the chopper while the offset term is calibrated with the 270 K of blackbody temperature which is taken every observation period.

Calibration against each OBL for all elements of Bands 1 to 3n will be carried out as follows. Monitor output will be checked if the VNIR output shows some change.

| | |
|---|---|
| Frequency | once every sixteen days for both A and B calibrator systems. |
| Strategy | See section 5.4. |
| Purpose | All coefficients of Bands 1 to 3n to be used for Level 1 processing will be generated from previous calibration coefficients and changes of OBL calibration data. |
| Review | The OBL calibration data are checked routinely every sixteen days by ERSDAC and if any anomaly is found a special review meeting will be held from the request by the Japanese ASTER Team Leader. |

## 5.3.3. Vicarious Calibraiton Activity during Normal Operation Period

Vicarious calibration is defined here as the use of ground and atmospheric measurements as inputs to radiative transfer codes to predict the top-of-the-atmosphere radiances for in-flight spacecraft calibration purposes. Unlike OBCs, a field-instrument malfunction can be corrected, with the loss of only one calibration. Also. such calibrations are likely to improve in accuracy with time as instrumentation and techniques are refined. OBCs are likely to degrade with time on orbit.

Intensive vicarious measurements will be made during the three mouth activation and evaluation (A and E) phase by Japanese and US ASTER Science Team members and others, these activities will continue through the lifetime of ASTER. These results, included in the "Vicarious Calibration" box in Figures 5-8, 5-9 and 5-10, will be combined with the on-board calibrator results.

Two kinds of the vicarious calibrations are planned. The vicarious calibration 1 will be carried out at Deserts as follows.

```
Testsite          Deserts in Saudi Arabia and other areas
                  (Non occupant areas)
Method            Using uniform image data and averaging
Frequency         Every forty-eight days
Precision         2.8 % (TBR)
Purpose 1         Calibration of all elements of Bands 3b against 3n
Purpose 2         uniformity Calibration among all elements in Bands 1 to 3n and 3b
```

The vicarious Calibration 2 will be carried out as follows.

Purpose          Calibration of center elements of Bands 1 to 3n and 3b

| Institute | Airborne | Testsite | Frequency |
|---|---|---|---|
| U. of A. | Helicopter | White Sands | Five times ? |
| JPL | AVIRIS | Lunar Lake etc. | Once (Three test site)? |
| GSJ | | Tsukuba, Nemuro | |
| Saga U | | Ariake Bay | |
| USGS/NAu | | | |
| JPL | MAS | | |
| CNR | MIVIS | | |
| CSIRO | | Ocean north-west Tasmania | |
| MISR | | | |
| CNES | | | |
| S. Dakota State | | | |
| Canada | | | |
| ESA | | | |

## 5.3.4.  In-flight  Cross-Calibration  Activity

In-flight cross-calibration will provide a particularly sensitive way to monitor the calibration change.  The type of site required is one having constant spectral distribution, not necessarily constant radiance. The moon and desert areas are good example of the type of site required.

Cross-calibration will be conducted by several groups.  These calibrations will be made between instruments on the EOS-AM1 or other stable or well-calibrated instrumentson other platforms.  The spectral reflectance/radiance and the atmospheric characteristics of the sites used need to be known if the measurements are made at different times from instruments on different platforms.

Because of the ease with which cross-calibration can be made between instruments on the same platform, it is anticipated that such comparisons may be carried out frequently.  The results of these calibration are included with those in the "Vicarious Calibration" box in Figure 5-8, 5-9 and 5-10.  They will be combined with the on-board calibrator results according to the method described in Section 5.4.

The cross-calibration with MODIS will be carried out as follows.

Institute    JPL, GSJ, Saga U, U of A, U of Wisconsin (MODIS), CSIRO, MISR, CNES
             S. Dakota State, Canada, ESA, etc.

Cross-calibration wiht Landsat, Spot and AVNIR are also planned

## 5.4. Strategy for Radiometric Coefficient Generation

### 5.4.1. Two sets of Radiometric Calibration Coefficients

Note that there are two radiometric coefficients. One is used for level 1 processing. The other is for the revised coefficients for higher accuracy. The former need to be determined as soon as possible after the calibrations because Level 1 Processing should be done within 48 hours (TBR) from data acquisition. The basic plan is to use the prelaunch calibration data corrected for the change in the on-board calibration data which will, if necessary, be further corrected by vicarious calibration and inflight cross-calibration data. The latter coefficients will be determined later considering for various calibration data even with data taken after the image acquisition in order to be more reliable and will be made public through newsletters, an internet server and/or other means.

Figure 5-11 shows an idea of two sets of Radiometric Calibration Coefficients, one is for Level 1 processing derived from OBC and prelaunch data, and the other is for notification of Radiometric Calibration Coefficients derived from not only OBC and prelaunch data but also Vicarious Calibration data and Inflight Cross-Calibraiotn data.
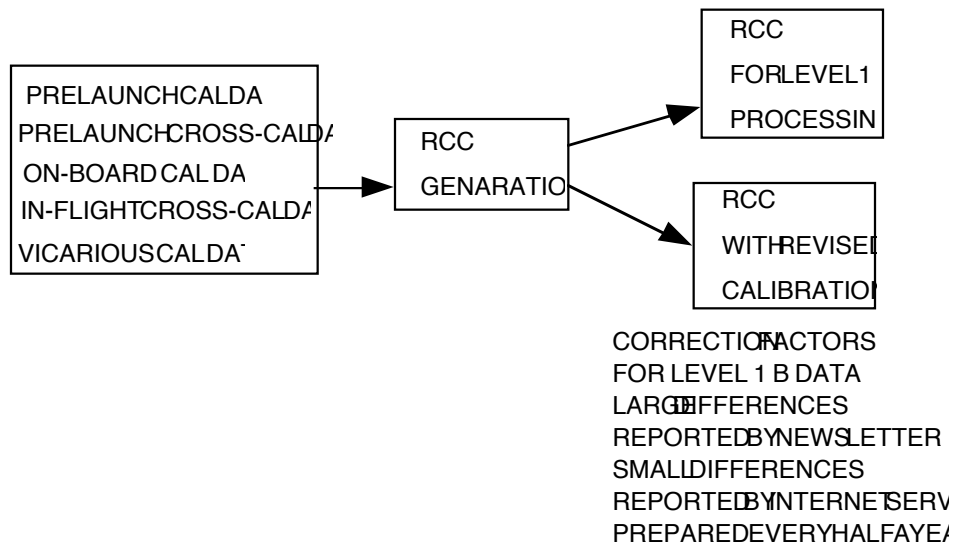
Figure 5-11  Two set of Radiometric Calibration Coefficients.

### 5.4.2. Review for ASTER Cal/Val

| | |
|---|---|
| Frequency | Twice a year |
| Member | Japanese coefficient review members, etc. |
| Language | English |
| Purpose | For reviewing the calibration coefficients for both used for Level 1 Processing and revised one. |
| Final Authority | ASTER Team Leader will owe the final responsivity of the calibration coefficients generation. |

### 5.4.3. Basic Flow of Determination

Figure 5-12 shows an example for the trend of On-board Calibration Data, Vicarious Calibration Data and Cross calibration Data. In every review, On-board Calibration Data and

prelaunch data together with trend analysis are used for determination of Radiometric Calibration Coefficients for level 1 processing.  If the On-Board Calibration Data shows more than 4 % of difference and the output from VNIR, SWIR and TIR show the situation shown in Figures 5-13, 5-14 and 5-15, Vicarious and Cross Calibration Data are included.   Then Updated Radiometric Calibration Coefficients are determined.  At this stage, a smooth curve is determined and extraporate for the next review.
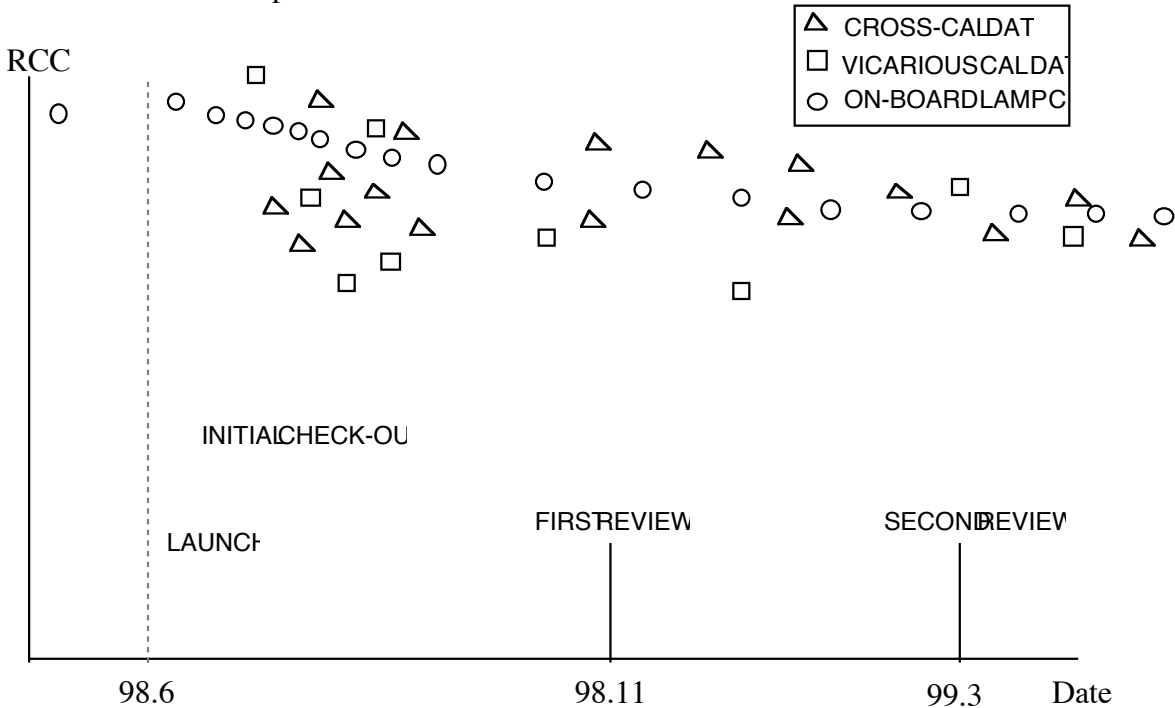


Figure 5-12  A trend of On-Board, vicarious and Cross Calibration Data
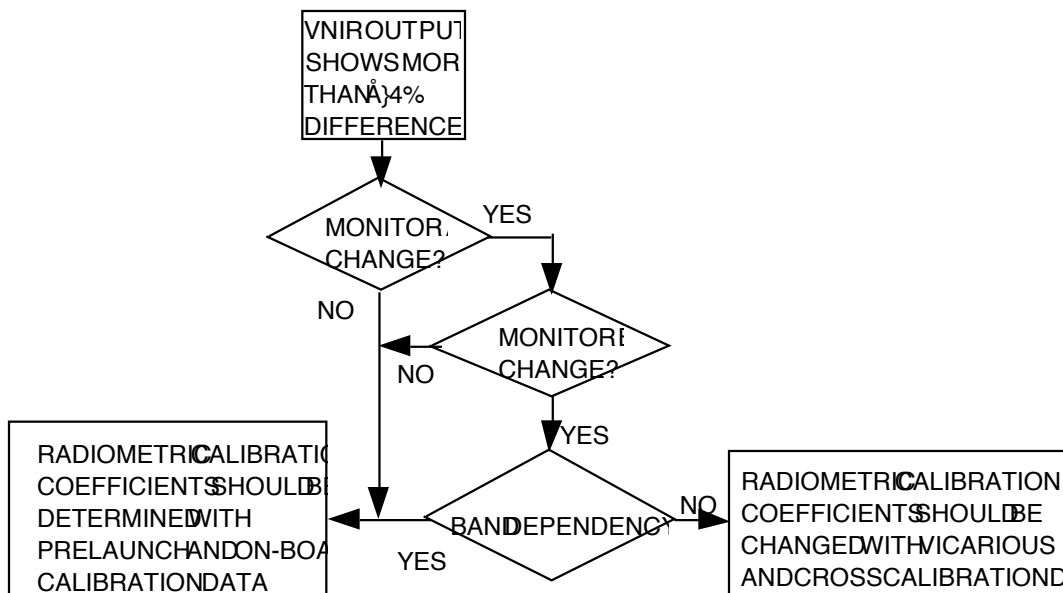


Figure 5-13  Strategy for determination of Radiometric Calibration for VNIR
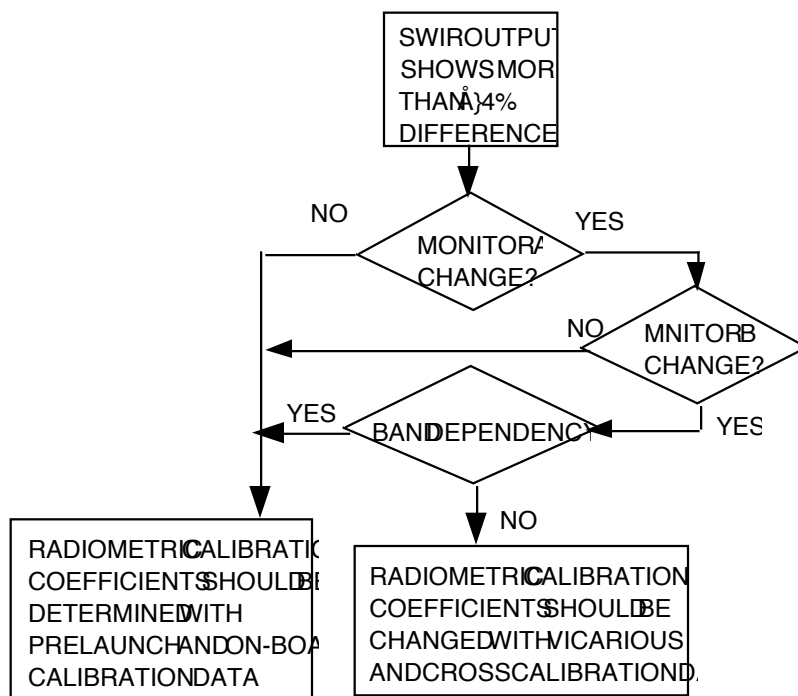
Figure 5-14  Strategy for determination of Radiometric Calibration Coefficients for SWIR.
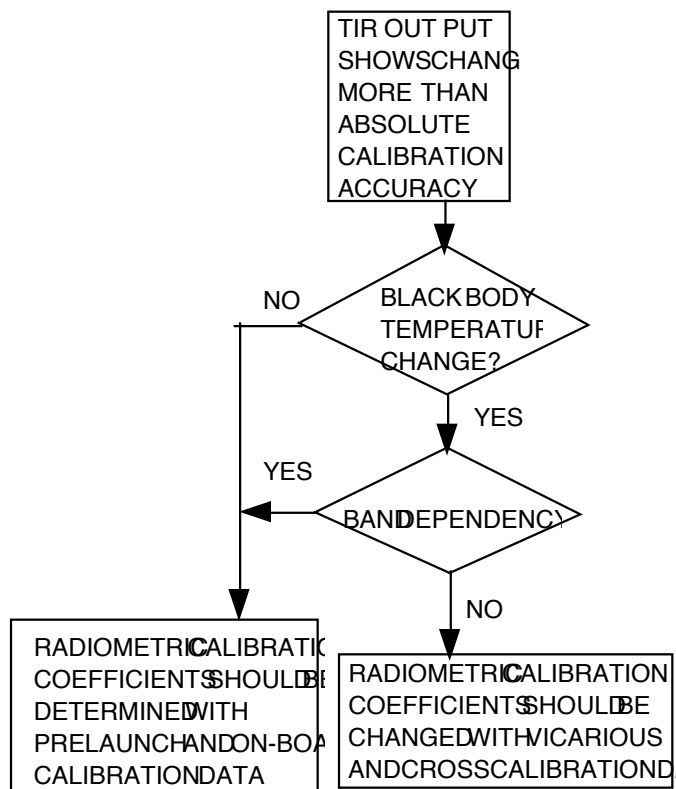


Figure 5-15  Strategy for determination of Radiometric CalibrationCoefficients for TIR.

### 5.4.4. Strategy under the discussion

For convenience we have used the following abbreviations:

A&E:        activation and evaluation (a period of between 3 and 6 months for system
            check-out and establishing the initial in-flight calibration coefficients)
CC:         Cross calibration (on orbit, between, say MODIS, MISR and Landsat-7,
            which will be in close formation with the AM-1 platform)
OBC:        on-board calibration or calibrator
PFC:        pre-flight calibration
RCC:        radiometric calibration coefficient
VC:         vicarious calibration

OBC results alone will be used in level 1B processing during the A&E phase. At the end of that phase there will be a meeting between those involved with CC, OBC, PFC, and VC to discuss the results and agree on the most accurate calibration coefficients as a function of time during the A&E phase. This agreement will be based on a weighted average of the results from the various methods. The weightings will be decided at this meeting although there will be further discussions on this subject before launch and perhaps during the A&E phase as the initial results become available.

The procedure to be followed for the processing of data following this review meeting is the topic of intensive discussion. Two methods are presently being considered. The first makes use of OBC data only for the production of Level-1B data, throughout the mission lifetime. More accurate calibration data, derived from combining OBC data with CC and VC data, will be made available to the user approximately every three months. The second method determines a set of trend equations at the end of the A&E phase and uses this until the next calibration review. At this time it may be necessary to derive a new set of equations for the period from the start of the mission to the next review. It is expected that, for a monotonically changing sensor, convergence will soon be reached between the extrapolated and actual results. Obviously the Level-1 processing algorithm is more complicated in the second case under consideration.

Items under the discussion are as follows.
- On-board Calibration Strategy
- Dark signal confirmation
- Confirmation that dark signals are in the normal range
- Comparison with the previous results
- Lamp voltage confirmation
- Confirmation that lamp voltage is in the normal range
- Comparison with the previous results
- Photodiode monitor signal at lamp confirmation
- Confirmation that monitor signal is in the normal range
- Comparison with the previous results
- Photodiode monitor signal at optics confirmation
- Confirmation that monitor signal is in the normal range
- Comparison with the previous results
- Optical calibration data
- Dark signal correction
- Confirmation that corrected optical calibration data are in the normal range
- Comparison with the previous results
- Comparison with redundant system
- Confirmation that difference is within allowance limit
- Average calculation
- New coefficient calculation
- Replace the coefficients in radio metric calibration data base to new data

# 6.   GRANULARIZATION

At the level 1 processing, the data shall be "granularized" to the unit of one scene for the convenience of further standard processing.  The data shall be divided into the scene every 60 km in the cross-track direction.   As a product, one scene size shall be 63 km including an overlap of 5 % with neighboring scenes except for band 3B.  For band 3B the scene size shall be 69 km including an additional overlap of 6 km to compensate the terrain error contribution, that is, 7.5 km overlap with the previous scene and 1.5 km overlap with the next scene.  For the along-track direction, the  overlap between two consecutive scenes are useful for the data interpretation of large area.

# 7.  ALGORITHM  EVALUATION

## 7.1.  Generation  of  Simulation  Data

Algorithm for band-to-band registration is an essential part  of level 1 processing, and this algorithm should be carefully evaluated.  Current candidates of the algorithm should be evaluated, and, based on the selected algorithm, operational program should be computed before the launch of ASTER.  To evaluate the candidate, misregistered ASTER simulation images was produced.  Since 1) intra-telescope misregistration of SWIR and 2) inter-telescope misregistration between VNIR, SWIR and TIR are two critical problems for the band-to-band registration, misregistered ASTER simulation data set including the above-mentioned two misregistration was produced.  Considering the availability of airborne data, Cuprite, Nevada, was selected as a target area.  To produce the data set, NASA/JPL's AVIRIS data were used for VNIR and SWIR band data, and NASA/JPL's TIMS data were used for TIR.  Relation between AVIRIS/TIMS and ASTER is shown in Table 7-1.  Also, Digital Elevation Model (DEM) of 15 m data interval, which was digitized from existing 1/24000 topographic map, was used to generate the shift caused by parallax.

Processing follows to generate the misregistered image are as follows
(1) to correct the AVIRIS and the TIMS data to coregistered topographically to the DEM data.
(2) to synthesize VNIR and SWIR bands ( bands 6 & 7) by summing up the AVIRIS bands,
    (TIMS bands 2 & 5 are selected for ASTER bands 11 & 13, because of the limited spectral
    bands of TIMS)
(3) to simulate inter-telescope misregistration  by shifting ASTER/VNIR and TIR data in cross
    track direction, referring to DEM effect.
(4) to simulate intra-telescope misregistration by shifting ASTER/SWIR in along track
    direction, using DEM data.
(5) to average SWIR data spatially to change the pixel size to 30 m , and TIR data , to 90 m,
    respectively.

The flow chart is shown in this Figure 7-1.  Generated data is shown in Figure 7-2.  As seen in the Figure 7-2 correlation between VNIR and SWIR band seems to be high while correlation between VNIR and TIR seems to be low or even negative.  For SWIR, parallax effect can be easily confirmed by stereo viewing because of the high correlation.  The data set created by the above process was used to evaluate the algorithm  for band-to-band registration.  The cuurent data set has following limitations.
(1) TIMS is not thoroughly same as the ASTER/TIR band; so, AAS ( Airborne ASTER
    Simulator) will be used in future, when the data is good enough for simulation.
(2) Pixel number for cross track direction is limited, because of the limited pixel number of
    airborne data in the cross-track direction,  In future, more complete data set should be
    considered.
(3) Radiometric consideration was not done.  So, the histogram doesn't well simulate ASTER
    data .
(4) Band number is also limited.  It is needed to check  whether the current band selection is
    best for matching.

Table 7-1  Band and Wavelength of Simulation Images

| ASTER | | Used Data | | Mis-registration |
|---|---|---|---|---|
| Band | Wavelength (μm) | Band | Wavelength (μm) | |
| VNIR 2 | 0.63-0.69 | AVIRIS 26-31 | 0.63678-0.68653 | Inter-telescope |
| SWIR 6 | 2.185-2.225 | AVIRIS 193-196 | 2.19237-2.22215 | Inter-telescope |
| SWIR 7 | 2.235-2.285 | AVIRIS 197-202 | 2.23207-2.28164 | Inter-telescope |
| TIR 11 | 8.475-8.825 | TIMS 2 | 8.6-9.0 | Inter-telescope |
| TIR 13 | 10.25-10.95 | TIMS 5 | 10.2-11.2 | Inter-telescope |

AVIRIS:  date=June 03, 1992,  time=18:05 (UTC)
TIMS:  date=September 01, 1990,  time=11:30 (Local Time)
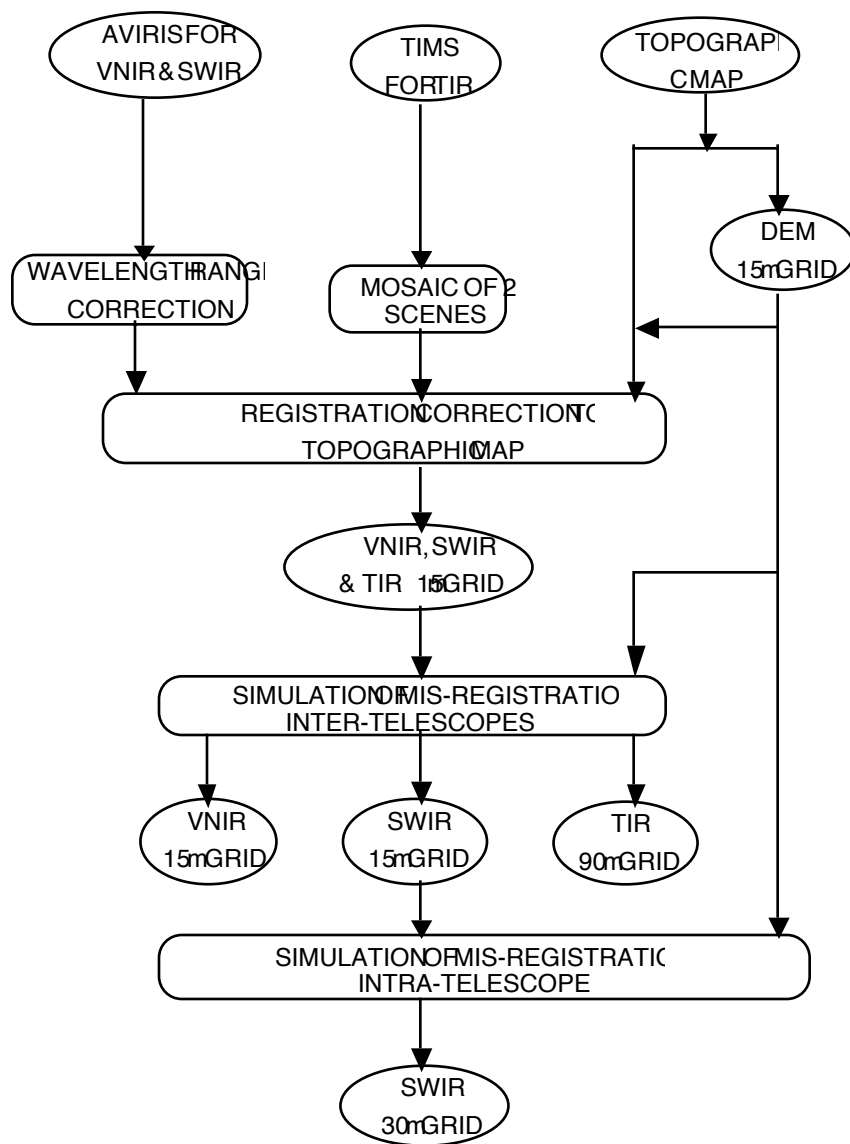


Figure 7-1  Data Processing Flow of Simulation Images
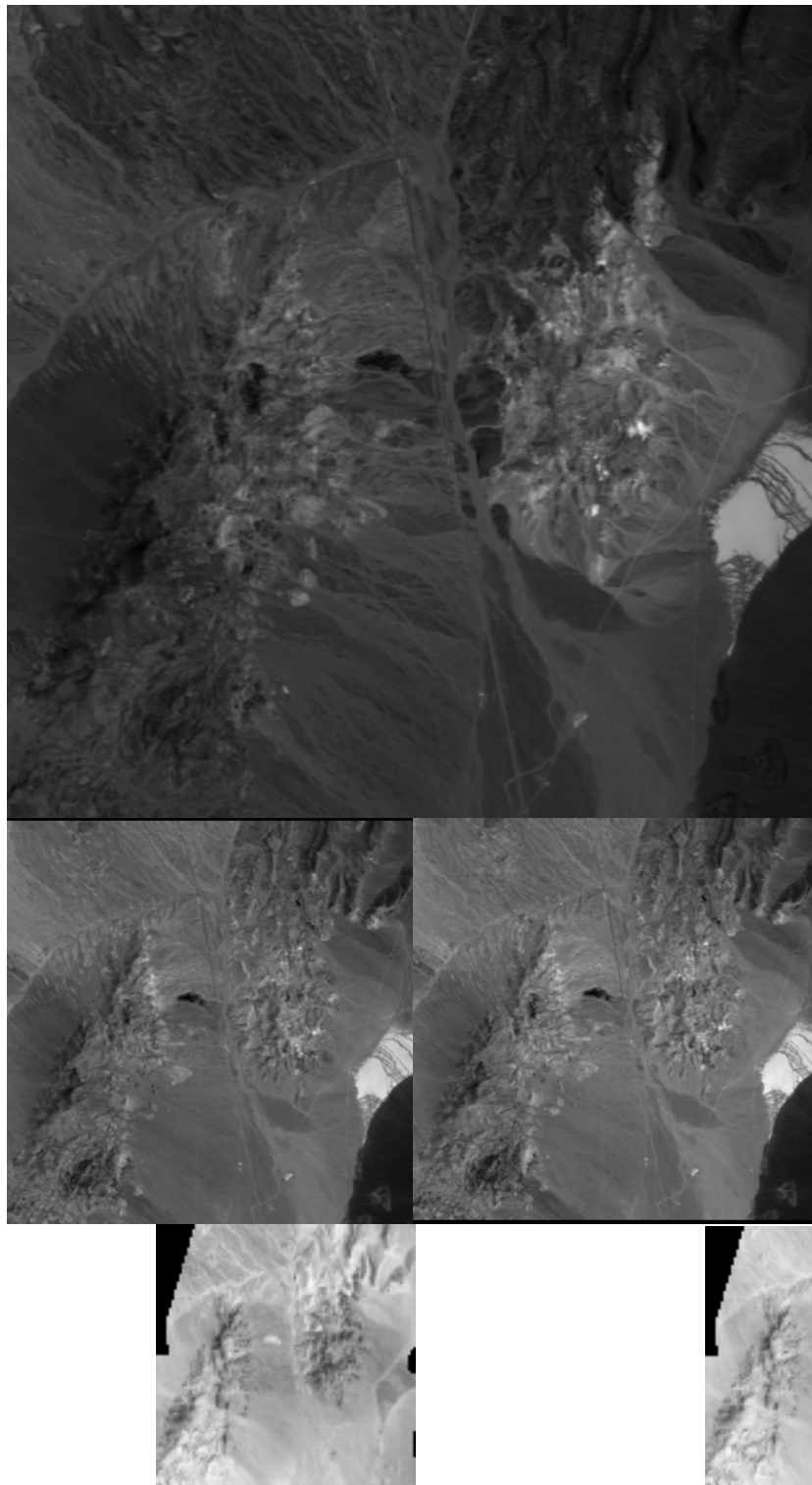
Mis-registration simulation images
Band 2
Band 6,  Band 7
Band 11,  Band 13

Figure 7-2 Generated Simulation Data (Cuprite)

## 7.2. TM and GEOSCAN Images for Algorithm Evaluation

In addition to the simulation image data described in previous section 7.2., several Landsat TM images and GEOSCAN airborne sensor images were used for the algorithm evaluation of the SWIR intra-telescope registration and the inter-telescope registration, although the spectral regions of these images are not completely same as ASTER bands. Figure 7-3 shows the TM band 7 images for the SWIR intra-telescope registration by the image matching. A cloud pattern was artificially superimposed on the TM original images to simulate the cloud coverage. Figure 7-4 shows the TM bands 3, 7 and 6 images for the inter-telescope registration by the image matching.

←--------------------- 30 km ------------------→



(Honduras TM#7)



(Honduras TM#7 with cloud)



(Death Valley TM#7)



(Death Valley TM#7 with cloud)
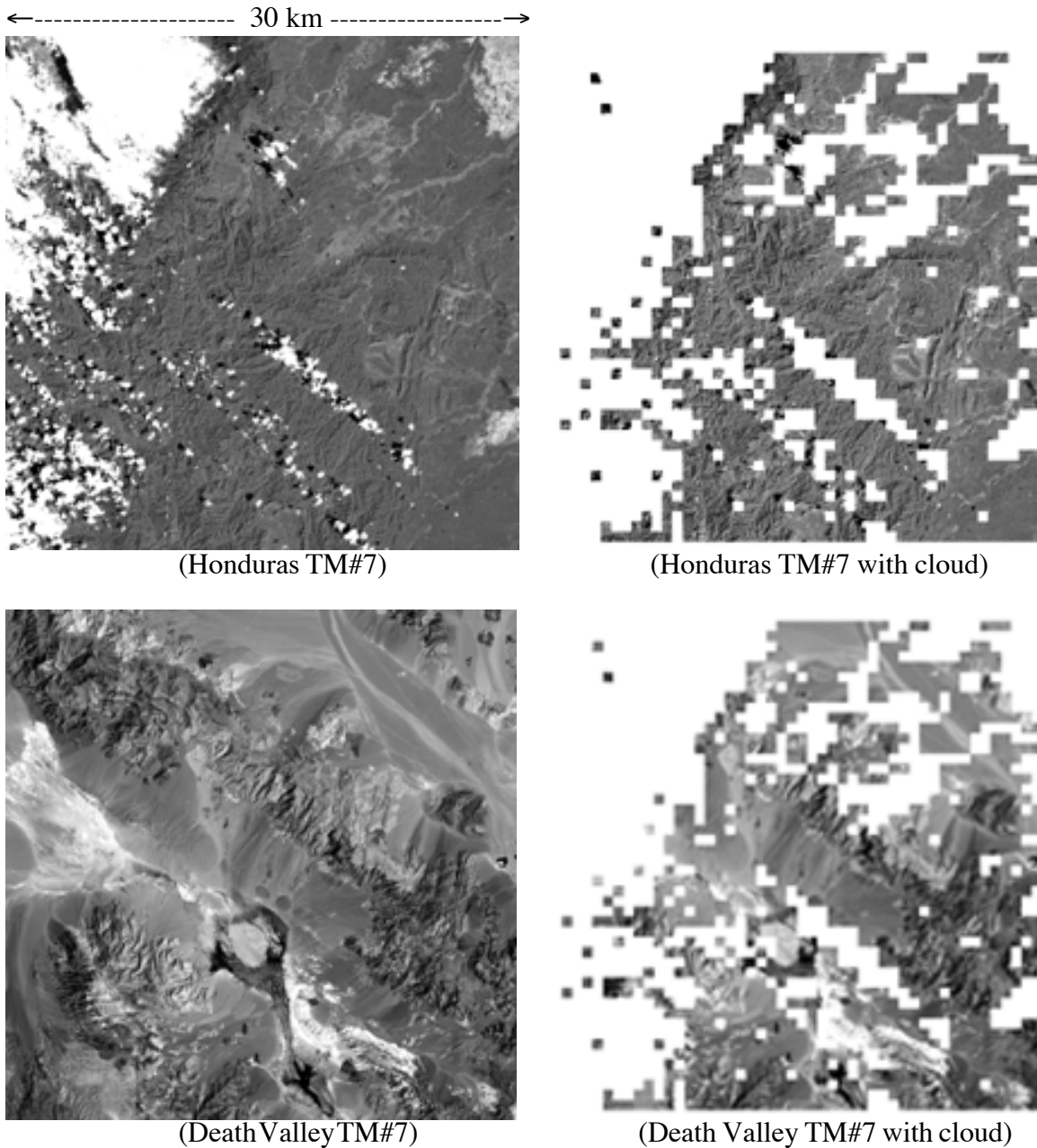
Figure 7-3  TM band 7 Images for Evaluation of SWIR Intra-telscope resgistration Algorithm
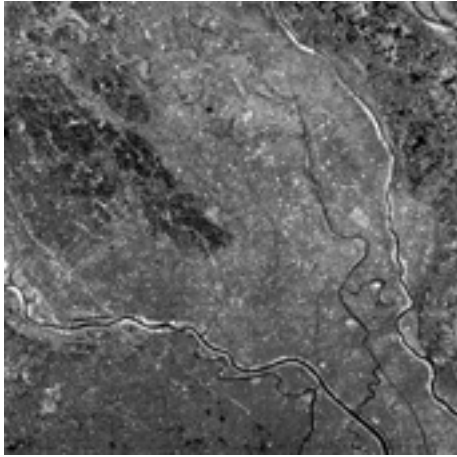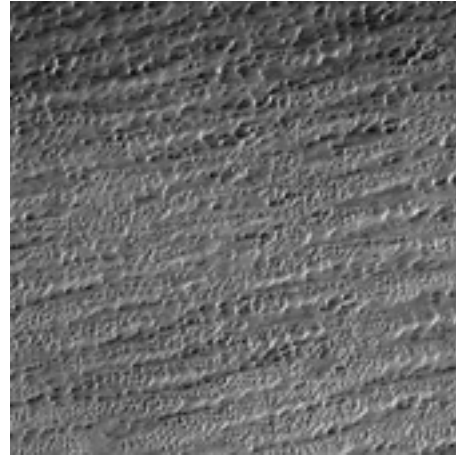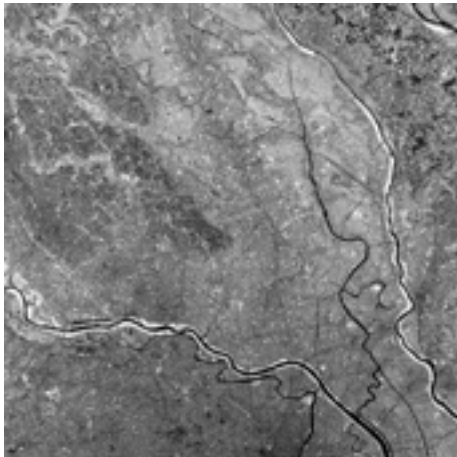
(Kanto TM#3)                          (Saudi TM#3)
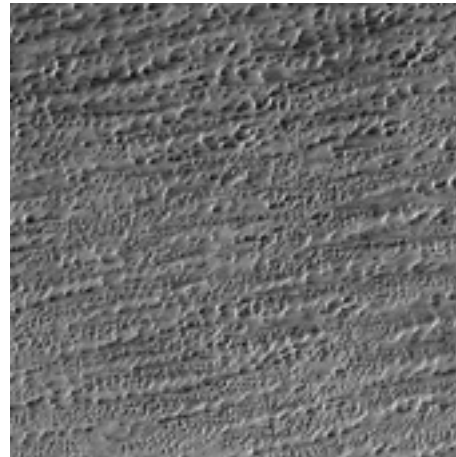


(Kanto TM#7)                          (Saudi TM#7)
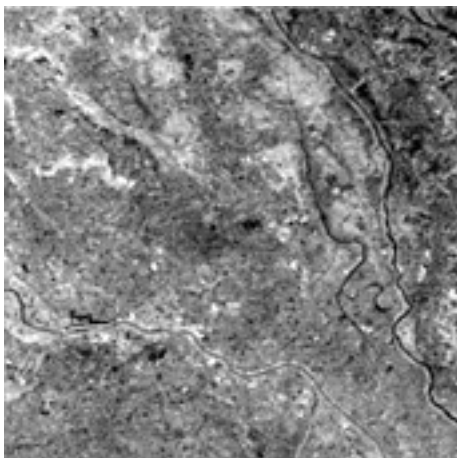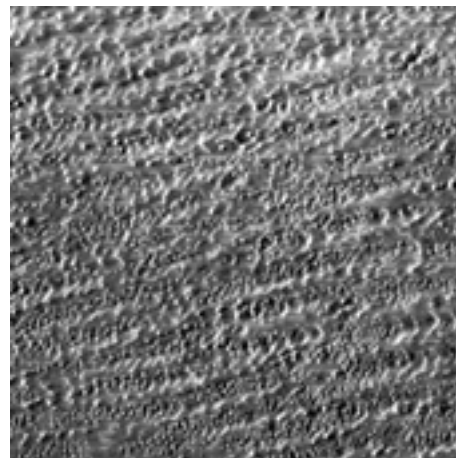


(Kanto TM#6)                          (Saudi TM#6)

Figure 7-4(a) TM bands Images for Evaluation of Inter-telscope resgistration Algorithm
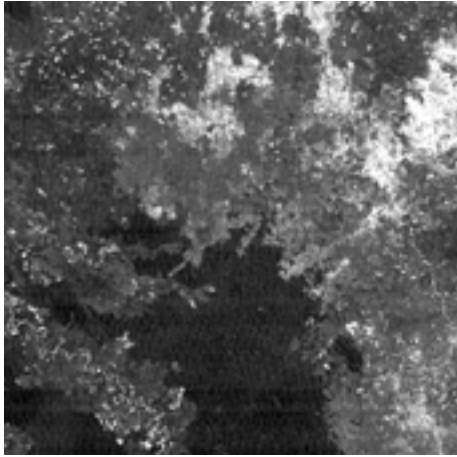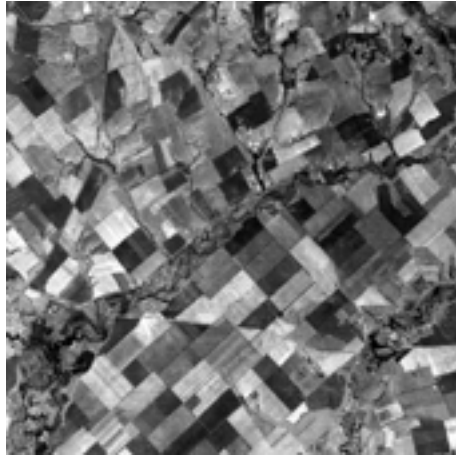
(Indonesia TM#3)            (Kazakhstan TM#3)
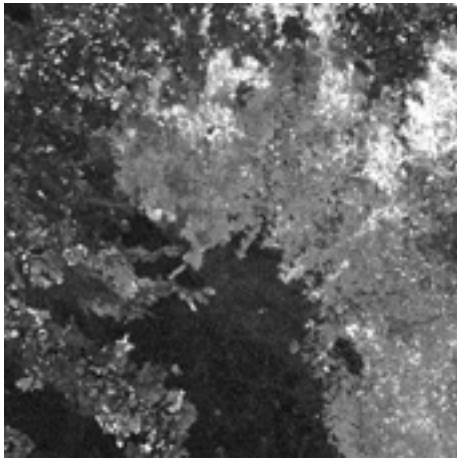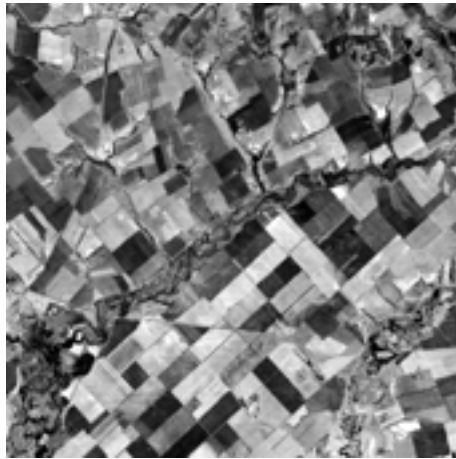
(Indonesia TM#7)            (Kazakhstan TM#7)
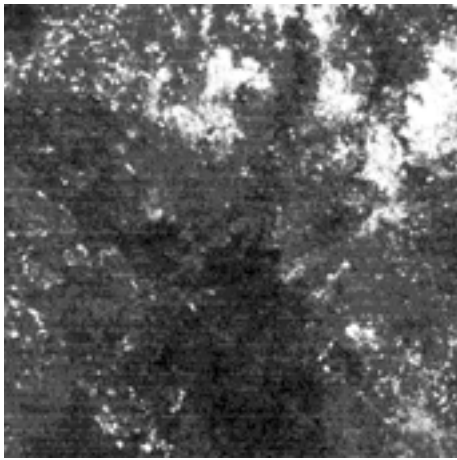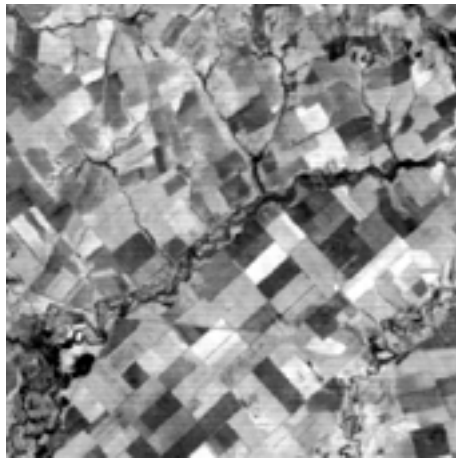
(Indonesia TM#6)            (Kazakhstan TM#6)

Figure 7-4(b) TM bands Images for Evaluation of Inter-telscope resgistration Algorithm
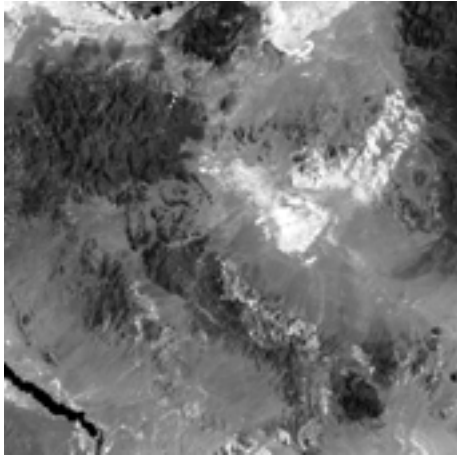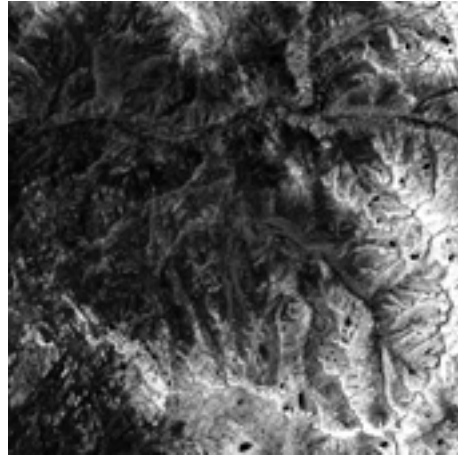
(YeilingtonTM#3)
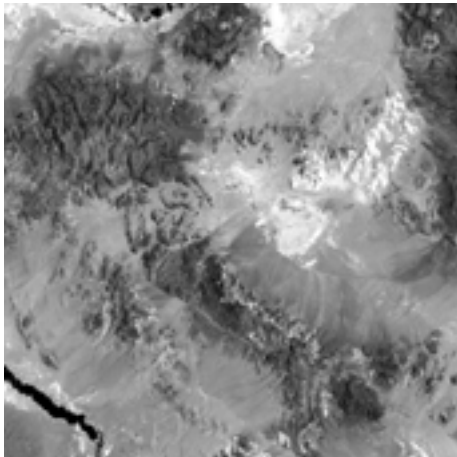


(Sierra TM#3)



(YeilingtonTM#7)
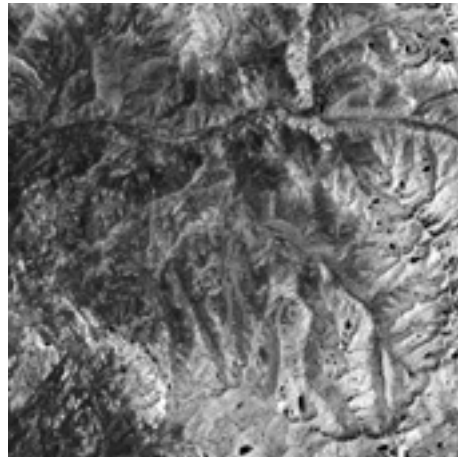


(Sierra TM#7)
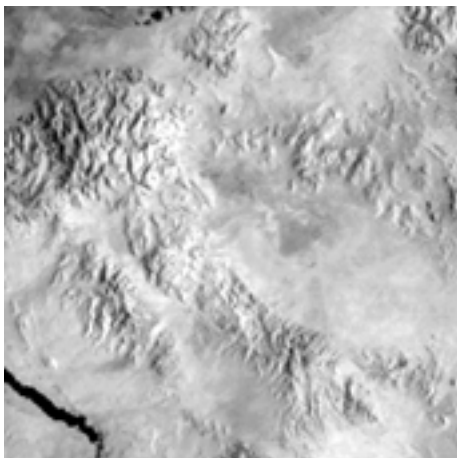


(YeilingtonTM#6)
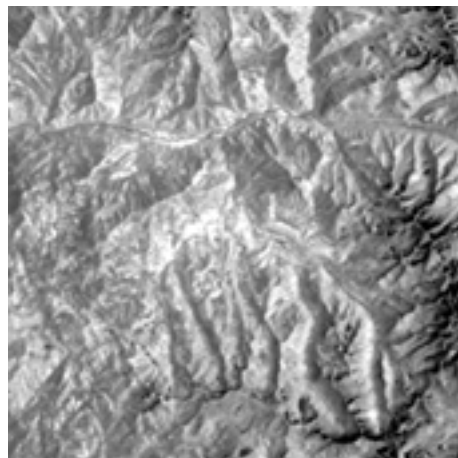


(Sierra TM#6)

Figure 7-4(c) TM bands Images for Evaluation of Inter-telscope resgistration Algorithm

Figure 7-5 shows the GEOSCAN airborne sensor images with an original spatial resolution of 6 m. The image pixel size was changed to 30 m for SWIR/VNIR image matching and 90 m for TIR/VNIR image matching.

←--- --------- 6 km --------→



| (a) VNIR | (b) SWIR | (c) TIR |
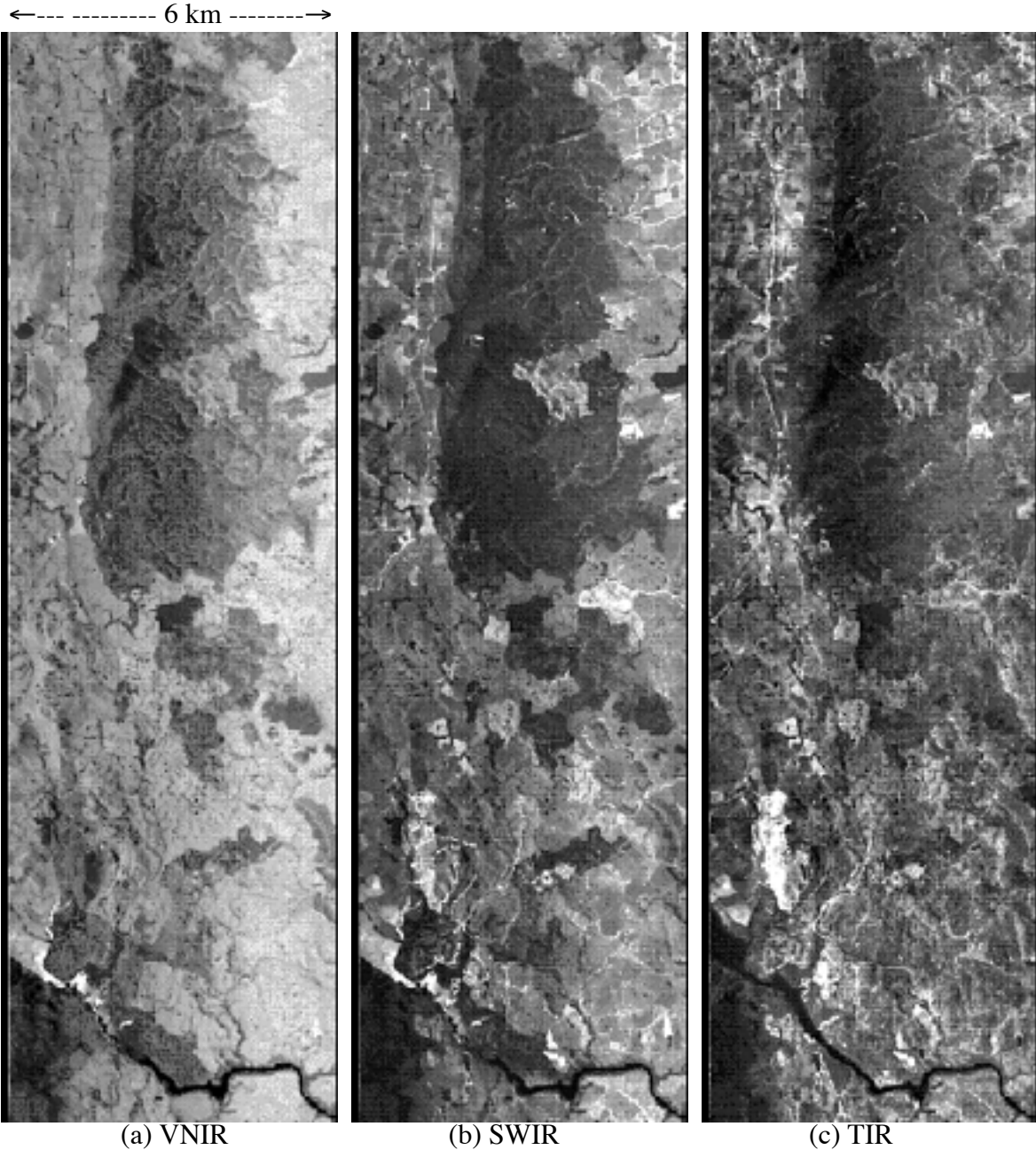
Figure 7-5 GEOSCAN Images for Evaluation of Inter-telescope Registration Algorithm (Tawpo)

## 7.3. Algorithm Evaluation of SWIR Intra-telescope Registration

The algorithm used for SWIR intra-telescope registration is a combination of the image matching correlation method and the coarse DEM method. An evaluation for the Ver.1 algorithm based on the previous ATBD version (Ver.2.1) was carried out by using simulation images shown in Figures 7-2 and 7-3. These images are generated from the airborne sensors and Landsat TM images. Mis-registration due to the parallax error was intentionally introduced to these images by using DEM data. The mis-registration was detected with the method of the image matching technique every 21 x 21 pixel window and the results were compared with the intentionally introduced values.

The coarse DEM data were used for the windows which were failed for the image matching. The sub-pixel accuracy was obtained by the interpolation of the correlation factors.

The error distributions are shown in Figures 7-6, 7-7, 7-8 and 7-9 with the Gaussian curves which were calculated from the measured $\sigma$ (RSS) values. The error distribution is roughly coincide with the Gaussian curve which means that the error process is random except for the case of the Honduras image. Figure 7-10 shows the error histogram. Judging from these results the 99 % data are within 0.3 pixels for all images, although the results are not satisfied the requirement (0.2 pixels). A part of the error seems to be attributed to the method of the combination of the image matching and the coarse DEM. This method will be improved for the version-2 algorithm.
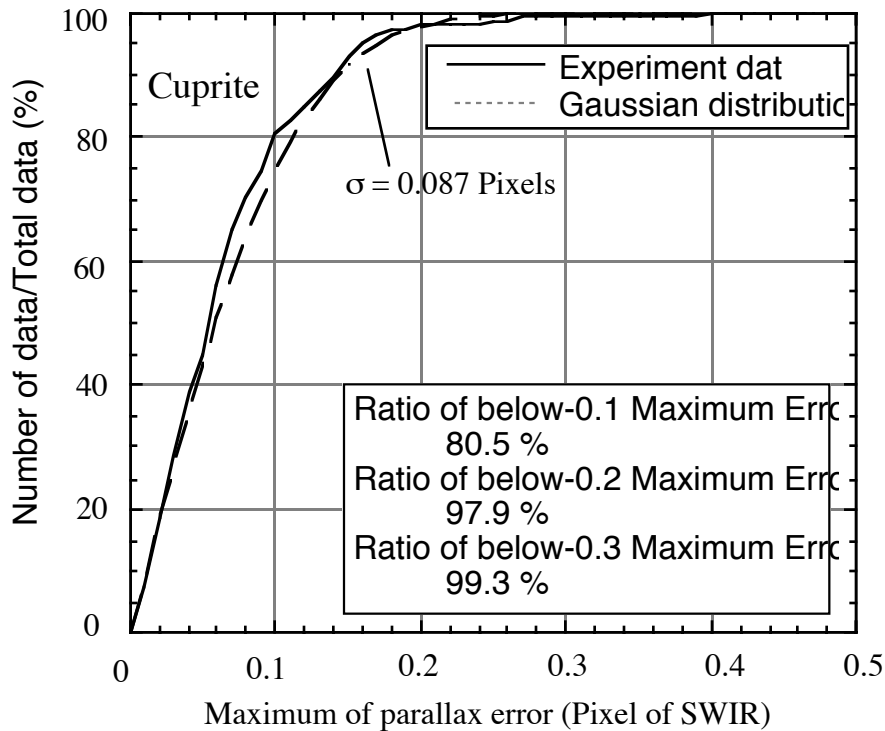


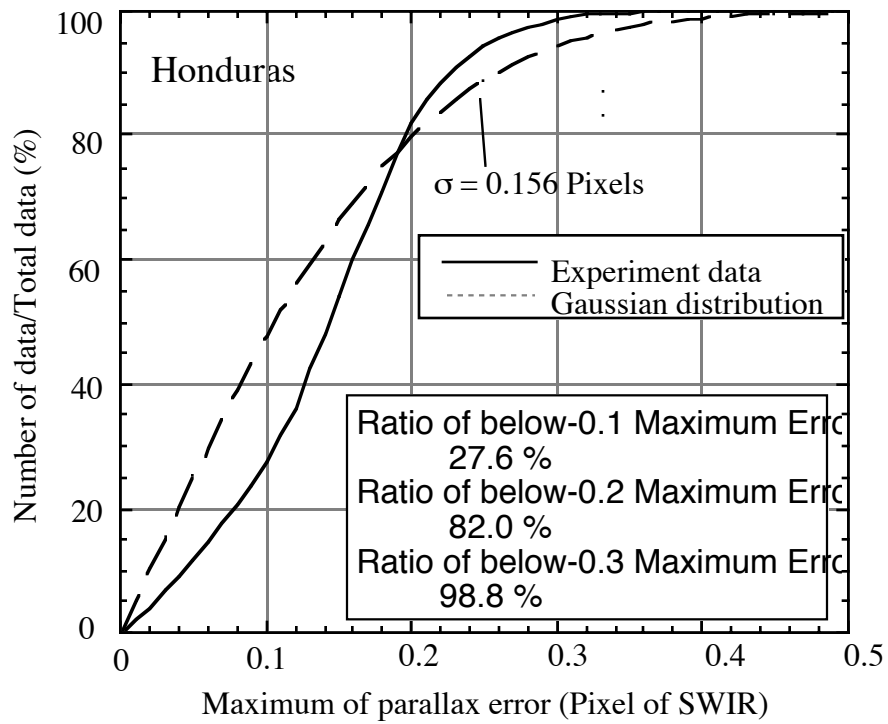Figure 7-6 SWIR Parallax Correction Error Distribution for Cuprite Image

Figure 7-7  SWIR Parallax Correction Error Distribution for Hondulas Image
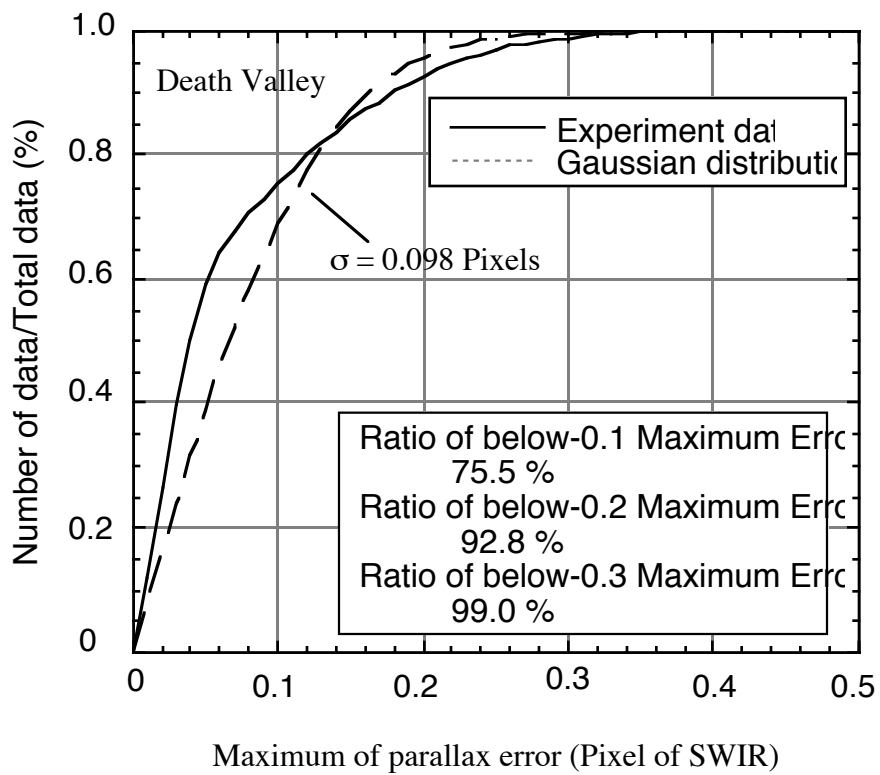


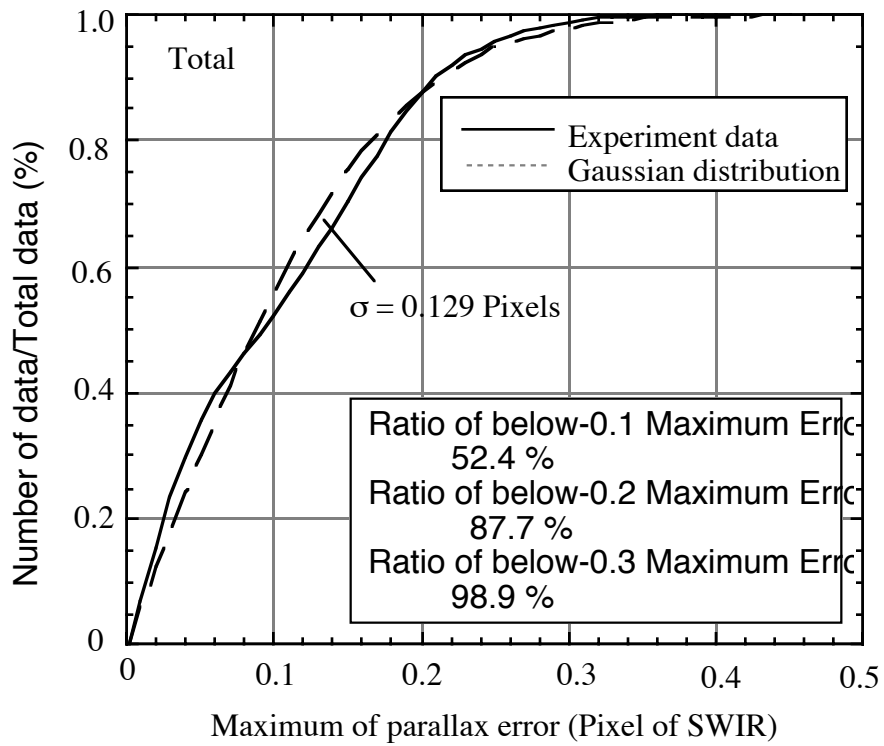Figure 7-8  SWIR Parallax Correction Error Distribution for Death Valley Image

Figure 7-9  SWIR Parallax Correction Error Distribution for Total Images
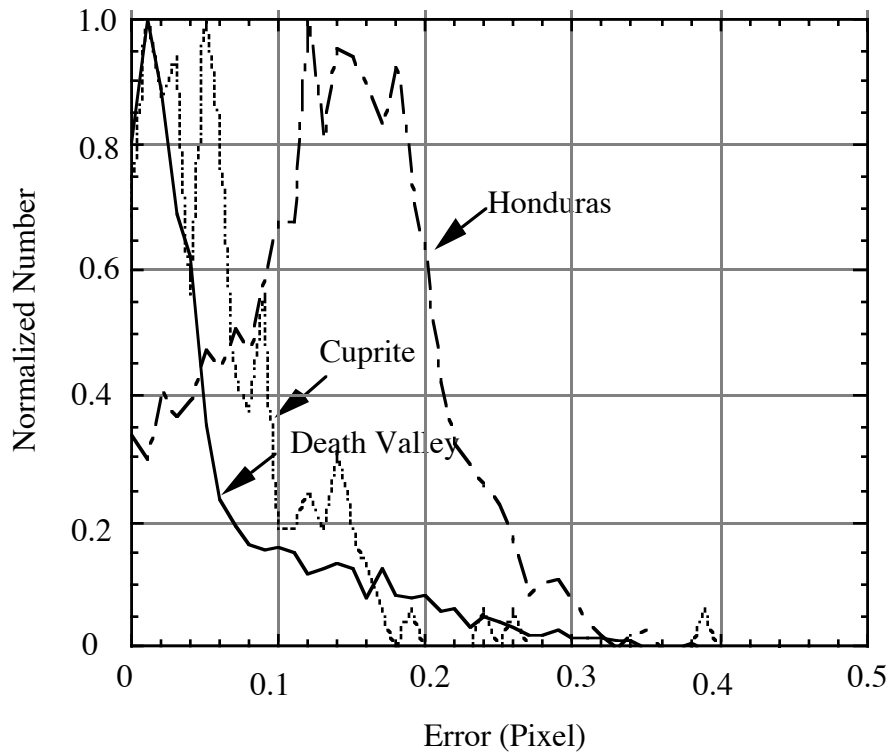


Figure 7-10  Error histogram

## 7.4. Algorithm Evaluation of Inter-telescope Registration

The algorithm used for the inter-telescope registration is the method using the image matching correlation. An evaluation for the Ver.1 algorithm based on the previous ATBD version (Ver.2.1) was carried out by using seven kinds of simulation images shown in Figures 7-4 and 7-5. These images are generated from Landsat TM images and the GEOSCAN images. TM band 3 images correspond to ASTER band 2 were used as reference images for the SWIR/VNIR and the TIR/VNIR inter-telescope registrations. TM bands 7 and 6 images were used as representative images of SWIR and TIR bands, respectively.

Evaluation results for the image matching between VNIR and SWIR bands are shown in Figures 7-11 and 7-12. The error distributions are shown in Figure 7-11 with the Gaussian curves which were calculated from the measured σ values. A threshold value of 0.7 is adopted for the correlation coefficients. Data which deviate over 3σ from the average are also excluded. The error distribution is roughly coincide with the Gaussian curve. The 3σ accuracy was calculated from the standard deviation (σ) for the averaging. Figure 7-12 shows the accuracy as a function of the number of the samples. The accuracy decreases with the number of the samples as a function of $N^{-1/2}$.

Evaluation results for the image matching between VNIR and TIR bands are shown in Figures 7-13 and 7-14. The error distributions are shown in Figure 7-13 with the Gaussian curves which were calculated from the measured σ values. The image matching quality was evaluated as the same way as SWIR/VNIR case. The error distribution is roughly coincide with the Gaussian curve. Figure 7-14 shows the results with the same feature as the SWIR/VNIR case.

Judging from these results a required accuracy of 0.3 pixels (3σ) for the inter-telescope registration will be achievable by averaging a lot of the image matching data in the same observation unit, if the boresight of each telescope is stable during a maximum observation time of 16 minutes. A hundred data will be enough for averaging to have a good accuracy and then to satisfy a required accuracy of 0.3 pixels at 3σ.

These evaluation proved that the quality judgment function has an excellent effect for selection of the high quality data.
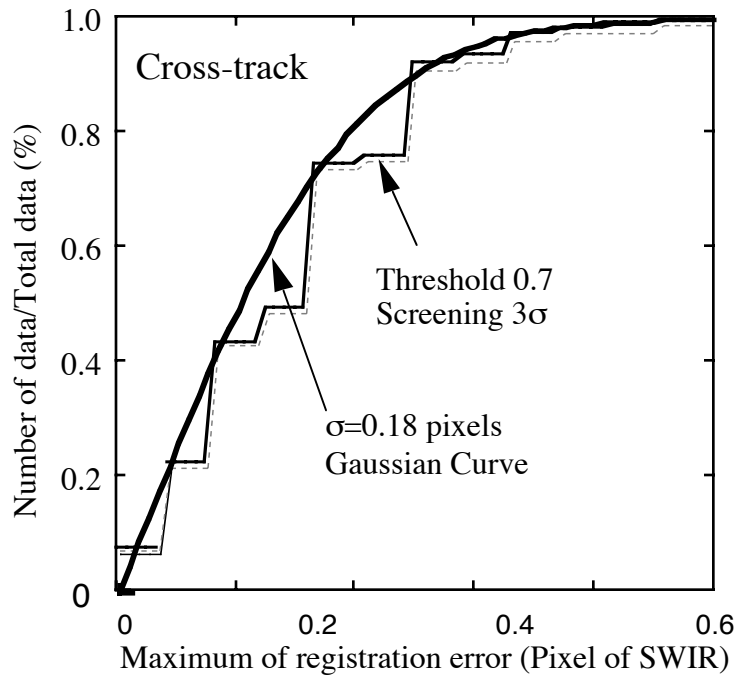
Figure 7-11(a)  SWIR/VNIR Inter-telescope Registration Correction Error Distribution
(21x21 SWIR matching window size, Error for one image matching data)
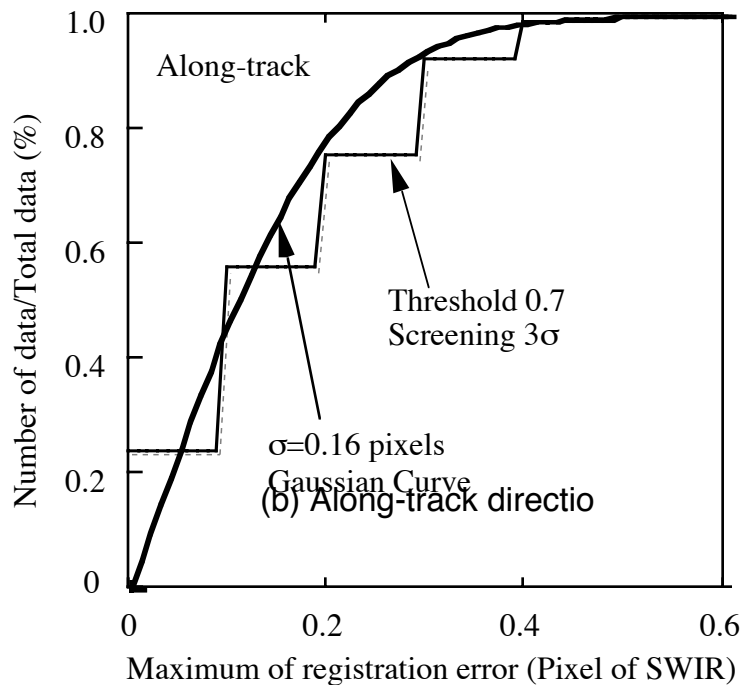(Cross-track Direction)



Figure 7-11(b)  SWIR/VNIR Inter-telescope Registration Correction Error Distribution
(21x21 SWIR matching window size, Error for one image matching data)
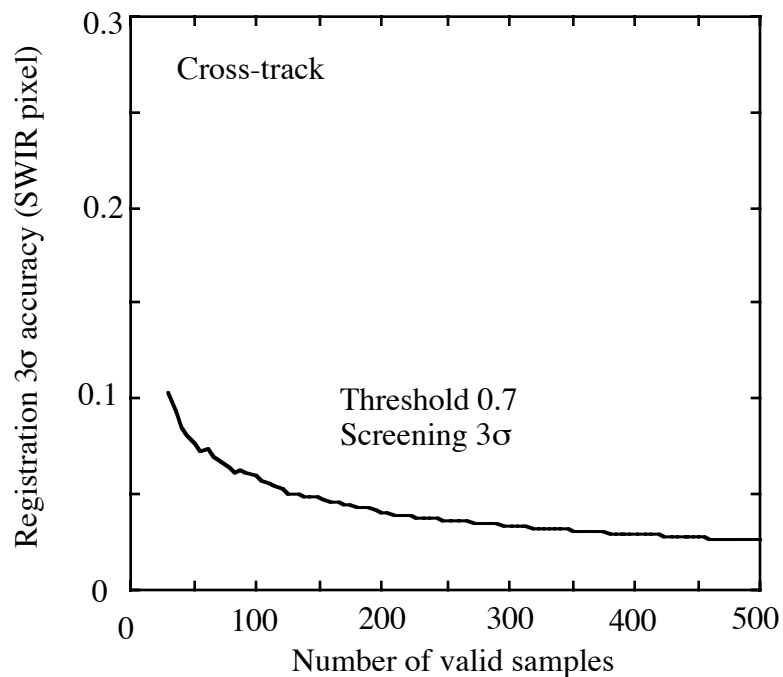(Along-track Direction)

Figure 7-12(a)  Averaging effect for SWIR/VNIR inter-telescope registration
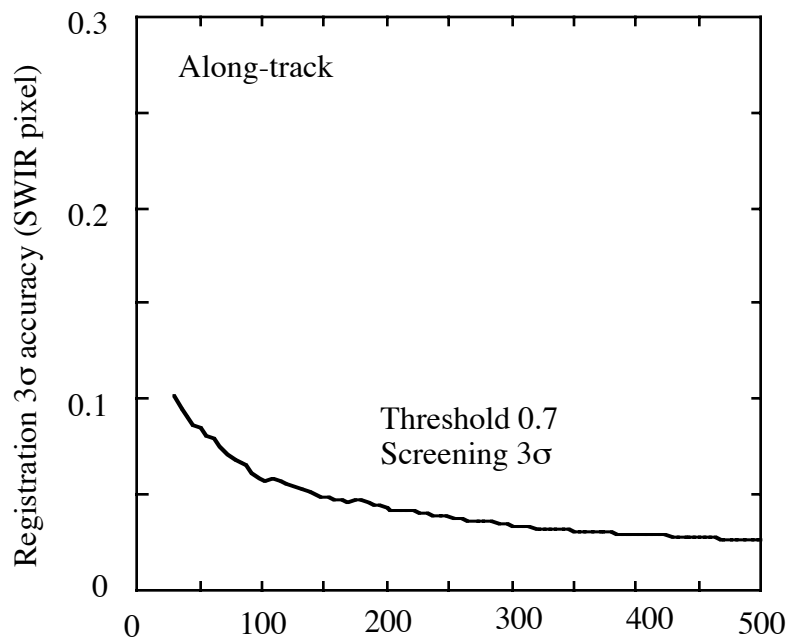(Cross-track Direction)



Figure 7-12(b)  Averaging effect for SWIR/VNIR inter-telescope registration
(Along-track Direction)

Figure 7-13(a)  TIR/VNIR Inter-telescope Registration Correction Error Distribution
(21x21 TIR matching window size, Error for one image matching data)
(Cross-track Direction)
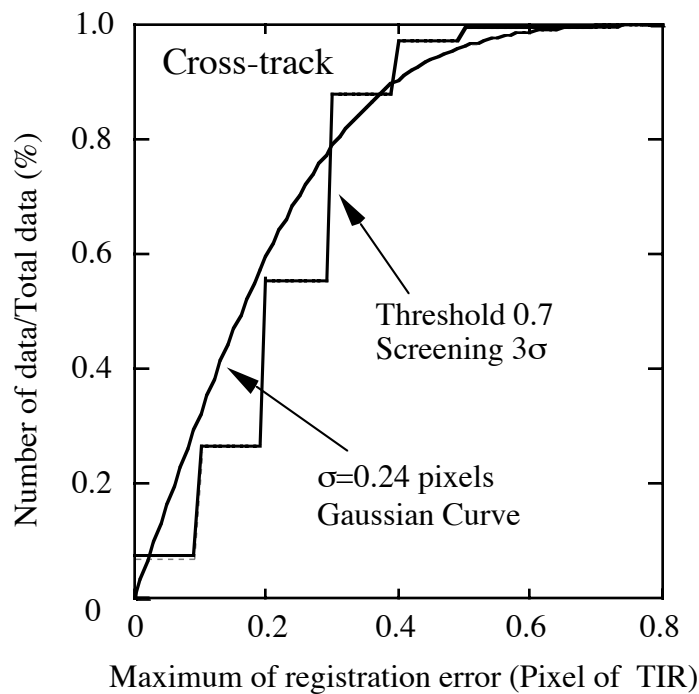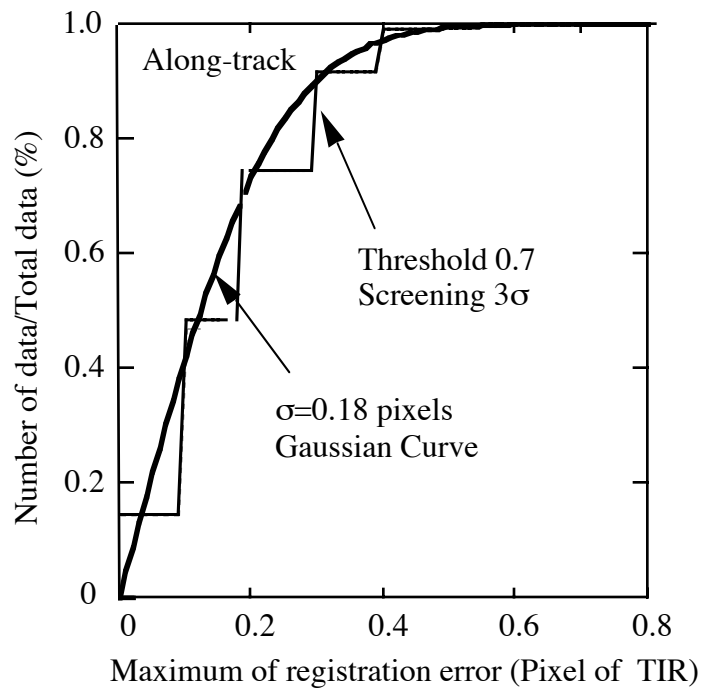


Figure 7-13(b)  TIR/VNIR Inter-telescope Registration Correction Error Distribution
(21x21 TIR matching window size, Error for one image matching data)
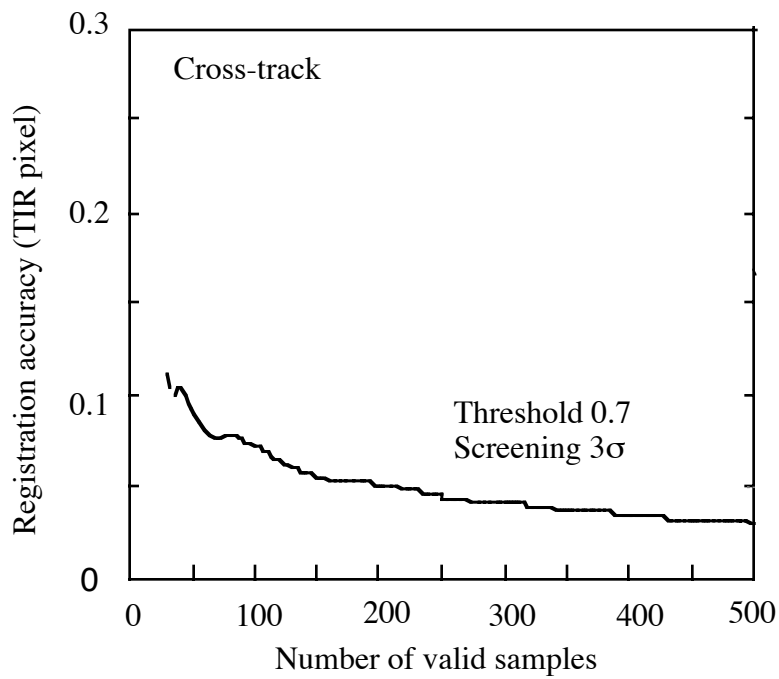(Along-track Direction)

Figure 7-14(a)  Averaging effect for  TIR/VNIR inter-telescope registration
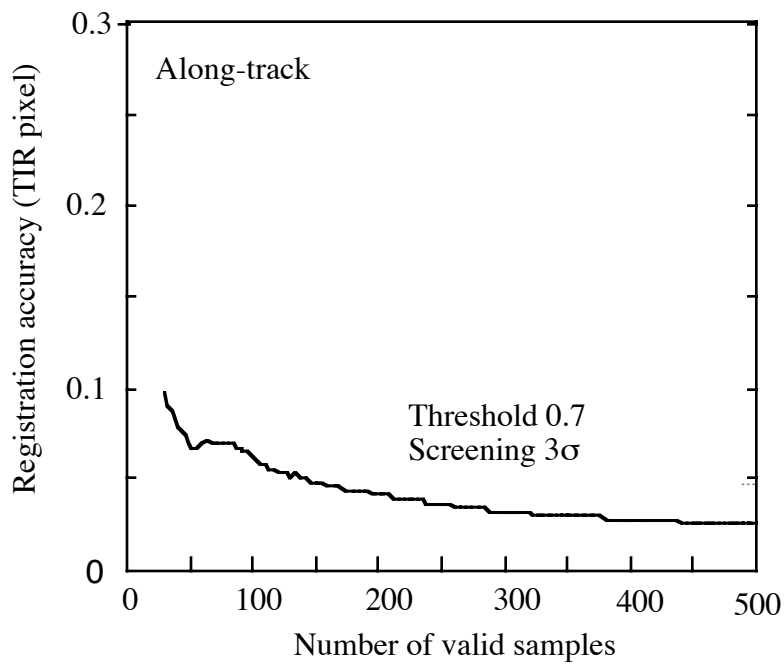(Cross-track Direction)



Figure7-14(b)  Averaging effect for  TIR/VNIR inter-telescope registration
(Along-track Direction)

# 8. THEORETICAL BASIS OF ALGORITHMS

## 8.1. Band Selection for Image Matching

ASTER data have two major mis-registrations, 1) inter-telescope misregistration among VNIR, SWIR, and TIR bands, and 2) inter-telescope misregistration including the parallax error of SWIR bands.  In this chapter, background for band selection to be used for correction of intra- and inter-telescope mis-registration will be discussed.  The former is caused mainly by parallax and the latter is caused by lack of accuracy in the telescope pointing mechanism.

Regarding the processing flow, inter-telescope registration within SWIR used correlation and registered SWIR and TIR data should be corrected using VNIR data as a reference.  Data from each of the different telescopes has different spatial resolution (VNIR : 15m, SWIR : 30m, TIR : 90m) and different spectral characteristics.  Those physical characteristics make inter-telescope registration difficult.  At present, matching between VNIR and SWIR can be done by spatial correlation.  However, correlation between VNIR and TIR seems to be more complicated.  In some cases, matching by spatial correlation is possible, but in most cases the correlation is low, and it can be negative.

The current plan is to find areas having good correlation and to select them to use for some contiguous scenes which have no change in pointing.  Other alternatives are also being investigated.

### 8.1.1. Band Selection of Intra-telescope Registration of SWIR

Band-to-band misregistration within a telescope of SWIR is caused by the difference of look direction of the 6 SWIR bands.  The two major causes of local misregistration are the parallax by different local altitude and the attitude change of the spacecraft.  At present, the former is considered to be a dominant factor of misregistration.  So, matching calculation should be taken with relatively small interval and calculation could be some burden for computer.  As the method of matching, conventional spatial correlation method is being considered.  Within the SWIR region, the correlation between bands is generally high, and matching algorithm does work. Furthermore, correlation is higher, in most cases, for the two adjacent bands which are spectrally close.

Then, problem is to determine which adjacent bands are the best. At first, the band 4 (1.6 micron band) may be excluded because it is spectrally far from the other 5 bands. The bands 8 and 9 may be relatively noisy because of lower incident energy. Consequently, there remain the bands 5, 6 and 7.

On the other hand, in order to produce maximum parallax misregistration, the two bands against which correlation calculation will be done, these bands should be placed at the two extremities.  And, as most frequent application, ratio is taken between the bands 5 and 6 considering the significant absorption feature at the band 6, and consequently, these two bands are recommended in adjacent locations.  As a result, the bands 6 and 7 are selected for the calculation of correlation and, by the current design, these two bands are located at the two extremities.

### 8.1.2. Band Selection for Inter-telescope Registration

Inter-telescope misregistration is caused by the pointing inaccuracy of the three telescopes as described previously.  Since the relative pointing direction of each telescope are stable, matching will be needed within a time span of this stability. So, matching between two bands from different telescopes will be needed at least two different locations over this time span. By

the consideration of Level-1 processing, VNIR bands are selected as reference and, by current design, matching between VNIR and SWIR and that between VNIR and TIR are considered. SWIR bands have a problem of mis-registration within them, it is not appropriate as reference.

To select the bands for matching, TM bands are used for consideration. At the next step, ASTER simulation data mentioned in the Section 7.1. will be used. The relation of the band pass of ASTER with LANDSAT/TM is shown in the Table 8-1. Based on this table, image correlation of LANDSAT/TM band 7 with bands 2,3 and 4 were calculated to infer the correlation of ASTER SWIR band with VNIR bands 1,2 and 3. And, in the same manner, image correlation of LANDSAT/TM band 6 with other bands were calculated to infer the correlation of ASTER TIR bands with VNIR or SWIR bands. At this study, difference of the pixel size was ignored. Used data as follows :

        Landsat/TM D109-36 13MAR86    Nagoya and Biwa Lake, Japan
        Landsat/TM D147-32 13JUL86    Tarim Basin, China
        Landsat/TM D140-30 17JAN89    Turpan Basin, China

The size of calculated area is approximately from 100 x 100 pixels to 200 x250 pixels. The results are summarized in Tables 8-2 to 8-7.

Following conclusions were obtained by this study.

(a) Image correlation between LANDSAT/TM band 7 and VNIR bands are generally good and consequently, this method can be used for ASTER inter-telescope BBR for VNIR and SWIR. The band 2 and the band 6 of ASTER can be used for the calculation of image correlation.

(b) Image correlation between LANDSAT/TM band 6 and other VNIR and SWIR bands are sometimes good and sometimes not good. In the no-good cases, correlation can be very low or can be even worse : negative. But, as mentioned above, it is not necessary to calculate correlation very often as the cases of intra-telescope calculation, so, the cases having good correlation can be selected. However, it is possible that no good correlation can be calculated. For such possibilities, further study using other kinds of matching methods are also under study. Examples are feature matching method and template matching method.

Table 8-1. Relation between LANDSAT
-TM and ASTER Band

| Landsat/TM | ASTER | μm |
|:---:|:---:|:---|
| 2 | 1 | 0.52 - 0.60 |
| 3 | 2 | 0.63 - 0.69 |
| 4 | 3 | 0.76 - 0.86(TM : 0.90) |
| 5 | 4 | 1.60 - 1.70(TM : 1.55 - 1.75) |
| 6 | 10-14(TIR) | |
| 7 | 5 -9(SWIR) | |

Table 8-2. Correlation Coefficients of TM Band 7 with TM Band 2, 3, and 4
( LANDSAT / TM  D109-36 13MAR86 Nagoya / Biwa Lake, Japan)

| Description of the Area | Band 2 | Band 3 | Band 4 |
|---|---|---|---|
| a. Vegetation / Mountains | 0.71 | 0.77 | 0.46 |
| b. Vegetation / Mountains / Urban (Wide Area) | 0.86 | 0.89 | 0.20 |
| c. Vegetation / Urban | 0.67 | 0.73 | 0.17 |
| d. Urban / River | 0.80 | 0.92 | 0.91 |
| e. Vegetation / Snow / Mountains | 0.24 | 0.28 | 0.38 |
| f. Urban / Vegetation / Mountains | 0.82 | 0.84 | 0.63 |
| g. Vegetation / Plain | 0.62 | 0.67 | 0.17 |
| h. Harbor / Sea | 0.94 | 0.97 | 0.97 |
| i. Land / Sea | 0.92 | 0.95 | 0.95 |
| a. Lake | 0.07 | 0.06 | 0.12 |
| b. Land / Lake | 0.84 | 0.89 | 0.91 |
| c. Snow / Mountains | -0.13 | -0.11 | -0.04 |
| d. Vegetation / Mountains | 0.78 | 0.83 | 0.56 |
| e. Mountains / Urban | 0.90 | 0.91 | -0.24 |
| f. Urban | 0.53 | 0.54 | 0.56 |
| g. Mountains / Lake | 0.85 | 0.91 | 0.83 |

Table 8-3  Correlation Coefficients of TM Band 7 with TM Band 2, 3, and 4
(LANDSAT / TM  D147-32 13JUL86 Tarim Basin, China)

| Description of the Area | Band 2 | Band 3 | Band 4 |
|---|---|---|---|
| a.  Arid Area (No-Vegetation) Carbonate Rock Mountains | 0.79 | 0.80 | 0.82 |
| b.  Arid Area (No-Vegetation) Sandstone Mountains | 0.87 | 0.92 | 0.92 |
| c.  Arid Area (No-Vegetation) Fan | 0.90 | 0.91 | 0.89 |
| d.  Arid Area (No-Vegetation) Carbonate Rock Mountains | 0.93 | 0.93 | 0.86 |
| e.  Vegetation | 0.84 | 0.83 | -0.19 |
| f.  Arid Area (No-Vegetation) Mountains | 0.91 | 0.92 | 0.86 |
| g.  Arid Area (No-Vegetation) Fan | 0.79 | 0.80 | 0.81 |

Table 8-4   Correlation Coefficients of TM Band 7 with TM Band 2, 3, and 4
(LANDSAT / TM  D140-30 17JAN89 Turpan Basin, China)

| Description of the Area | Band 2 | Band 3 | Band 4 |
|---|---|---|---|
| a. Dune | 0.87 | 0.93 | 0.94 |
| b. Desert | 0.05 | 0.16 | 0.37 |
| c. Arid Area | 0.75 | 0.80 | 0.84 |
| d. (Cirrus) Cloud / Desert | 0.61 | 0.66 | 0.70 |
| e. Snow / Mountains | -0.17 | -0.08 | 0.01 |
| f.  Desert | 0.82 | 0.86 | 0.88 |

Table 8-5 Correction Coefficients of TM Band 6 with Other Bands
(LANDSAT / TM  D109-36 13MAR86 Nagoya / Biwa Lake, Japan)

| Area | Band 1 | Band 2 | Band 3 | Band 4 | Band 5 | Variance | Band 7 |
|---|---|---|---|---|---|---|---|
| a. Vegetation Mountains | 0.34 | 0.43 | 0.42 | 0.37 | 0.64 | 31.8 | 0.62 |
| b. Vegetation Mountains Urban (Wide Area) | 0.69 | 0.67 | 0.69 | 0.05 | 0.72 | 54.8 | 0.78 |
| c. Vegetation Urban | 0.35 | 0.32 | 0.35 | -0.12 | 0.44 | 9.8 | 0.55 |
| d. Urban River | 0.55 | 0.57 | 0.77 | 0.87 | 0.87 | 96.0 | 0.85 |
| e. Vegetation Snow Mountains | -0.61 | -0.57 | -0.56 | -0.36 | 0.40 | 33.8 | 0.16 |
| f.  Urban Vegetation Mountains | 0.75 | 0.79 | 0.82 | 0.57 | 0.81 | 49.1 | 0.83 |
| g. Vegetation Plain | 0.22 | 0.20 | 0.22 | 0.14 | 0.21 | 5.3 | 0.18 |
| h.  Harbor Sea | 0.83 | 0.89 | 0.93 | 0.95 | 0.95 | 120.6 | 0.96 |
| i.  Reclamation of Land Sea | 0.51 | 0.55 | 0.62 | 0.70 | 0.69 | 91.0 | 0.66 |
| a. Lake | 0.03 | 0.02 | 0.01 | 0.02 | 0.03 | 0.5 | 0.02 |
| b. Land Lake | 0.79 | 0.85 | 0.92 | 0.94 | 0.91 | 70.7 | 0.88 |
| c.  Snow Mountains | -0.48 | -0.49 | -0.47 | -0.40 | 0.48 | 10.1 | 0.44 |
| d. Vegetation Mountains | 0.43 | 0.53 | 0.52 | 0.66 | 0.67 | 16.8 | 0.60 |
| e .Mountains Urban | 0.84 | 0.83 | 0.84 | -0.34 | 0.62 | 28.7 | 0.81 |
| f. Urban | 0.05 | 0.02 | 0.03 | 0.03 | 0.08 | 11.1 | 0.06 |
| g Mountains Lake | 0.54 | 0.79 | 0.85 | 0.81 | 0.91 | 58.8 | 0.91 |

Table 8-6  Correction Coefficients of TM Band 6 with Other Bands
(LANDSAT / TM  D147-32 13JUL86 Tarim Basin, China)

| Description of the Area | Band 1 | Band 2 | Band 3 | Band 4 | Band 5 | Variance | Band 7 |
|---|---|---|---|---|---|---|---|
| a. Arid Area (No-Vegetation) Carbonate Rock Mountains | 0.30 | 0.28 | 0.25 | 0.17 | 0.20 | 79.8 | 0.27 |
| b. Arid Area (No-Vegetation) andstone Mountains | -0.21 | -0.20 | -0.12 | -0.10 | -0.14 | 28.3 | -0.08 |
| c. Arid Area (No-Vegetation) Fan | -0.19 | -0.18 | -0.16 | -0.17 | -0.11 | 23.1 | -0.12 |
| d. Arid Area (No-Vegetation) Carbonate Rock Mountains | 0.64 | 0.66 | 0.65 | 0.70 | 0.70 | 184.9 | 0.69 |
| e. Vegetation | 0.38 | 0.39 | 0.39 | -0.15 | 0.36 | 29.6 | 0.41 |
| f. Arid Area (No-Vegetation) Mountains | 0.75 | 0.74 | 0.75 | 0.57 | 0.66 | 185.6 | 0.71 |
| g. Arid Area (No-Vegetation) Fan | 0.38 | 0.41 | 0.42 | 0.46 | 0.45 | 15.9 | 0.47 |

Table 8-7.  Correction Coefficients of TM Band 6 with Other Bands
(LANDSAT / TM  D140-30 17JAN89 Turpan Basin, China)

| Description of the Area | Band 1 | Band 2 | Band 3 | Band 4 | Band 5 | Variance | Band 7 |
|---|---|---|---|---|---|---|---|
| a. Dune | 0.56 | 0.76 | 0.80 | 0.80 | 0.80 | 61.0 | 0.81 |
| b. Desert | -0.33 | -0.38 | -0.34 | -0.19 | 0.07 | 0.9 | 0.19 |
| c. Arid Area | 0.34 | 0.49 | 0.56 | 0.60 | 0.49 | 49.4 | 0.53 |
| d. (Cirrus) Cloud / Desert | -0.12 | -0.12 | -0.16 | -0.14 | -0.05 | 1.0 | 0.06 |
| e. Snow / Mountains | -0.28 | -0.16 | -0.08 | 0.01 | 0.77 | 80.3 | 0.77 |
| f. Desert | 0.41 | 0.36 | 0.35 | 0.35 | 0.45 | 4.8 | 0.50 |

## 8.2. Theoretical Basis of Geometric System Correction

The geometric system correction is divided into several parts as follows:

(1) The pointing correction
(2) The coordinates transformation from Navigation Base Reference of the spacecraft to the Orbital Reference Frame
(3) The coordinates transformation from the Orbital Reference Coordinate Frame to the Earth Inertial coordinate Frame
(4) The coordinates transformation from the Earth Inertial Coordinate Frame to the Earth Greenwich Coordinate Frame
(5) Identification of a cross-point between the earth surface and an extended line of the vector

### 8.2.1. Basic Relation

The coordinates rotation is a basic coordinate frame transformation function. When the coordinates are transformed from the Coordinates 1 to the Coordinates 2 with the rotations for x, y, z by the angles of $\theta_x$, $\theta_y$ and $\theta_z$, the expression of the vector $P$ in the Coordinates 1 is transformed to the Coordinates 2 as follows.

$$\begin{bmatrix} X_2 \\ Y_2 \\ Z_2 \end{bmatrix} = F_z F_y F_x \begin{bmatrix} X_1 \\ Y_1 \\ Z_1 \end{bmatrix} \tag{8.2-1}$$

where $X_1, Y_1, Z_1$ : x, y and z components of the vector $P$ in the Coordinates 1, respectively,
$X_2, Y_2, Z_2$ : x, y and z components of the vector $P$ in the Coordinates 2, respectively,

$$F_x = \begin{bmatrix} 1 & 0 & 0 \\ 0 & \cos\theta_x & \sin\theta_x \\ 0 & -\sin\theta_x & \cos\theta_x \end{bmatrix}$$

(8.2-2)

$$F_y = \begin{bmatrix} \cos\theta_y & 0 & -\sin\theta_y \\ 0 & 1 & 0 \\ \sin\theta_y & 0 & \cos\theta_y \end{bmatrix}$$

(8.2-3)

$$F_z = \begin{bmatrix} \cos\theta_z & \sin\theta_z & 0 \\ -\sin\theta_z & \cos\theta_z & 0 \\ 0 & 0 & 1 \end{bmatrix}.$$

(8.2-4)

In the orbit x, y and z axes correspond to the roll, the pitch and the yaw axes, respectively.

## 8.2.2. Pointing Correction

The line of sight vector changes with the rotation for the pointing axis by an angle of $\beta$ from $S_0$ to $S$ as follows.

$$\begin{bmatrix} S_X \\ S_Y \\ S_Z \end{bmatrix} = M^{-1} \begin{bmatrix} 1 & 0 & 0 \\ 0 & \cos\beta & -\sin\beta \\ 0 & \sin\beta & \cos\beta \end{bmatrix} M \begin{bmatrix} S_{0X} \\ S_{0Y} \\ S_{0Z} \end{bmatrix} \qquad (8.2\text{-}5)$$

where

$S_{0x}, S_{0y}, S_{0z}$ : x, y , z components of the line of sight vector $S_0$ befor pointing,
$S_x, S_y, S_z$    : x, y, x components of the line of sight vector $S$ after pointing,

$$M \equiv \begin{bmatrix} \cos\theta_{yaw} & \sin\theta_{yaw} & 0 \\ -\sin\theta_{yaw} & \cos\theta_{yaw} & 0 \\ 0 & 0 & 1 \end{bmatrix} \begin{bmatrix} \cos\theta_{pitch} & 0 & -\sin\theta_{pitch} \\ 0 & 1 & 0 \\ \sin\theta_{pitch} & 0 & \cos\theta_{pitch} \end{bmatrix}, \qquad (8.2\text{-}6)$$

$$M^{-1} \equiv \begin{bmatrix} \cos\theta_{pitch} & 0 & \sin\theta_{pitch} \\ 0 & 1 & 0 \\ -\sin\theta_{pitch} & 0 & \cos\theta_{pitch} \end{bmatrix} \begin{bmatrix} \cos\theta_{yaw} & -\sin\theta_{yaw} & 0 \\ \sin\theta_{yaw} & \cos\theta_{yaw} & 0 \\ 0 & 0 & 1 \end{bmatrix}, \qquad (8.2\text{-}7)$$

$$\Delta\theta_{yaw} \equiv \sin^{-1}(P_y) , \qquad (8.2\text{-}8)$$
$$\Delta\theta_{pitch} \equiv -\tan^{-1}(P_z / P_x) , \qquad (8.2\text{-}9)$$

$P_x, P_y, P_z$ : x, y, z componets of the pointing axes unit vector in the NBR Coordinate Frame.

Figure 8-1 shows the relation between the pointing axis and the NBR Coordinate Frame. The angles $\Delta\theta_{yaw}$ and $\Delta\theta_{pitch}$ are the yaw and the pitch rotation angles, respectively, to coalign the $X_{NBR}$ to the pointing axis.
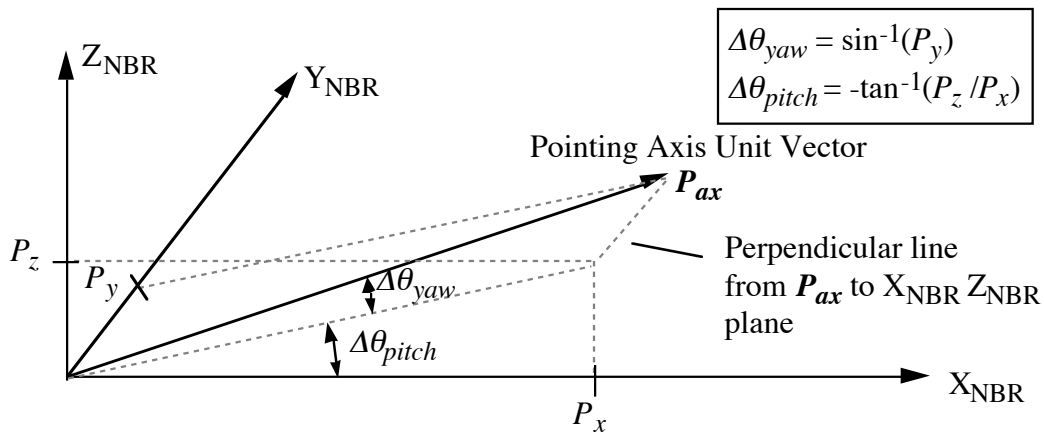


Figure 8-1    Pointing Axis Vector in NBR Coordinate Frame

### 8.2.3. Spacecraft NBR to Orbit Reference Frame

The line of sight vectors in the Spacecraft NBR Coordinate Frame can be converted to the expression in the Orbital Reference Frame using the attitude angle data in the spacecraft ancillary data as follows.

$$S_{OR} = F_{SO \cdot yaw} \, F_{SO \cdot pitch} \, F_{SO \cdot roll} \, S \quad , \tag{8.2-10}$$

where $S$ :  the line of sight vector expressed in the NBR Coordinate Frame,
$\quad S_{OR}$ :  the line of sight vector expressed in the Orbit Reference Coordinate Frame,

$$F_{SO \cdot roll} \equiv \begin{bmatrix} 1 & 0 & 0 \\ 0 & \cos(-\alpha_{roll}) & \sin(-\alpha_{roll}) \\ 0 & -\sin(-\alpha_{roll}) & \cos(-\alpha_{roll}) \end{bmatrix} , \tag{8.2-11}$$

$$F_{SO \cdot pitch} \equiv \begin{bmatrix} \cos(-\alpha_{pitch}) & 0 & -\sin(-\alpha_{pitch}) \\ 0 & 1 & 0 \\ \sin(-\alpha_{pitch}) & 0 & \cos(-\alpha_{pitch}) \end{bmatrix} , \tag{8.2-12}$$

$$F_{SO \cdot yaw} \equiv \begin{bmatrix} \cos(-\alpha_{yaw}) & \sin(-\alpha_{yaw}) & 0 \\ -\sin(-\alpha_{yaw}) & \cos(-\alpha_{yaw}) & 0 \\ 0 & 0 & 1 \end{bmatrix} , \tag{8.2-13}$$

$\alpha_{roll}, \alpha_{pitch}, \alpha_{yaw}$ : roll, pitch, yaw components of the attitude data, respectively, in the spacecraft ancillary data

### 8.2.4. Orbital Reference Frame to Earth Inertial Frame

The line of sight vectors in the Orbital Reference Coordinate Frame can be converted to the expression in the Earth Inertial Coordinate Frame as follows.

$$S_{EI} = F_{OI} \, S_{OR}, \tag{8.2-14}$$

where $S_{OR}$ :  the line of sight vector expressed in the Orbit Reference Coordinate Frame,
$\quad S_{EI}$ :  the line of sight vector expressed in the Eartt Inertial Coordinate Frame,

$$F_{OI} \equiv (T_x \, T_y \, T_z), \tag{8.2-15}$$

$T_x \, T_y \, T_z$ : unit vector components of x, y and z axes of the Orbital Coordinate Frame expressed in the Earth Inertial Coordinate Frame and defined as

$$\begin{aligned} T_x &\equiv T_y \times T_z \\ T_y &\equiv \text{unit} \, (-R \times V) \\ T_z &\equiv \text{unit} \, (-R) \end{aligned} \tag{8.2-16}$$

$R, V$ : the spacecraft position and velocity vectors expressed in the Earth Inertial Frame

For more accurate calculation the Precession matrix $P$ and the Nutation matrix $N$ shall be applied to the line of sight vector $S_{EI}$ in the Earth Inertial Coordinate Frame.

## 8.2.5. Earth Inertial Frame to Earth Fixed Frame

The line of sight vectors in the Earth Inertial Coordinate Frame can be converted to the expression in the Earth Fixed Coordinate Frame as follows.

$$S_{EF} = F_{IF} \, S_{EI} ,$$

(8.2-17)

where $S_{EI}$: the line of sight vector expressed in the Eartt Inertial Coordinate Frame,
$S_{EF}$ : the line of sight vector expressed in the Eartt Fixed Coordinate Frame,

$$F_{IF} \equiv \begin{bmatrix} \cos \theta_g & \sin \theta_g & 0 \\ -\sin \theta_g & \cos \theta_g & 0 \\ 0 & 0 & 1 \end{bmatrix},$$

(8.2-18)

$\theta_g$ : Greenwich true sidereal hour angle.

## 8.2.6. Identification of Observing Earth Surface

The observing earth surface can be identified calculating the crossing point between the extension line of the LOS vector and the earth surface.  The extension line of the LOS vector can be expressed as follows.

$$x = X + S_{EF \cdot x} \, r$$
$$y = Y + S_{EF \cdot y} \, r$$

(8.2-19)

$$z = Z + S_{EF \cdot z} \, r$$

where $S_{EF \cdot x}$, $S_{EF \cdot y}$, $S_{EF \cdot z}$ : x, y, z components of the LOS vector $S_{EF}$ in the Earth
Fixed Coordinate Frame,
X, Y, Z : x, y, z components of the Spacecraft position vector in the Earth
Fixed Coordinate Frame
r : parameter.

The earth surface can be expressed as follows.

$$(x^2 + y^2)/a^2 + z^2/b^2 = 1,$$

(8.2-20)

where

$a = 6378137m$   (earth radius at equator--WGS-84),
$b = a(1 - f)$     (earth radius at pole----WGS-84),     (8.2-21)
$f = 1/298.2572$ .

The crossing point can be calculated from eqs.(8.2-19) and (8.2-20).  When the observing point
is expressed as $P_x$, $P_y$, and $P_z$ , the geocentric latitude $\psi$ and the longitude $\lambda$ can be expressed as follows.

$$\psi = \tan^{-1}\{P_z/(P_x{}^2 + P_y{}^2)^{1/2}\}, \tag{8.2-22}$$
$$\lambda = \tan^{-1}(P_y/P_x). \tag{8.2-23}$$

## 8.2.7. Panoramic Correction

As mentioned above, the altitude of the sensor (or the distance between the earth surface and the sensor) has some geometric impact to the data, This altitude changes predominantly by following three factors.

1) Change of the spacecraft orbit :
   Nominal major axis of the spacecraft orbit is 7078 km as shown in the table 2-1. This gives an altitude of 700 km at the equator, assuming the WGS 84 Earth parameter : Considering the small flattening factor f of the orbit ($1/f = 1.389 \times 10^{-6}$), the radius of the orbit may change only slightly. So, the radius can be considered constant for few cycles. However, long term change of the radius may occur so that the change is of magnitude of 11km.
2) Change of the earth radius

   By the WGS 84(World Geodetic System 84), the earth major axis a is 6378.137km and 1/f ( f : flattening factor ) = 298.25723563 ( the earth minor axis b is 6356.752 km ) So, if the orbit of the spacecraft is close to a circle, the distance from the ellipsoid changes with magnitude of 21 km .

3) Topographic change.
   Since the geoid height ,which is the distance between the mean sea level and the earth ellipsoid, is of order of 20 - 30 meters at most, it can be negligible. However, the topography may change from 0 meter to 9000 m, and there is an influence to the altitude. Currently, a coarse DEM ( Digital Elevation Model ) which has a spatial resolution corresponding to one scene is considered to be needed.

Getting these parameters, panoramic effect can be considered. The swath $L_{ct}$ and pixel size change in cross track direction. $L_{ct}$ is given by

$$L_{ct} = R\ [\arcsin\{\ (R{+}H)/R\ \sin(\theta{+}\Delta\theta)\ \}{-}\arcsin\{\ (R{+}H)/R\ \sin(\theta{-}\Delta\theta)\ \}{-}2\Delta\theta)]$$
where
   $R$ : radius for local curvature of the earth
   $H$ : altitude of the spacecraft
   $\theta$: look direction angle of the central pixel
          $\Delta\theta$: look direction angle difference of the edge pixel from the direction $\theta$

## 8.2.8. Correction for Earth Rotation

In addition to the panoramic correction, the earth rotation gives rise to skew effect. The skew angle $\Phi_\varepsilon$ can be calculated by

$$\tan \Phi_\varepsilon = \{\omega_e/\omega_s \sin(\alpha \cos\omega_s t)\}/(1+\omega_e/\omega_s \cos\alpha)$$

where
   $\omega_e$ angular velocity of the earth rotation
   $\omega_s$: angular velocity of the spacecraft
   $\alpha$: orbit inclination angle
   $t$ : time spent from the equator

The skew angle makes the spacecraft track on the earth surface deviate from the perpendicular direction to the cross track direction. The skew angle has its maximum value of 3.85 degree at the equator and becomes zero at the high latitude point.

### 8.2.9. Map Projection

Although map projection is a geometric transformation rather than correction, earth surface data which is a part of the sphere cannot be projected on a two dimensional plane without map projection.

Considering the scale of the ASTER data to be 1/100,000 ~ 1/250,000, UTM (Universal Transverse Mercator) is the most common map cylindrical map projection, the earth surface is divided into 60 Mercator Zone having 6 degree longitude width. There will be some data encompassing two UTM Zones. In such case, one of the UTM Zone should be extended to the other . As a disadvantage of the UTM to the level 1 processing is that the two adjacent scenes located at the border of the two UTM zones cannot be mosaiced easily, while, in the case of SOM (Space Oblique Mercator), this continuity is guaranteed. However as a standard map projection, SOM is not of general use. Further more, conversion factor will be able to calculated so that the data can be projective by SOM, starting form level-1A data.

On the other hand at the high latitude regions, each UTM zone becomes narrow. So, alternative map projection should be considered. Currently, LCC (Lambert Conformal Conic) projection is being considered.

## 8.3 Theoretical Basis of Radiometric Correction

### 8.3.1 VNIR Radiometric Coefficients Correction

VNIR observes spectral reflectance characteristics of the ground cover targets with the solar irradiance through the atmospheric influences due to scatterings and absorptions. The input radiance $L$ is converted into the output voltage as follows.

$$V_{ij} = G_i A_{Lij} L_{ij} + D_{Lij \bullet G} , \qquad (8.3\text{-}1)$$

where the subscripts $i$ and $j$ denote the band number and the pixel number, respectively. The values $A_{Lij}$ and $B_{Lij}$ are the sensitivity and the offset of each detector, respectively. The value $G_i$ is the gain factor. The notation $D_{Lij \bullet G}$ means that the offset depends on the gain settings.

The input radiance for each pixel can be calculated from the output voltage as follows.

$$L_{ij} = A_{Vij} V_{ij} /G_i + D_{vij \bullet G} , \qquad (8.3\text{-}2)$$

where

$$A_{Vij} \equiv 1/A_{Lij} \qquad (8.3\text{-}3)$$
$$D_{Vij \bullet G} \equiv -D_{Lij \bullet G} /(A_{Lij} G_i) . \qquad (8.3\text{-}4)$$

The detector temperature dependence of the sensitivity and the offset can be expressed with a good accuracy as follows.

$$A_{Lij} = A_{L0ij} \{1 + a_{ij}(\Delta T_{DET}/T_{DET0})\} \qquad (8.3\text{-}5)$$
$$D_{Lij \bullet G} = D_{L0ij \bullet G} \{1 + b_{ij}(\Delta T_{DET}/T_{DET0})\},$$
$$(8.3\text{-}6)$$

where

$T_{DET}$ : the detector temperature

$T_{DET0}$ : the reference detector temperature

$\Delta T_{DET0} \equiv T_{DET} - T_{DET0}$ .

The values $A_{L0ij}$ and $D_{L0ij \cdot G}$ are $A_{Lij}$ and $D_{Lij \cdot G}$ at $T_{DET} = T_{DET0}$ , respectively. The temperature coefficients $a_{ij}$, and $b_{ij}$ can be evaluated by the preflight subsystem test and will be used throughout all mission life period.

Using the relation of Eqs.(8.3-5) and (8.3-6), Eqs.((8.3-3) and (8.3-4) become

$$A_{Vij} = A_{V0ij} \{1 + a_{ij}(\Delta T_{DET}/T_{DET0})\}^{-1} \qquad (8.3\text{-}7)$$

$$D_{Vij \cdot G} = D_{V0ij \cdot G}\{ 1 + a_{ij}(\Delta T_{DET}/T_{DET0})\}^{-1}\{1 + b_{ij}(\Delta T_{DET}/T_{DET0})\}. \qquad (8.3\text{-}8)$$

When the detector temperature difference from the reference temperature is very small, Eqs.(8.3-7) and (8.3-8) can be approximated by a following linear dependence.

$$A_{Vij} = A_{V0ij} \{1 + c_{ij}(\Delta T_{DET}/T_{DET0})\} \qquad (8.3\text{-}9)$$

$$D_{Vij \cdot G} = D_{V0ij \cdot G}\{ 1 + d_{ij}(\Delta T_{DET}/T_{DET0})\} , \qquad (8.3\text{-}10)$$

where

$c_{ij} \equiv -a_{ij}$

$d_{ij} \equiv -a_{ij} + b_{ij}$ .

The values $A_{V0ij}$ and $D_{V0ij \cdot G}$ can be evaluated by the calibration activity and the dark target observation data in the preflight and the flight periods.

The parameters $A_{V0ij}$ , $D_{V0ij \cdot G}$ , $c_{ij}$ , $d_{ij}$ and $T_{DET0}$ are accommodated in the radiometric correction data base file. The coefficients $A_{Vij}$ , $D_{Vij \cdot G}$ are corrected using Eqs. (8.3-9) and (8.3-10) by the detector temperature in the supplement data at each observation and will be appended in the Level-1A data products as the radiometric coefficients of each detector.

The temperature dependence factors $c_{ij}$ and $d_{ij}$ are assumed to depend on each pixel even in the same band. However, there is some possibility to have a same value for the same band. The final decision on the detector dependence will be made after PFM subsystem test.

## 8.3.2 SWIR Radiometric Coefficients Correction

SWIR observes spectral reflectance and high temperature thermal radiation characteristics of the ground cover targets. The input radiance $L$ is converted into the output voltage as follows.

$$V_{ij} = G_i A_{Lij} L_{ij} + D_{Lij \cdot G} , \qquad (8.3\text{-}11)$$

where the subscripts $i$ and $j$ denote the band number and the pixel number, respectively. The values $A_{Lij}$ and $B_{Lij}$ are the sensitivity and the offset of each detector, respectively. The value $G_i$ is the gain factor. The notation $D_{Lij \cdot G}$ means that the offset depends on the gain settings.

The input radiance for each pixel can be calculated from the output Voltage as follows.

$$L_{ij} = A_{Vij} V_{ij} /G_i + D_{vij \cdot G} , \qquad (8.3\text{-}12)$$

where

$$A_{Vij} \equiv 1/A_{Lij} \tag{8.3-13}$$

$$D_{Vij \bullet G} \equiv -D_{Lij \bullet G} /(A_{Lij} G_i) . \tag{8.3-14}$$

The sensitivity depends on the detector temperature and its dependence can be expressed with a linear relation as follows.

$$A_{Lij} = A_{L0ij} \{1 + a_{ij}(\Delta T_{DET}/T_{DET0})\}. \tag{8.3-15}$$

While the offset depends on both the detector temperature and the dewar temperature. The detector temperature dependence is approximated up to the second order term of the temperature change when the temperature range is within 77K ± 3K range, although it is basically exponential. The dewar temperature dependence can be approximated with a linear relation. The total offset can be expressed as follows.

$$D_{Lij \bullet G} = D_{L0ij \bullet G} \{1 + b_{1ij}(\Delta T_{DET}/T_{DET0}) + b_{2ij}(\Delta T_{DET}/T_{DET0})^2 + b_{3ij}(\Delta T_{DEW}/T_{DEW0})\}, \tag{8.3-16}$$

where

$T_{DET}$ : the detector temperature
$T_{DET0}$ : the reference detector temperature
$\Delta T_{DET} \equiv T_{DET} - T_{DET0}$
$T_{DEW}$ : the dewar temperature
$T_{DEW0}$ : the reference dewar temperature
$\Delta T_{DEW} \equiv T_{DEW} - T_{DEW0}$ .

The values $A_{L0ij}$ and $D_{L0ij \bullet G}$ are $A_{Lij}$ and $D_{Lij \bullet G}$ at $T_{DET} = T_{DET0}$ and $T_{DEW} = T_{DEW0}$, respectively.

By using the relation of Eqs.(8.3-15) and (8.3-16), Eqs.((8.3-13) and (8.3-14) become

$$A_{Vij} = A_{V0ij} \{1 + a_{ij}(\Delta T_{DET}/T_{DET0})\}^{-1} \tag{8.3-17}$$

$$D_{Vij \bullet G} = D_{V0ij \bullet G} \cdot \{ 1 + a_{ij}(\Delta T_{DET}/T_{DET0})\}^{-1}\{1 + b_{1ij}(\Delta T_{DET}/T_{DET0})$$
$$+ b_{2ij} (\Delta T_{DET}/T_{DET0})^2 + b_{3ij}(\Delta T_{DEW}/T_{DEW0})\}. \tag{8.3-18}$$

The values $A_{V0ij}$ and $D_{V0ij \bullet G}$ are $A_{Vij}$ and $D_{Vij \bullet G}$ at $T_{DET} = T_{DET0}$ and $T_{DEW} = T_{DEW0}$, respectively. The temperature coefficients $a_{ij}$, $b_{1ij}$ , $b_{2ij}$ , and $b_{3ij}$ can be evaluated by the preflight subsystem test and will be used throughout all mission life period. When the temperature change is small, Eqs (8.3-17) and (8.3-18) can be approximated by the following equations.

$$A_{Vij} = A_{V0ij} \{1 + c_{ij}(\Delta T_{DET}/T_{DET0})\} \tag{8.3-19}$$

$$D_{Vij \bullet G} = D_{V0ij \bullet G} \{ 1 + d_{1ij}(\Delta T_{DET}/T_{DET0}) + d_{2ij}(\Delta T_{DET}/T_{DET0})^2 + d_{3ij}(\Delta T_{DEW}/T_{DEW0})\}, \tag{8.3-20}$$

where

$c_{ij} \equiv -a_{ij}$
$d_{1ij} \equiv -a_{ij} + b_{1ij}$
$d_{2ij} \equiv b_{2ij}$
$d_{3ij} \equiv b_{3ij}$ .

The values $A_{V0ij}$ and $D_{V0ij\bullet G}$ can be evaluated by the calibration activity and the dark target observation data in the preflight and the flight periods.

The parameters $A_{V0ij}$, $D_{V0ij\bullet G}$, $c_{ij}$, $d_{1ij}$, $d_{2ij}$, $d_{3ij}$, $T_{DET0}$ and $T_{DEW0}$ are accommodated in the radiometric correction data base file. The coefficients $A_{Vij}$ and $D_{Vij\bullet G}$ are corrected using Eqs. (8.3-17) and (8.3-18) by the detector temperature and the dewar temperature in the supplement data at each observation and will be appended in the Level-1A data products as the radiometric coefficients of each detector.

The temperature dependence factors $c_{ij}$, $d_{1ij}$, $d_{2ij}$, and $d_{3ij}$ are assumed to depend on each pixel even in the same band. However, there is some possibility to have a same value for the same band. The final decision on the detector dependence will be made after PFM subsystem test.

### 8.3.3 TIR Radiometric Coefficients Correction

TIR observes thermal radiation of the ground cover targets through the atmospheric absorptions. Not only direct emission from the targets but also the emission from the atmospheric molecule and the reflected sky radiance at the ground are included in the input radiance.

Input radiance $L$ in front of the optics of the TIR system can be evaluated from output voltage by the following second order non-linear equation.

$$L_{ij} = A_{Vij}V_{ij} + C_{Vij}V_{ij}^2 + D_{vij} \qquad (8.3\text{-}21)$$

where the subscripts $i$ and $j$ denote the band number and the pixel number, respectively. The values $A_{Vij}$, $C_{vij}$ and $D_{Vij}$ are the linear sensitivity, non-linear sensitivity and the offset of each detector, respectively.

The linear and non-linear sensitivities depend on the detector temperature with linear relations as follows.

$$A_{Vij} = A_{V0ij} \{1 + c_{1ij}(\Delta T_{DET}/T_{DET0})\} \qquad (8.3\text{-}22)$$
$$C_{Vij} = C_{V0ij} \{1 + c_{2ij}(\Delta T_{DET}/T_{DET0})\}. \qquad (8.3\text{-}23)$$

While the offset depends on the telescope, the chopper and the lens temperatures. When the temperature change is a few degrees around a normal operating temperature of 300 K. The temperature dependence is approximated with a linear relation as follows.

$$D_{Vij} = D_{V0ij}\{ 1 + d_{ij}(\Delta T_{TEL}/T_{TEL0}) + g_{ij}(\Delta T_{CHP}/T_{CHP0}) + h_{ij}(\Delta T_{LNS}/T_{LNS0})\}, \qquad (8.3\text{-}24)$$

where
$T_{DET}$ : the detector temperature
$T_{DET0}$ : the reference detector temperature
$\Delta T_{DET} \equiv T_{DET} - T_{DET0}$
$T_{TEL}$ : the telescope temperature
$T_{TEL0}$: the reference telescope temperature
$\Delta T_{TEL} \equiv T_{TEL} - T_{TEL0}$
$T_{CHP}$ : the chopper temperature
$T_{CHP0}$: the reference chopper temperature
$\Delta T_{CHP} \equiv T_{CHP} - T_{CHP0}$
$T_{LNS}$ : the lens temperature
$T_{LNS0}$: the reference lens temperature

$$\Delta T_{LSN} \equiv T_{LNS} - T_{LNS0} \, .$$

The values $A_{V0ij}$, $D_{V0ij}$ and $C_{V0ij}$ are $A_{Vij}$, $D_{Vij}$ and $C_{Vij}$ at $T_{DET} = T_{DET0}$, $T_{TEL} = T_{TEL0}$, $T_{CHP} = T_{CHP0}$ and $T_{LNS} = T_{LNS0}$ respectively, and can be evaluated with the variable temperature blackbody in the preflight test period. The variable temperature range is from 100 K to 370 K. The least square method may be used to calculate these parameters from several measurement values. The input radiance of the blackbody can be calculated by Plank's law as functions of the wavelength and the blackbody temperature as follows.

$$L(\lambda_i , T_{BB}) = \frac{C_1}{\pi \lambda_i^5} \frac{1}{\exp\left(\dfrac{C_2}{\lambda_i T_{BB}}\right) - 1} \tag{8.3-25}$$

where

$\lambda_i$ : the wavelength
$T_{BB}$ : the blackbody temperature
$C_1 = 3.7415 \times 10^4$ (W cm$^{-2}$ μm$^4$)
$C_2 = 1.4388 \times 10^4$ (μm K) .

The wavelength $\lambda_i$ can be represented by the center wavelength of each spectral band with a small error as shown in Figure 8-1 later. The temperature coefficients $c_{1ij}$, $c_{2ij}$, $d_{ij}$, $g_{ij}$ and $h_{ij}$ can also be evaluated in the preflight test period. These temperature coefficients and non-linear sensitivity coefficient will be used throughout all mission life.

The linear sensitivity coefficient $A_{vij}$ and the offset $D_{vij}$ can be evaluated by the regular long term calibration activity even in the flight period and will be revised if necessary. For the long term in-flight calibration activity the on-board blackbody temperature will be varied from 270 K to 340 K. The least square method may be used to calculate these parameters from several measurement values.

The offset values $D_{vij}$ will be evaluated more frequently every observation at a on-board blackbody temperature of 270 K. This calibration activity is called the short term calibration. In the case that the offset data based on the short term calibration is available, only two sensitivity coefficients will be corrected by using Eqs. (8.3-22) and (8.3-23) for each observation.

In the case that the offset data based on the short term calibration is not available, the offset values $D_{vij}$ will be evaluated from the previous long term calibration data using Eq. (8.3-24).

The values $A_{V0ij}$, $C_{V0ij}$, $D_{V0ij}$, $c_{1ij}$, $c_{2ij}$, $d_{ij}$, $g_{ij}$, $h_i$, $T_{DET0}$, $T_{TEL0}$, $T_{CHP0}$, and $T_{LNS0}$ are accommodated in the radiometric correction data base file. The coefficients $A_{Vij}$, $C_{Vij}$ and $D_{Vij}$ are corrected using Eqs. (8.3-22), (8.3-23) and (8.3-24) depending on the temperatures of some components mentioned above at each observation and will be appended in the Level-1A data products as the radiometric coefficients of each detector.

The temperature dependence factors are assumed to depend on each pixel in the same band. However, there is some possibility to have a same value for each detector in the same band. The final decision on the detector dependence will be made after PFM subsystem test.

When the radiance is calculated from the blackbody temperature by a representative value at the center wavelength of each band, the calculation error is expressed as

$$E_C = \frac{W(\lambda_{ic}, T_{BB})\Delta\lambda_i}{\int_{\lambda_{i1}}^{\lambda_{i2}} W(\lambda_i, T_{BB})d\lambda_i} \quad , \qquad\qquad\qquad (8.3\text{-}26$$

where

        *i:* Band number

        $\Delta\lambda_i \equiv \lambda_{i2} - \lambda_{i1}$(Band width)

        $\lambda_{i1}$: Lower band edge

        $\lambda_{i2}$: Upper band edge

        $\lambda_{ic}$ : Center wavelength

        $T_{BB}$ : Blackbody temperature .

Figure 8-1 show the calculation error for each band as a function of the temperature. The error is very small.
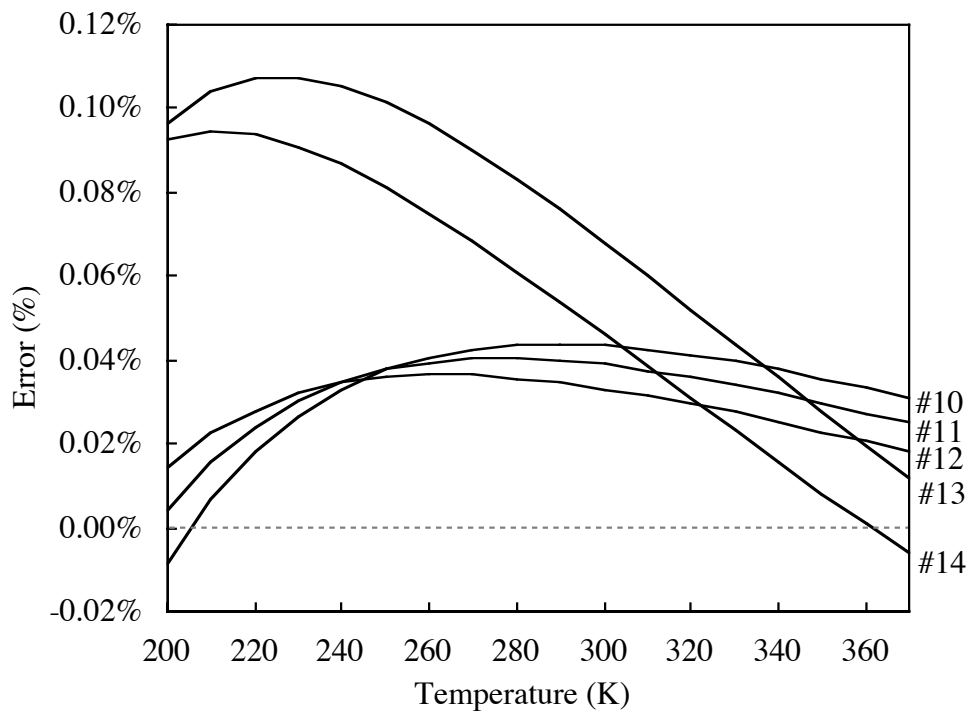


Figure 8-1  Calculation Error from Temperature to Radiance for
Approximation at Center Wavelength  of Each Band


## 8.3.4.  Radiance   Conversion   Coefficients

The radiance values of the Level-1 product shall be converted to 8 bits digital numbers for the VNIR and the SWIR bands, and 16 bits digital numbers for the TIR bands as follows.

$$L_{DNij} = L_{ij} /( L_{ni} /G_i ), \qquad\qquad\qquad (8.3\text{-}27)$$

where $L_{DNij}$ is the DN value for $L_{ij}$ which corresponds to the radiance of band $i$ and pixel $j$ . The conversion  coefficient $L_{ni}$ is the radiance of unit DN for the band $i$  in the normal gain.  The

radiance conversion coefficients for the gain other than the normal gain can be obtained by $L_{ni}$ /$G_i$ .

The conversion coefficient for each band shall be defined as a common value throughout the mission life such that the specified maximum input radiance corresponds to 256 DN (8 bits) for VNIR and SWIR, and 4096 DN (12 bits) for TIR. The specified maximum input radiance for each band is described in Section 2.2.3.

### 8.3.5. TIR DC Clamp Correction

The DC clamp correction shall be carried out subtracting the correction value $\Delta V_{DNCLij}$ from the image data DN value. The correction value $\Delta V_{DNCLij}$ can be calculated as follows.

$$\Delta V_{DNCLij} \equiv V_{DNCLij} - V_{CL0i} /V_{ni} , \qquad (8.3\text{-}28)$$

where
$V_{CL0i}$ : the DC Clamp voltage for the band $i$ which correspond to -1.4 V for the bands 10-12 and -0.9 V for the bands 13 and 14
$V_{DNCLij}$ : the average output DN value for the $ij$ detector when the chopper plate is observed by the detectors every scan
$V_{ni}$ : the voltage of unit DN for the band $i$ .

### 8.3.6. TIR Chopper Temperature Drift Correction

The chopper temperature of TIR may slightly change during an observation period which is 16 minutes in the maximum case. This correction shall be carried out subtracting the correction value $\Delta V_{DNCHPij}$ from the image data DN value. The correction value $\Delta V_{DNCHPij}$ can be calculated as follows.

$$\Delta V_{DNCHPij} \equiv f_{DNij} \Delta T_{CHP} , \qquad (8.3\text{-}29)$$

where

$\Delta T_{CHP} \equiv T_{CHP} - T_{CHP \bullet S}$
$T_{CHP}$ : the chopper temperature for each scan
$T_{CHP \bullet S}$ : the chopper temperature in the short term calibration period for each scan

$f_{DNij}$ : the output DN change of $ij$ detector for the unit $\Delta T_{CHP}$ which can be evaluated during the preflight test.

# 9.   ASSUMPTIONS  AND  LIMITATIONS

## 9.1.   Assumptions

(1) It is assumed that the pointing stability of the spacecraft meets requirements shown in Table 2-3.

(2) It is assumed that the jitter and stability meet requirements shown in Table 2-16.

(3) It is assumed that the accuracy of detector configuration meets specification shown in Table 2-15.

(4) It is assumed that the pointing stability meet specification shown in Table 2-18.

(5) It is assumed that the boresight-to-boresight stability due to the spacecraft deformation is smaller than 0.3 pixels of coarser pixels, though it is not required and specified.

(6) It is assumed that the  input radiance for TIR can be expressed by offset, linear and square terms of output signal.

## 9.2.   Limitations

(1) SWIR parallax correction is carried out only for  scenes with smaller cloud coverage than some threshold value.

(2) SWIR parallax correction is carried out only on average of 21 by 21 pixels.

# 10. REFERENCES

1) Y. Yamaguchi, H. Tsu  and H. Fujisada,  "Scientific Basis of ASTER Instrument Design",Proc. SPIE, vol. 1939, pp. 150-160, 1993 Orlando

2) H. Fujisada,  "Overview of ASTER instrument on EOS-AM1 platform",   Proc. SPIE, vol. 2268, pp. 14-36, 1994  San Diego

3) H. Fujisada,  "Design and performance of ASTER instrument",  Proc. EUROPTO/SPIE, Vol.2583, 1995 Paris

4) A. Ono and F. Sakuma,  "ASTER Instrument Calibration Plan",  Proc. SPIE, vol. 1939, pp. 198-209, 1993 Orlando

5) H. Fujisada and H. Watanabe, "ASTER Level-1 Data Processing Concept", Proc. EUROPTO/SPIE, vol. 2317, pp. 6-17, 1994 Rome

6) M. Ono, "Parallax Error Correction Techniques by Image Matching for ASTER/SWIR Band-to-band Registration", Proc. EUROPTO/SPIE, vol. 2317, pp. 18-27, 1994 Rome

7) H. Watanabe and Y. Kannari, Band-to-band Registration Techniques among ASTER Images obtained by Different Telescope", Proc. EUROPTO/SPIE, vol. 2317, pp. 28-35, 1994 Rome

8) I. Sato, K. Fukue and K. Arai, "Basic Concept and Development of ASTER Data Processing System", Proc. EUROPTO/SPIE, vol. 2317, pp. 36-41, 1994 Rome

9) F. Sakuma, A. Ono and K. Arai, "Radiometric Calibration Techniques for ASTER" Proc. EUROPTO/SPIE, vol. 2317, pp. 42-48, 1994 Rome

10) P. N. Slater, S. F. Bigger, K. J. Thome, D. I. Gellman, and P. R. Spyak, "The In-flight Radiometric Calibration of ASTER by Reference to Well-characterized Scenes" Proc. EUROPTO/SPIE, vol. 2317, pp. 49-60, 1994 Rome

11) T. Ezaka and H. Watanabe, "ASTER Simulation Data for Evaluation of Level-1 Processing Algorithms", Proc. EUROPTO/SPIE, vol. 2317, pp. 61-69, 1994 Rome

12) S. P. Neeck, T. J. Venator and J. T. Bolek. "Jitter and Stability Calculation for the ASTER Instrument", Proc. EUROPTO/SPIE, vol. 2317, pp. 70-80, 1994 Rome